博士論文

Evaluation and development of remote sensing techniques for accurate water quality monitoring in turbid lakes and coastal areas

（閉鎖性及び海岸水域における高精度な水質モニタリングに向けたリモートセンシング技術の開発)

Salem Ibrahim Salem Mohamed Salem

サレム　イブラヒム　サレム　モハメット　サレム

37-147189

Adviser

Assoc.Prof. Kazuo Oki

A dissertation submitted to the Department of Civil Engineering, Graduate School of Engineering, The University of Tokyo in partial completion of the requirements for the degree of:

Doctor of Engineering

September 2017

Acknowledgements

The following words express my gratitude to ALLAH and people who morally and financially supported me to achieve my Ph.D. degree. First and foremost, I would like to express my deepest appreciation to my supervisor, Assoc. Prof. Kazuo Oki, for accepting me to be a member of Oki Laboratory. I am sincerely grateful to his guidance, supervisions, instructions, valuable advices and suggestions during my Ph.D. studies. From the bottom of my heart, I also wish to thank professor Taikan Oki for his leadership and ethical support during the three-years of my Ph.D. study in Oki Laboratory. In addition, I would like to thank Dr. Hiroto Higa for his continuous guidance to consolidate my background in ocean remote sensing and for providing me the experience and data that allow me to achieve my Ph.D.

I would like to acknowledge the funding received from the Japanese Ministry of Education, Culture, Sports, Science, and Technology (MEXT) to conduct my doctoral research. I wish to express my gratitude for professor Hiroshi Kobayashi and Dr. Hiroto Higa for including me in the GCOM-C RA6 project from Japan Aerospace eXploration Agency (JAXA) to perform in-situ measurements in many Japanese lakes and coastal areas.

My special thanks go to all Oki laboratory's member for the friendly atmosphere we have. I am grateful to Assoc. Prof. Hyungjun Kim for his continuous guidance. I am also grateful to Dr. Nobuyuki Utsumi and Hideaki Kamiya for the effective discussion that helped me a lot during my research. I am thankful to our secretary, Ms. Ayako Kurosawa, for her endless support which I have greatly benefited.

In order to have today achievements, I would like to express my deep gratitude to my father and mother, who believed in me more than I believed in myself. Whatever I am today is because of their belief in me and in my capability. On this occasion, I would also like to express my greatest appreciation to my brothers, Osama and Ahmed, my sister, Heba, and my children, Shery and Bebo for the happiness they have made in my life.

Finally, I would like to dedicate this achievement, Doctor Degree, to my wife, Mai Mohamed Bedeir. She is my source of inspiration and first person who hear my thoughts. For my wife, I wish to say "You are not just my wife, you are my life".

Summary

Many approaches have been proposed for monitoring the eutrophication of Case 2 waters using remote sensing data. Semi-analytical algorithms, neural network and spectrum matching with look-up table are three major approaches for chlorophyll-a (Chla) retrieval. However, there is no continuous monitoring for water quality in Case 2 waters (e.g., lakes and coastal areas). These approaches are evaluated during this study to address the strength and limitation of these approaches, and a new approach is proposed. Firstly, an evaluation of seven Chla retrieval processors developed for Medium Resolution Imaging Spectrometer (MERIS) sensor was performed using 10-year of MERIS archive data. Although the mission of MERIS was ended in 2012, the recent launched Ocean and Land Colour Instrument (OLCI) sensor is considered the follow-up mission for MERIS. The OLCI has similar configuration of MERIS. The seven processors will be adopted for OLCI. These processors are based on neural network and band height techniques. Results indicate that these processors tend to underestimate or overestimate the retrieved Chla. Therefore, local calibration using regression approach (e.g., linear regression) should be incorporated. Result from the calibration and validation stages indicate that four processors represent band height (i.e., Maximum Chlorophyll Index (MCI_L1) and Fluorescence Line Height (FLH_L1)) and neural network (i.e., Eutrophic Lake (EUL) and Case 2 Regional (C2R)) introduce reasonable retrieval accuracy with R^2 in the range of 0.42 – 0.65. The MCI_L1 provide the highest retrieval accuracy during the calibration and validation stages (R^2 = 0.65, RMSE = 22.18 mg m^{-3}, MARE = 36.88 %). In contrast, the results from Boreal Lake (BOL) and Free University of Berlin (FUB) highlighted their limitation to accurately retrieve Chla, resulting in high MARE for BOL (56.20 %) and FUB (57.00 %). Mapping the spatial distribution of Chla concentrations across Lake Kasumigaura using the seven processors show that all the processors except for BOL and FUB are able to accurately capture the Chla distribution for moderate and high Chla concentrations. MCI_L1 and C2R processors were evaluated over 10 years of time series as they demonstrated the best retrieval accuracy from the both groups (i.e., band height and neural network, respectively). The retrieved Chla of MCI_L1 is more precise than C2R to track the seasonal and annual variation of Chla with slight overestimation occur during springtime.

Secondly, seven semi-analytical algorithms are assessed with different band combinations of multispectral and hyperspectral bands with linear, polynomial and power regression approaches, resulting in 43 combinations of algorithms. These algorithms are evaluated by using simulated and measured datasets. Two simulated datasets of 500,000 reflectance spectra

each based on local and wide ranges of specific inherent optical properties (IOPs) are generated for calibration stage. A dependent simulated dataset of 500,000 reflectance spectra based on wide ranges of IOPs is used to validate the proposed algorithms. Results from simulated datasets reveal that algorithms calibrated with local IOPs introduced higher error comparing with wide range IOPs with overall RMSE of 95.92 mg m^{-3} and 30.10 mg m^{-3} for local and wide range IOPs, respectively. The spatial distribution of the best three algorithms for various combinations of Chla and NAP concentrations show that the two-, three-, four-band, and NDCI algorithms tend to provide acceptable accuracy among measured and simulated dataset, while some other algorithms provide high error (i.e., synthetic chlorophyll index (SCI) algorithms). In addition, the algorithms' indices are much important than the regression approach to achieve higher retrieval accuracy. 3b_680_QP and 3b_tuning_QP algorithms outperform other algorithms in terms of minimum RMSE frequency for local (27.78 %) and wide range (33.19 %) scenario, respectively. In addition, the spatial distribution emphasize that no single algorithm can provide outstanding accuracy for Chla retrieval, and multi-algorithms should be included to reduce the error.

The proposed technique combines the semi-analytical algorithms with look-up table. Semi-analytical algorithms provide indices correlated with phytoplankton characteristics, (e.g., maximum and minimum absorption peaks). Algorithms' indices are correlated with measured Chla through regression process. The main drawback of the semi-analytical algorithms is that the derived relation is location and data limited. Spectrum matching and look-up table approach rely on matching the measured reflectance with a large library of simulated reference corresponding to wide ranges of water properties. The spectral matching approach taking hyperspectral measured reflectance as an input, leading to difficulties in incorporating data from multispectral satellite. Consequently, multi-algorithm indices and look-up table (MAIN-LUT) technique is proposed to combine the merits of semi-analytical algorithms and look-up table which can be applied to multispectral data. Eight combinations of four algorithms (i.e., 2-band, 3-band, maximum chlorophyll index, and normalized difference chlorophyll index) are investigated for the MAIN-LUT technique. In-situ measurements and MERIS sensor data are used to validate MAIN-LUT. In general, the MAIN-LUT provide a comparable retrieval accuracy with locally tuned algorithms. The most accurate of the locally tuned algorithms varied among dataset, revealing the limitation of these algorithms to be applied universally. In contrast, the six out of the eight combinations of MAIN-LUT technique provided comparable high retrieval accuracy in Tokyo Bay (R^2 = 0.65, RMSE = 22.2 mg m^{-3}), Lake Kasumigaura (R^2 = 0.85, RMSE = 11.98 mg m^{-3}), and MERIS data (R^2 = 0.552, RMSE = 34.38 mg m^{-3}). The

simulated reflectance library of MAIN-LUT was generated based on inherent optical properties of Tokyo bay; however, the MAIN-LUT provided higher retrieval accuracy for lake Kasumigaura than Tokyo bay due to the fact that the abovementioned algorithms are more appropriate for highly turbid water bodies. Furthermore, these results emphasize that the MIAN-LUT can be applied for similar turbid water bodies. 4-indices-[680] combination is recommended for MERIS data to overcome the limitation of other combinations which underestimated Chla concentration > 50 mg m^{-3}.

Publication Lists

Peer-Reviewed Papers

Salem Ibrahim Salem, Hiroto Higa, Hyungjun Kim, Komatsu Kazuhiro, Hiroshi Kobayashi, Kazuo Oki, and Taikan Oki, 2017. Multi-Algorithm Indices and Look-Up Table for Chlorophyll-a Retrieval in Highly Turbid Water Bodies Using Multispectral Data. Remote Sens. 9, 556. doi:10.3390/RS9060556

Salem Ibrahim Salem, Hiroto Higa, Hyungjun Kim, Hiroshi Kobayashi, Kazuo Oki, and Taikan Oki. Assessment of chlorophyll-a algorithms considering different trophic statuses and optimal bands. Sensors, 2017, 1746. doi:10.3390/S17081746

Salem Ibrahim Salem, Marie Hayashi Strand, Hiroto Higa, Hyungjun Kim, Komatsu Kazuhiro, Kazuo Oki, and Taikan Oki, 2017. Evaluation of MERIS chlorophyll-a retrieval processors in a complex turbid Lake Kasumigaura through 10-year mission. Remote Sens. (**revised and re-submitted**)

Presentations on Conferences/Symposium (as participant)

Salem Ibrahim Salem, Hiroto Higa, Hyungjun Kim, Komatsu Kazuhiro, Hiroshi KoBayashi, Kazuo Oki, and Taikan Oki. Evaluation of Chlorophyll Retrieval in a Complex Turbid Inland Lake Using MERIS 10-Year Mission. International Symposium on Remote Sensing, May 17-19, 2017. Nagoya University, Nagoya, Japan.

Salem Ibrahim Salem, Hiroshi KoBayashi, and Hiroto Higa. In-situ measurements for development of an atmosphere and in-water combined algorithm basing on classification of coastal and lake water optical property characterization. Joint PI Meeting of Global Environment Observation Mission 2016, January 23-27, 2017. Tokyo, japan.

Salem Ibrahim Salem, Hiroto Higa, Hyungjun Kim, Hiroshi KoBayashi, Kazuo Oki, and Taikan Oki. Continuous Monitoring of Water Quality for Japan's Lakes & Coastal Areas. Joint Hydro-Science Meeting: Tsinghua University and The University of Tokyo, March 8th, 2016. The University of Tokyo, Tokyo, Japan.

Salem Ibrahim Salem, Hiroto Higa, Hyungjun Kim, Hiroshi KoBayashi, Kazuo Oki, and Taikan Oki. Retrieval Accuracy Assessment with Gap Detection for Case 2 Waters Chla Algorithms. AGU Fall Meeting, December 12-16, 2016. San Francisco, California, USA.

Table of Contents

REFERENCES 90

List of Tables

List of Figures

CHAPTER 1

Introduction

1.1. Eutrophication problem

During the last 40 years, many industrialized countries including Japan have applied several actions to reduce the nutrient loadings that flow into lakes and coastal areas by constructing sewage treatment plants and banning phosphorus materials in many industries (Finger et al., 2013). As a result, the nutrients loading significantly decreased in some areas to the extent that it caused environmental problem such as declining in the fishing yield and primary production (i.e., that known as oligotrophication) (Terauchi et al., 2014). On the other hand, the eutrophication (i.e., means nutrient enrichment in water bodies) still a serious environmental problem in many lakes and coastal waters because of the extensive use of fertilizers and rapid urbanization all over the world (Le et al., 2009). The eutrophication causes serious problem for environment and society (e.g., mortality of fishes, crop damage and foul smelling). Governments legislated laws to control the deteriorating situation such as Law Concerning Special Measures for Improving Riverhead Areas (1973), Ibaraki Prefectural Eutrophication Prevention Act (1981), and Law Concerning Special Measured for Preserving Lake Water Quality (1984) (NIES, 2016). In addition, regular in-situ measurements have been established to monitor water quality in lake and coastal areas. For example, the National Institute for Environmental Studies (NIES) and the Ministry Of Land Infrastructure Transport And Tourism (MLIT) collecting monthly water quality parameters from Lake Kasumigaura, whereas the Chiba Prefectural Government preforming monthly in-situ measurements in Tokyo Bay.

1.2. Ocean color sensors

In-situ measurements and remote sensing are two alternative techniques to assess water quality. Although the in-situ measurements provide accurate values for sampling sites, they are time consuming and they do not provide the spatial distribution of the water constituents over the water body (Tyler et al., 2016). In contrast, the remote sensing has been considered as a valuable tool to monitor water bodies. Ocean color satellites have provided synoptic observation for oceans, coastal areas and inland water bodies (Bresciani et al., 2011). Coastal Zone Color Scanner (CZCS) was the first ocean color satellite which enables ocean community to map the spatial distribution of ocean properties (Shi et al., 2014), such as the diffuse attenuation coefficient (Austin and Petzold, 1981) and chlorophyll-a (Chla) concentration

(Yoder et al., 1987). After a gap of 10 years from the end of CZCS mission, the Sea-viewing Wide Field-of-view Sensor (SeaWiFS) was launched in 1997, since then, continuous monitoring of water bodies is achieved through many satellite (IOCCG, 2014, 2006). Most of these satellites provided multispectral data with reasonable spatial and temporal resolution (IOCCG, 2010), and it is freely available (Kutser, 2004; Majozi et al., 2014). Monitoring of Chla concentration in Case 1 waters using satellite sensors has been established, due to the fact that the phytoplankton is governing the optical properties (Matsushita et al., 2012; Mishra and Mishra, 2012). Monitoring water quality in Case 2 waters is a challenging problem due to the complex interaction among three constituents (chlorophyll-a (Chla), non-algal particles (NAP), and colored dissolved organic matter (CDOM)) properties (Binding et al., 2011) as shown in Fig. 1.1.

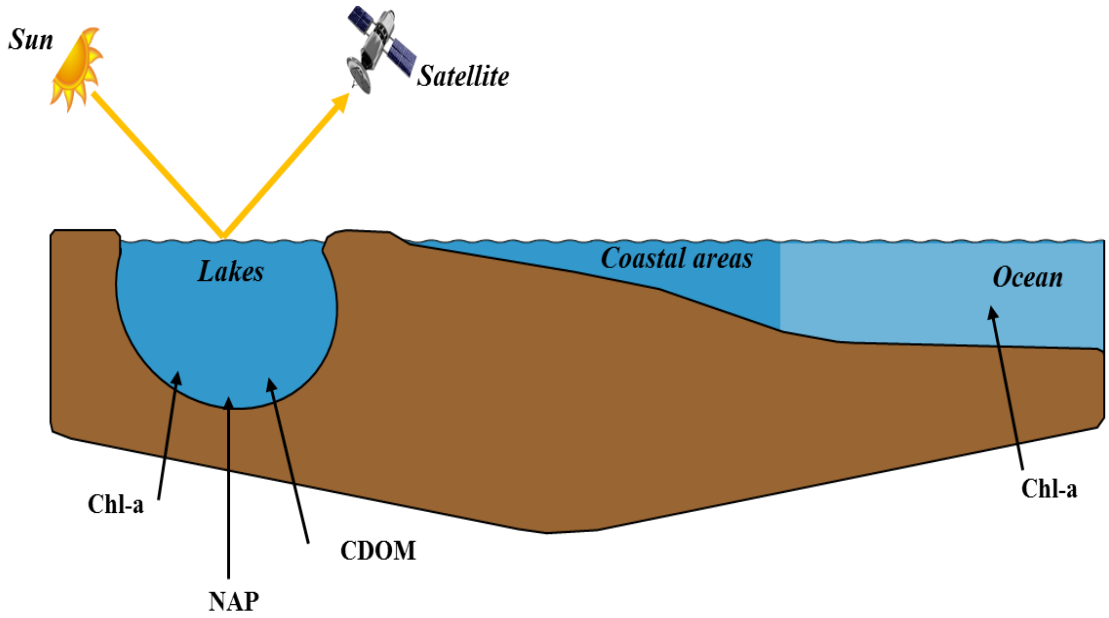

Fig. 1.1. Schematic diagram of ocean color satellite for Case 1 and Case 2 waters.

1.3. Purpose of this study

Japanese lakes and coastal areas suffer from major problems, for example, Tokyo bay suffers from the blue tide due to the depletion of dissolved oxygen and presence of sulfur, while Seto-Inland Sea affected by an excessive harmful bloom of dinoflagellate (i.e., red tide). These problems revealing the importance of accurate monitoring for Japanese lakes and coastal areas using satellites. The reflected sunlight from water bodies that recorded by satellite sensors provides the information of Chla, NAP and CDOM existing in water column. The retrieval of these constituents' concentration from remote sensing reflectance still a challenging task. A lot

of effort has been made to overcome that complexity, resulting in several approaches have been proposed, including bands ratio algorithms (Gons, 1999; HAN et al., 1994; Oki and Yasuoka, 2002, 1996), semi-analytical algorithms (Dall'Olmo et al., 2003; Le et al., 2009; Lyu et al., 2015), semi-analytical inversion/optimization approach (Brando et al., 2009; Hedley et al., 2009; Klonowski et al., 2007; Lee et al., 1999), spectrum matching and look-up tables (Louchard et al., 2002; Mobley et al., 2005), and neural network (NN) (Baruah et al., 2001; Doerffer and Helmut, 2000; Doerffer and Schiller, 2007). However, there is no accurate continuous monitoring for those optically complex waters. Accordingly, this dissertation aims to achieve the following goals; 1) evaluating the current algorithms to address the strength and limitations of these algorithms; 2) develop a new technique for Chla retrieval based on algorithms' indices and look-up table; and 3) evaluate the performance of proposed technique in different water bodies. In order to achieve the proposed goals, three kind of data are required, which are satellite data, in-situ measurements, and simulated water-leaving reflectance. The simulated dataset is required because of the limitation of in-site measurements as recently reported by many researchers such as (Zhang et al., 2015).

1.4. Dissertation outline

Chapter 2 describes the selected sites for field campaigns, and the in-situ and laboratory measurements to colleting the inherent optical properties (e.g., absorption and backscattering coefficients) and apparent optical properties (e.g., the remote sensing reflectance). In addition, the description of the bio-optical model to generate simulated reflectance is also provided.

Chapter 3 illustrate an intercomparison of seven Chla retrieval processors developed for MERIS sensor. These processors represent the neural network and band height technique. The seven processors are evaluated using MERIS achieve data during 2002 – 2012.

Chapter 4 represents an extensive evaluation of 43 algorithms' combinations to understand the strength and limitation of these algorithms under different conditions such as changing the optimal band and regression approaches. In-situ measurements and simulated reflectance were used to conduct the evaluation.

Chapter 5 provides a description and validation of the Multi-Algorithm Indices and Look-Up Table (MAIN-LUT) technique. The MAIN-LUT is a novel technique that combine the spectral matching technique with the existing semi-analytical algorithms to provide high chlorophyll-a retrieval accuracy over turbid lakes and coastal areas. The MAIN-LUT technique was validated using in-situ and satellite datasets.

CHAPTER 2

Material and methods

2.1. Observation sites

In-situ measurements are very important task to provide ground truth data to validate theoretical techniques. During this study, there were two criteria to select field observation sites; these sites should 1) represent coastal and inland water bodies; and 2) cover various water properties. Thus, Tokyo Bay and Lake Kasumigaura were selected (Fig. 2.1). Tokyo Bay (35 ° 25′ N; 139° 47′ E) is located in the center of Japan. Many rivers flow into the northern and western sides of the bay. Tokyo Bay has a surface area of 1500 km^2, with a mean and maximum water depth of 40 and 70 m, respectively. Lake Kasumigaura (36° 2' 57" N; 140° 22' 45"E), which is the second largest lake in Japan after Biwa Lake, is located approximately 70 km north of Tokyo Bay (Fig. 2.1). Lake kasumigaura is consider as a shallow water body with 4 m average depth and surface area of 220 km^2. A total of 56 rivers flows into the lake causing rapid deterioration of water quality (HIGANO and SAWADA, 1995). Table 2.1 summarizes the sampling points' coordinates of Tokyo Bay and Lake Kasumigaura.

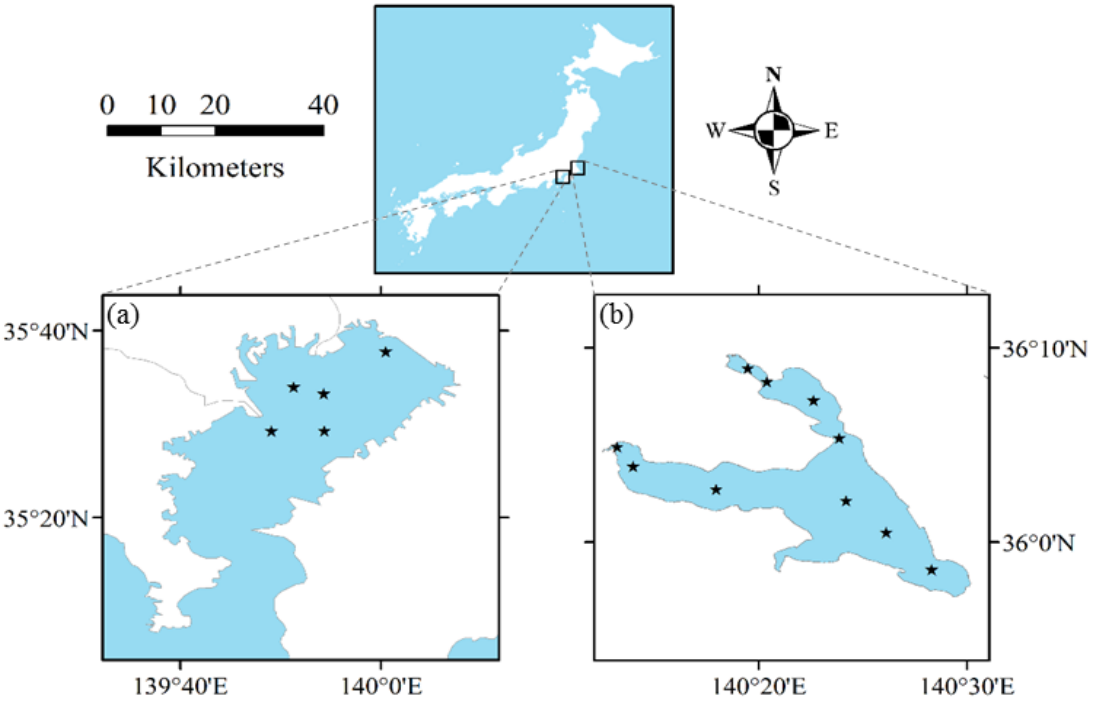

Fig. 2.1. Location of the sampling sites. (a) Tokyo Bay; and (b) Lake Kasumigaura.

Table 2.1 Coordinates of sampling point at Tokyo Bay and Lake Kasumigaura.

Station name	Latitude	Longitude
Tokyo Bay		
St. 8	35° 33' 16"	139° 54' 20"
St. 13	35° 29' 18"	139° 54' 24"
St. 97	35° 29' 16"	139° 49' 07"
St. 98	35° 33' 59"	139° 51' 21"
St. 99	35° 37' 45"	140° 00' 31"
Lake Kasumigaura		
St. 1	36° 08' 57"	140° 19' 30"
St. 2	36° 08' 15"	140° 20' 25"
St. 3	36° 07' 18"	140° 22' 39"
St. 4	36° 05' 21"	140° 23' 54"
St. 6	36° 04' 55"	140° 13' 13"
St. 7	36° 03' 54"	140° 14' 00"
St. 8	36° 20' 43"	140° 17' 58"
St. 9	36° 02' 09"	140° 24' 13"
St. 11	36° 00' 30"	140° 26' 09"
St. 12	35° 58' 36"	140° 28' 20"

2.2. In-situ and laboratory measurements

Water samples were collected during field campaigns at a depth of 0.5 m below the surface between 09:00 and 14:00 JST. Sixteen field campaigns were conducted in Tokyo Bay from June 2010 to August 2013 (71 stations), whereas eight field campaigns were performed in 2016 between February and November at Lake Kasumigaura (68 stations). Furthermore, water quality parameters were also collected monthly since 1977 by the National Institute for Environmental Studies (NIES, 2016). These monthly campaigns of NIES were compared with acquired MEdium Resolution Imaging Spectrometer (MERIS) sensor during 2002–2012 to extracted matched dates, resulting in 77 stations.

Chla concentrations were measured fluorometrically using a Turner Designs 10-AU fluorometer. Water samples of 20 ml were filtered onto 25 mm Whatman GF/F filters with 0.7 µm pore size. The filter was immediately soaked in a 6 ml of N,N-dimethylformamide (DMF) to extract the pigments and then stored in dark at 4°C for 4 hours (Suzuki and Ishimaru, 1990). Total suspended solids (TSS) were determined gravimetrically by filtering 300 ml of water samples through a pre-combusted Whatman GF/F filter (550 °C for 4 hrs). The filter with retained material was dried at 105 °C for 2 hrs and weighted for TSS, and then the filter was re-combusted again for 4 hrs at 550 °C to obtain inorganic suspended solids (ISS). Organic suspended solids (OSS) were estimated by subtraction ISS from TSS (American Public Health

Association., 2005). Table 2.2 summarized the basic characteristics of collected data, revealing that Lake Kasumigaura is a highly turbid water body comparing with Tokyo Bay.

Table 2.2 Descriptive statistics of the water quality parameters for Tokyo Bay, and Lake Kasumigaura. ***Tokyo Bay with IOPs*** dataset refers to stations where additional measurements of absorption and backscattering properties were performed along with remote sensing reflectance measurements. Lake kasumigaura *Dataset 1* and *Dataset 2* represent measurements collected in 2016 and during 2002 – 2012, respectively.

	Min	Max	Mean	Median	SD	RSD (%)
Tokyo Bay (N = 71)						
Chla (mg m^{-3})	0.76	102.07	25.14	13.94	25.85	102.82
TSS (g m^{-3})	2.99	26.29	8.29	7.99	0.49	5.87
Tokyo Bay with IOPs (N = 12)						
Chla (mg m^{-3})	2.9	42.6	18.31	11.85	14.99	81.87
TSS (g m^{-3})	2.99	9.86	6.34	6.81	2.24	35.38
ISS (g m^{-3})	0.81	6.13	2.96	2.22	1.63	55.24
OSS (g m^{-3})	0.96	7.16	3.39	2.9	1.75	51.63
$a_{ph}(440)$ (m^{-1})	0.23	1.03	0.65	0.6	0.27	41.3
$a_{NAP}(440)$ (m^{-1})	0.14	0.34	0.22	0.21	0.07	31.75
$a_{CDOM}(440)$ (m^{-1})	0.06	0.47	0.25	0.19	0.14	56.23
$b_{b,p}(442)$ (m^{-1})	0.01	0.04	0.02	0.03	0.01	41.16
Lake Kasumigaura (Dataset 1) (N = 68)						
Chla (mg m^{-3})	13.16	152.14	55.86	48.16	26.59	47.60
TSS (g m^{-3})	9.40	57.10	21.71	18.25	9.44	43.50
Lake Kasumigaura* (Dataset 2) (N = 77)						
Chla (mg m^{-3})	8.10	179.40	65.98	59.90	35.90	54.42
TSS (g m^{-3})	10.70	59.10	25.00	23.67	10.14	40.56

* Data was collected by the National Institute for Environmental Studies (NIES).
TSS, ISS and OSS stand for total, inorganic and organic suspended solids, respectively; $a_{ph}(440)$, $a_{NAP}(440)$ and a_{CDOM} (440) represent the measured absorption coefficients for phytoplankton, NAP and CDOM at 440-nm band, respectively; $b_{b,p}$ (442) denotes the measured backscattering at 442-nm band; *N* represents the number of samples; SD stands for standard deviation; and RSD denotes relative standard deviation = (SD / Mean × 100).

2.3. Remote sensing reflectance

Hyperspectral remote reflectance data for water surface were measured using Fieldspec HandHeld 2 Spectroradiometer in the spectrum range from 350 to 1075 nm with spectral resolution 1.0 nm. The instrument was manually held about one meter over the water surface with a viewing angle (θ_v) of 45° from the nadir and the azimuth angle (ϕ_v) of 135° from the projected plane of the sun's rays reflected (Fig. 2.2) to measure the Total radiance from both water and sky (L_{sw}) (Le et al., 2009). The radiance from white panel was measured immediately after measuring water leaving radiance with same viewing and

azimuth angles. The Handheld 2 then rotating 40° toward the sky to collect the sky radiance (L_{sky}). The described position will minimize the effects of sun glint, non-uniform sky radiance and overcome the instrument's shading problem (Mobley, 1999). The instrument was adjusted to take 15 scans to calculate the average value for a single radiance. For increasing the accuracy of the measurements, the three radiances (L_{sw}, L_{sky}, and $\mathrm{L_p}$) were repeated 5 times at each sampling point and these values were averaged to calculate remote sensing reflectance (Rrs) as:

$$R_{rs} = \frac{L_W}{E_d} = \frac{(L_{\mathrm{sw}} - rL_{sky})}{\pi \mathrm{L_p} / \rho_p} \quad (\mathbf{2.1})$$

where L_W is the water-leaving radiance, E_d denotes for downwelling Irradiance above water surface, r and ρp stand for skylight reflectance at air-water interface and white reference panel irradiance reflectance, respectively. Fig. 2.3 illustrates the remote sensing reflectance spectra collected at Tokyo Bay and Lake Kasumigaura. The red reflectance spectra shown in Fig. 2.3b represent 12 stations of Tokyo Bay where additional inherent optical measurements (i.e., Absorption and backscattering coefficients) were measured.

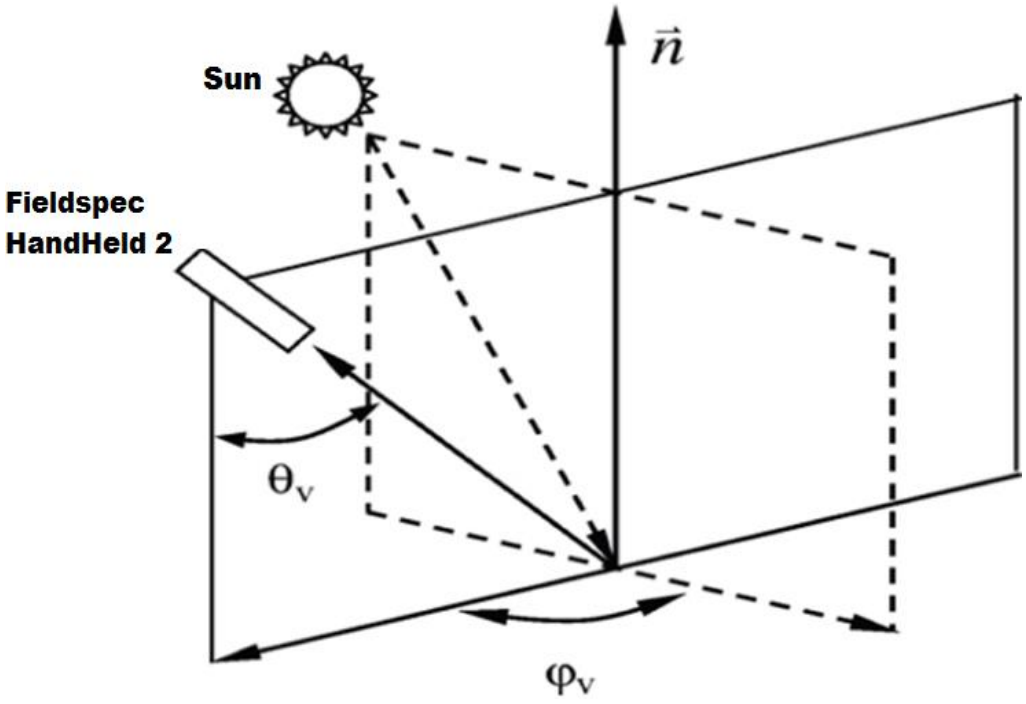

Fig. 2.2. Schematic diagram for measuring remote sensing reflectance using HandHeld 2.

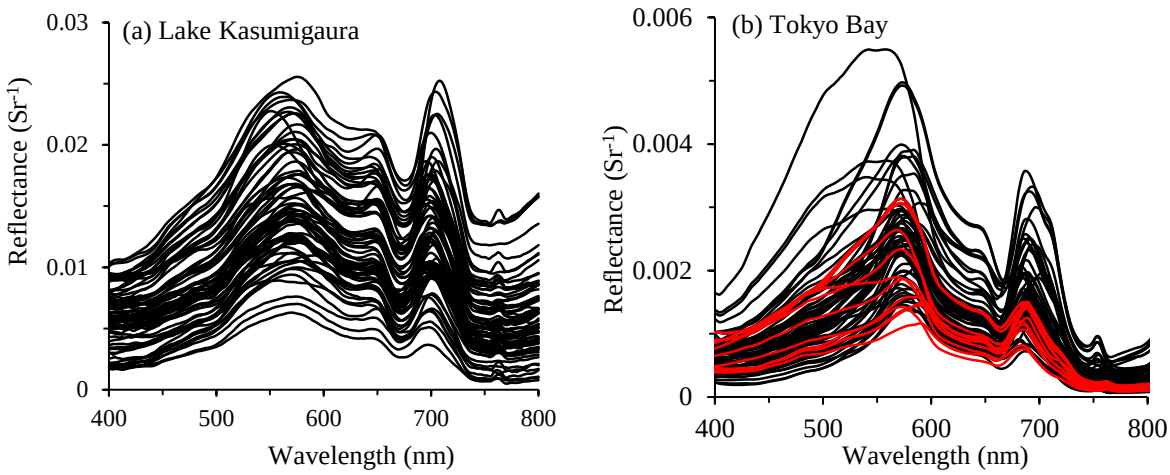

Fig. 2.3. Remote sensing reflectance collected from Lake Kasumigaura and Tokyo Bay. The red lines highlighted the 12 stations of Tokyo Bay that had additional measurements of absorption and backscattering properties along with remote sensing reflectance measurements.

2.4. Measurement of CDOM absorption coefficient

The absorption of CDOM (a_{CDOM}) is measured relative to ultrapure water (Milli-Q water). Water sample must be protected from photo-degradation during preparation and measurements. Thus, Mitchell et al. (2002) recommended Clear borosilicate Qorpak bottle than the Amber borosilicate Qorpak bottle with a volume of 250 ml to keep water sampling. The sampling bottles for CDOM measurements were stored under refrigeration between 4°C to 8°C till measurements in laboratory. The samples were warn to chamber temperature and filtered under 100 mmHg vacuum pressure through 0.2 mm Whatman Nuclepore (polycarbonate) filters. The UV/NIR spectrophotometer (V-550, Jasco) (Fig. 2.4) with two cuvette tubes were used to measure the CDOM absorption coefficient. The UV/NIR spectrophotometer should be warm for 30 minutes before the measurements. Firstly, the two tubes were filled with Milli-Q water and placed in the sample roam of the spectrophotometer to measure the optical density of blank ($OD_0(\lambda)$). Replace the MILLI-Q water from one tube with the sample water and place in the sampling chamber to measure the optical density of water sample ($OD_S(\lambda)$). The CDOM absorption coefficients of water sample was calculated as:

$$a_{CDOM}(\lambda) = \frac{\ln(10)}{l} * [OD_S(\lambda) - OD_{Null}] \quad (2.2)$$

where $a_{CDOM}(\lambda)$ refers to the absorption coefficient of CDOM; l represents the cuvette path length (0.1 m); and OD_{Null} stands for average optical density of the sample from 780 to 800 nm for the null point correction, because theoretically the values of aCDOM should be zero form 750 nm and toward longer wavelengths.

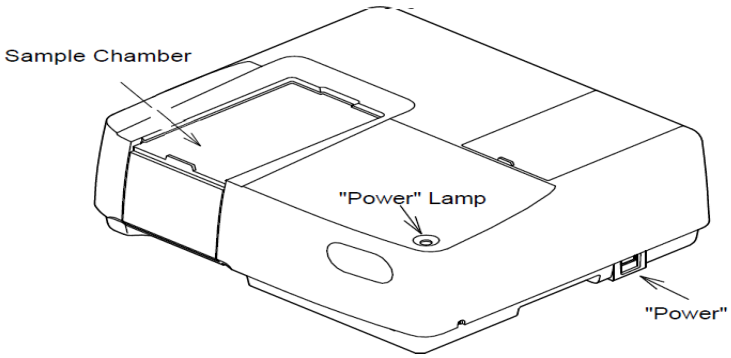

Fig. 2.4. Schematic of UV/NIR spectrophotometer (V-550, Jasco).

2.5. Measurement of non-algal particles and Phytoplankton absorption coefficients

The absorption of particles (a_P) and non-algal particles (NAP) (a_{NAP}) were measured relative to blank clean filter moistened with filtered seawater that filtered using 0.2 µm Whatman GF/F filter. Filtration and measurements should be executed in a dim light to minimize phot-degradation of the samples. Water samples were filtered through 0.7 µm Whatman GF/F filters under low vacuum pressure (100 mm Hg). Water volume (i.e., typically 0.5 L to 5.0 litres) were determined to maintain the optical density of the particles ($OD_P(\lambda)$) less than 0.4 (Zhang et al., 2009). Two blank GF/F filters were prepared by soaking them in 25 ml of 0.2 µm filtered seawater. After warming the spectrophotometer, the two moistened blank GF/F filters were placed in the sampling chamber of the spectrophotometer to measure the optical density of blank. The diameter of biomass retained over the filter (D_f) was measured with Vernier callipers and then replaced one of the blank GF/F filters located in the sampling chamber to measure the optical density of the particle sample ($OD_P(\lambda)$). The protocol of (Hirawake et al., 2001) was employed to calculate the absorption coefficients as:

$$OD_{SP}(\lambda) = 0.392 * OD_P(\lambda) + 0.655 * [OD_P(\lambda)]^2 \quad (\mathbf{2.3})$$

$$a_P(\lambda) = \frac{\ln(10) * A}{V_f} OD_{SP}(\lambda) \quad (\mathbf{2.4})$$

where $a_P(\lambda)$ refers to the absorption coefficient of particles; $OD_{SP}(\lambda)$ represents the corrected particle optical density; and V_f denotes filtered sample volume (m^3), and A represents the area of particulate matters held over the filter, which was calculated from diameter of biomass retained over the filter (D_f) as

$$A = \frac{\pi {D_f}^2}{4} \quad (\mathbf{2.5})$$

In order to remove pigments from the particles retained of the filter that used to measure $a_P(\lambda)$, the methanol was used as proposed by Kishino et al. (1985). The filter with the retained particles was soaked in 20 ml of 95% methanol and 5% Milli-Q water for 1.0 hour, then filter these 20 ml using low vacuum pressure (100 mm Hg). The de-pigmented filter was rescanned with the spectrophotometer using same protocol described for particles to measure the optical density of NAP. Pigment extraction is complete when the 675-nm chlorophyll a absorption peak is not present in measured spectrum, or the filter should be soaked again in methanol for addition 1.0 hour. The absorption coefficient of non-algal particles $\left(a_{NAP}(\lambda)\right)$ was calculated as:

$$OD_{Sd}(\lambda) = 0.392 * OD_d(\lambda) + 0.655 * [OD_d(\lambda)]^2 \quad (\mathbf{2.6})$$

$$a_{NAP}(\lambda) = \frac{\ln(10) * A}{V_f} OD_{Sd}(\lambda) \quad (\mathbf{2.7})$$

where $a_{NAP}(\lambda)$ represents the absorption coefficient of NAP; $OD_d(\lambda)$ and $OD_{Sd}(\lambda)$ denote the measured and corrected optical density of NAP. The phytoplankton absorption coefficients $\left(a_{Ph}(\lambda)\right)$ was calculated as

$$a_{Ph}(\lambda) = a_P(\lambda) - a_{NAP}(\lambda) \quad (\mathbf{2.8})$$

2.6. Measurement of non-algal particles and Phytoplankton absorption coefficients

The Vertical profiles of the total backscattering coefficients $(b_b(\lambda))$ were measured at the six wavelengths (420, 442, 488, 510, 550 and 676 nm) with a HydroScat-6 (HOBI Labs). The backscattering coefficients for particles $(b_{bp}(\lambda))$ were estimated by subtraction the backscattering of pure water (Dall'Olmo and Gitelson, 2006; Morel, 1974) from $b_b(\lambda)$ (Mélin et al., 2011).

2.7. Bio-optical model

Gordon et al. (1988) fitted the remote sensing reflectance just beneath the water surface, $r_{rs}(\lambda)$, with a polynomial function of inherent optical properties (IOPs), which can be simplified as

$$r_{rs}(\lambda) = \frac{f}{Q} * \left(\frac{b_b(\lambda)}{a(\lambda) + b_b(\lambda)} \right) \quad (\mathbf{2.9})$$

where $a(\lambda)$ and $b_b(\lambda)$ are the total absorption and total backscattering coefficients, respectively (all symbols are defined in Table 2.3); f is the light field factor; and Q denotes the light distribution factor. Kirk (1984) found that f is a function of the solar altitude, which is expressed as a linear function of the cosine of the zenith angle of the refracted photons μ_o:

$$f = 0.975 - 0.629\ \mu_o \quad \textbf{(2.10)}$$

The average value of f/Q (0.09) was determined by using the bio-optical model in stations that have both measured Rrs and IOPs in Tokyo Bay, which is consistent with that in Mishra et al. (2012). Both $a(\lambda)$ and $b_b(\lambda)$ are the sum of the contributions of pure water and optically active components in the water, which include three constituents: phytoplankton, non-algal particles and colored dissolved organic matter. The total absorption $a(\lambda)$ is expressed as

$$a(\lambda) = a_w(\lambda) + a_{ph}(\lambda) + a_{NAP}(\lambda) + a_{CDOM}(\lambda) \quad \textbf{(2.11)}$$

where $a_w(\lambda)$ is the absorption coefficient of pure water (Buiteveld et al., 1994); and $a_{ph}(\lambda)$, $a_{NAP}(\lambda)$, and $a_{CDOM}(\lambda)$ are the absorption coefficients for phytoplankton, NAP, and CDOM, respectively. The total backscattering coefficient $b_b(\lambda)$ can be described as

$$b_b(\lambda) = b_{b,w}(\lambda) + b_{b,p}(\lambda) \quad \textbf{(2.12)}$$

where $b_{b,w}(\lambda)$ is the backscattering coefficient of pure water (Dall'Olmo and Gitelson, 2006; Morel, 1974) and $b_{b,p}(\lambda)$ is the backscattering coefficient of particles. The radiance just above the surface was related to the radiance just below the surface by a factor of 0.544 (Austin, 1980). Therefore, the remote sensing reflectance just above the water surface, $R_{rs}(\lambda)$, can be calculated as

$$R_{rs}(\lambda) = 0.544 * \frac{f}{Q} * \left(\frac{b_b(\lambda)}{a(\lambda) + b_b(\lambda)} \right) \quad \textbf{(2.13)}$$

Table 2.3 Symbols and definitions

Symbol	Description	Units
[Chla]	Chlorophyll-a concentration	mg m^{-3}
[NAP]	Non-algal particle concentration	g m^{-3}
[CDOM]	Colored dissolved organic matter absorption at 440 nm	m^{-1}
$a_w(\lambda)$	Absorption coefficient of pure water	m^{-1}
$a_{ph}(\lambda)$	Absorption coefficient of phytoplankton	m^{-1}
$a_{NAP}(\lambda)$	Absorption coefficient of NAP	m^{-1}
$a_{CDOM}(\lambda)$	Absorption coefficient of CDOM	m^{-1}
$a(\lambda)$	Total absorption coefficient (= $a_w(\lambda) + a_{ph}(\lambda) + a_{NAP}(\lambda) + a_{CDOM}(\lambda)$)	m^{-1}
$b_{b,w}(\lambda)$	Backscattering coefficients of pure water	m^{-1}
$b_{b,p}(\lambda)$	Backscattering coefficients of suspendedparticles	m^{-1}
$b_{b,ph}(\lambda)$	Backscattering coefficients of phytoplankton	m^{-1}
$b_{b,NAP}(\lambda)$	Backscattering coefficients of NAP	m^{-1}
$b_b(\lambda)$	Total backscattering coefficient (=$b_{b,w}(\lambda) + b_{b,ph}(\lambda) + b_{b,NAP}(\lambda)$)	m^{-1}
$R_{rs}(\lambda)$	Above-surface remote sensing reflectance	sr^{-1}
$r_{rs}(\lambda)$	Subsurface remote sensing reflectance	sr^{-1}

2.8. Simulating the remote sensing reflectance

Numerous researchers proposed many models to generate simulated R_{rs} based on bio-optical models (Yang et al., 2013, 2011a; Zhu et al., 2014). The key variation between these models is the specific absorption and backscattering parameters (Kutser, 2004). The phytoplankton absorption, $a_{ph}(\lambda)$, and chlorophyll concentration, $[Chla]$, have a proportional relationship (Gilerson et al., 2007) that can be expressed as

$$a_{ph}(\lambda) = [Chla] * a^*_{ph}(\lambda) \quad (2.14)$$

where $a^*_{ph}(\lambda)$ refers to the specific absorption of phytoplankton. The specific IOPs for phytoplankton, NAP, and CDOM were computed by averaging their values for the 12 stations at Tokyo Bay. The absorption spectra of both NAP and CDOM had an exponential decay distribution with increasing wavelength and could be determined from their reference values at 440 nm as follows:

$$a_{NAP}(\lambda) = [NAP] * a^*_{Ph}(\lambda) = [NAP] * a^*_{NAP}(440) * e^{(-S_{NAP}(\lambda - 440))} \quad (2.15)$$

$$a_{CDOM}(\lambda) = [CDOM] * a^*_{CDOM}(\lambda) = [CDOM] * a^*_{CDOM}(440) * e^{(-S_{CDOM}(\lambda - 440))} \quad (2.16)$$

where $[NAP]$ is the concentration of NAP; $[CDOM]$ refers to the CDOM absorption at 440 nm; $a^*_{NAP}(\lambda)$ and $a^*_{CDOM}(\lambda)$ are the specific absorption of NAP and CDOM at any wavelength, respectively; $a^*_{NAP}(440)$ and $a^*_{CDOM}(440)$ stand for the specific absorption of NAP and CDOM at 440 nm, respectively; and S_{NAP} and S_{CDOM} represent the decay slope coefficients of NAP and CDOM, respectively.

The backscattering coefficient of particles, $b_{b,p}(\lambda)$, at different wavelengths was estimated by fitting the measured backscattering at the six wavelengths with an exponential function:

$$b_{b,p}(\lambda) = b_{b,p}(\lambda_o)\left(\frac{\lambda}{\lambda_o}\right)^{-n} \quad (\mathbf{2.17})$$

where n stands for the spectral slope of $b_{b,p}(\lambda)$; $b_{b,p}(\lambda_o)$ refers to the backscattering at the reference band (λ_o); and λ_o was assigned to 550 nm. The segregation of $b_{b,p}(\lambda)$ into the backscattering of phytoplankton $(b_{b,ph}(\lambda))$ and non-algal particles $(b_{b,NAP}(\lambda))$ was based on the assumption that their contributions to $b_{b,p}(\lambda)$ were proportionally correlated to their concentrations (Yang et al., 2011a). Separating NAP from the TSS with laboratory analysis is impossible (Oyama et al., 2009), so the approach of Gons et al. (Gons et al., 1992) was employed to divide the TSS into NAP and phytoplankton suspended solids (PSS). First, a linear regression model was created between Chla and OSS at 70 stations of Tokyo Bay. This relationship showed that the 1.0 mg m^{-3} Chla concentration approximately equaled 0.0687 g m^{-3} TSS. Therefore, the NAP concentration was calculated by subtracting the PSS (= 0.0687*Chla) from the TSS. Fig. 2.5 demonstrates the average specific inherent optical properties (SIOPs) measured in Tokyo Bay. Whereas, the specific phytoplankton absorption used for the wide range scenario was taken from Ciotti (Ciotti et al., 2002) with different weighting factors (Sf) range for microplankton and picoplankton as shown in Fig. 2.6.

The contribution of chlorophyll fluorescence emission to the remote sensing reflectance was simulated by Gilerson et al. (2007) for Case 2 waters. The fluorescence spectral distribution follows a Gaussian shape with a peak at 685 nm, a full-width half maximum of 25 nm and a standard deviation (σ) of 10.6 nm (Gower et al., 1999). Thus, the chlorophyll fluorescence emission reflectance $R_{rs,fl}(\lambda)$ was modeled as

$$R_{rs,fl}(\lambda)=\frac{fl(685)}{1000*E_d(685)}*\exp\left[-0.5*\left(\frac{\lambda-685}{\sigma}\right)^2\right] \quad (\mathbf{2.18})$$

where $E_d(685)$ refers to the downwelling irradiance just above the water surface at 685 nm with a value of 1.1 W m^{-2} nm^{-1} under clear sky conditions, and $fl(685)$ is the chlorophyll fluorescence at 685 nm, which was calculated as

$$fl(685)=\frac{0.0375\,[Chla]}{1+0.32\,a_{CDOM}(440)+0.01\,[NAP]+0.032\,[Chla]} \quad (\mathbf{2.19})$$

The total reflectance was calculated as the sum of the reflectance that was estimated in Eqs. (**2.13**) and (**2.18**) (Mishra and Mishra, 2012). Table 2.4 summarize the IOPs values that used for local and wide range simulated reflectance scenarios.

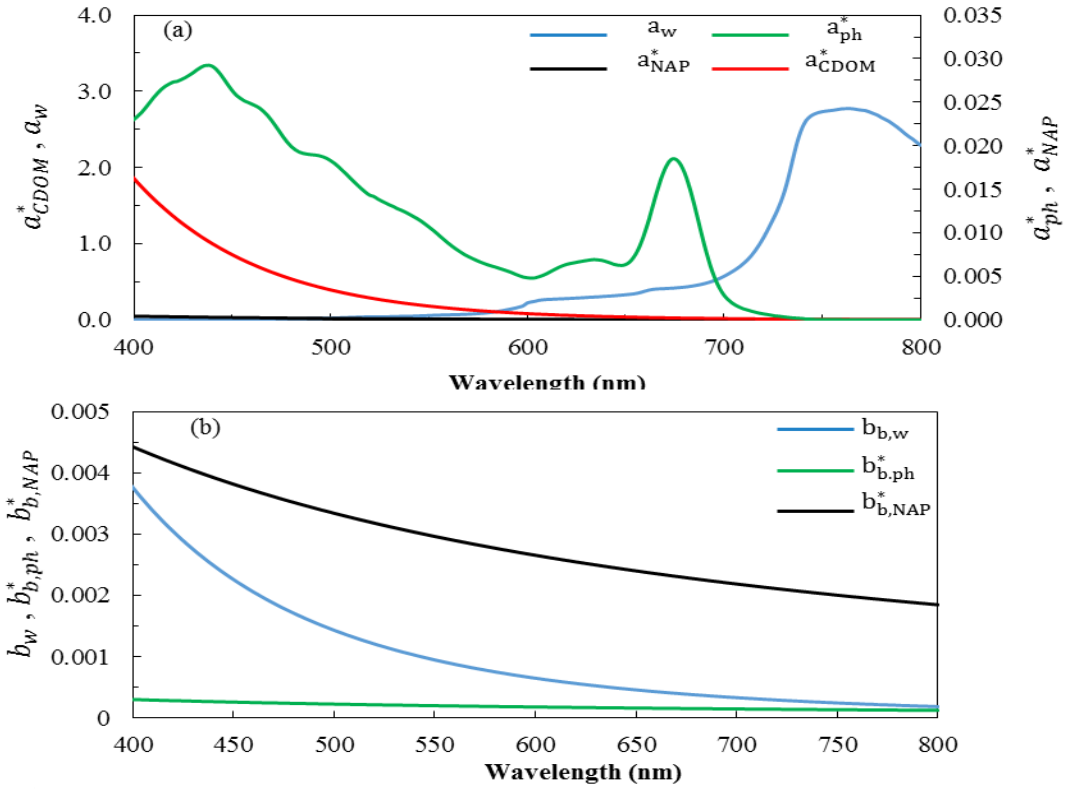

Fig. 2.5. Average specific inherent optical properties of Tokyo Bay. (a) a^*_{Ph} [m^2 mg^{-1}], a^*_{NAP} [m^2 g^{-1}], and a^*_{CDOM} [dimensionless] are the specific absorption coefficients of phytoplankton, NAP, and CDOM, respectively; and a_w [m^{-1}] refers to the absorption coefficient of pure water. (b) $b^*_{b,Ph}$ [m^2 mg^{-1}] and $b^*_{b,NAP}$ [m^2 g^{-1}] are the specific backscattering coefficients of phytoplankton and NAP, respectively; and $b_{b,w}$ [m^{-1}] denotes the backscattering coefficient of pure water.

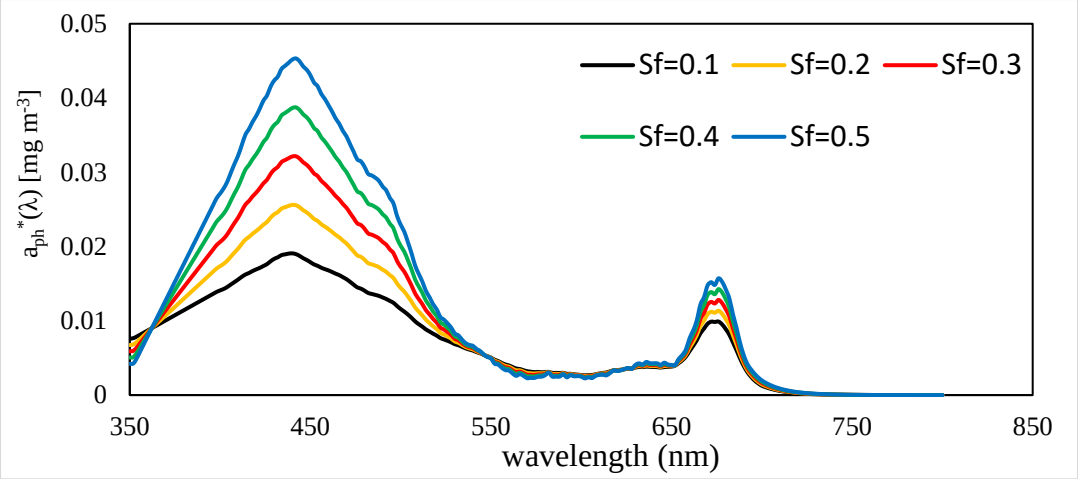

Fig. 2.6. Specific phytoplankton absorption used to generate simulated reflectance. Solid lines characterize specific phytoplankton absorption from Ciotti (Ciotti et al., 2002) based on different weighting factors (S_f) for microplankton and picoplankton. Dashed red line represents the specific phytoplankton absorption from Tokyo bay.

Table 2.4 Values of Specific inherent optical properties (SIOPs) used in the bio-optical model to generate simulated reflectance for local parameterization and wide range scenarios.

SIOPs	Local Parameterization*	Wide range**
$a^*_{NAP}(440)$ m^2 g^{-1}	0.03483	0.02 - 0.1
$a^*_{CDOM}(440)$	1.0	1.0
$b^*_{b,ph}(550)$	0.000204	0.0001 - 0.002
$b^*_{b,NAP}(550)$	0.00296	0.001 - 0.02
S_{NAP}	0.00899	0.007 - 0.015
S_{CDOM}	0.01547	0.01 - 0.02
n	1.25848	0.5 - 2.2

* based on Tokyo bay in-situ measurements.
** based on IOCCG database (2006) (IOCCG, 2006)

2.9. Accuracy assessment

The algorithms' performance was evaluated based on two indices: the root mean square error (RMSE) and the mean absolute relative error (MARE). These indices are defined as

$$RMSE = \sqrt{\frac{\sum_{i=1}^{N}\left(X_{i,input} - X_{i,retr}\right)^2}{N}} \qquad (\mathbf{2.20})$$

$$MARE = \frac{1}{N} * \sum_{i=1}^{N} \frac{\left| \left(X_{i,input} - X_{i,retr} \right) \right|}{X_{i,input}} * 100 \quad (\mathbf{2.21})$$

where $X_{i,input}$ and $X_{i,retr}$ denote the input (i.e., measured or reference concentrations) and retrieved Chla concentrations, respectively; and N is the total number of samples. The log-based error ($Error_{\log}$) was used as proposed by Zhu et al. (2014) to investigate the error of the Chla concentration.

$$Error_{\log} = \log_{10}\left(X_{i,input}\right) - \log_{10}\left(X_{i,retr}\right) \quad (\mathbf{2.22})$$

CHAPTER 3

Evaluation of MERIS band height and neural network processors

3.1. Introduction

Water constituents' concentrations significantly fluctuate over a short time period which requires continuous monitoring of water bodies (Gokul et al., 2014). Unlike the in-situ campaigns that provide point measurements, the remote sensing technique can detect the spatial and temporal variation in water bodies (Dall'Olmo and Gitelson, 2006; Oyama et al., 2009; Su et al., 2014). Water leaving reflectance, particularly in the visible and near infrared (NIR) spectrum, provides quantitative and qualitative information on the water constituents (Le et al., 2011). In clear waters, the optical properties are mainly governed by phytoplankton and the blue and green region of spectrum are commonly used to retrieve chlorophyll-a (Chla), which is the main pigment of phytoplankton (Gholizadeh et al., 2016; Gordon and Morel, 1983). The chla retrieval in turbid waters shifted from the blue and green to the red and NIR spectral region to avoid high absorption of colored dissolved organic matter (CDOM) and non-algal particles (NAP) (Dekker, 1993; Gons, 1999; Oki and Yasuoka, 1996).

Monitoring water quality of ocean from space started in 1978 using Coastal Zone Color Scanner (CZCS) sensor (Austin and Petzold, 1981; Gordon et al., 1988; Matsushita et al., 2016; Yoder et al., 1987). Since then, several ocean color sensors such as Sea-viewing Wide Field-of-view (SeaWiFS), Moderate Resolution Imaging Spectroradiometer (MODIS) and Medium Resolution Imaging Spectrometer (MERIS) were employed to monitor water quality in open ocean as well as inland lakes (IOCCG, 2000; Shi et al., 2014). MERIS sensor and its follow-up mission (i.e., Ocean and Land Colour Instrument sensor (OLCI)) contains some unique bands (i.e., 620- and 709-nm band) that were not incorporated in other ocean color sensors (Majozi et al., 2014; Matsushita et al., 2016; Ylöstalo et al., 2014). Kutser et al. (2006) demonstrated the importance of 620-nm band to distinguish the cyanobacterial blooms from other algae blooms; whereas the floating brown algae (i.e., *Sargassum*) was firstly detecting from space using 709-nm band (Gower et al., 2008a).

Several algorithms based on band height were developed for MERIS sensor, namely, the fluorescence line height (FLH) (Gower et al., 1999), maximum chlorophyll index (MCI) (Gower et al., 2008b, 2005) and maximum peak height (MPH) (Matthews et al., 2012). Regression approach (e.g., linear) is required to establish a relation between Chla indices (i.e., FLH and MCI) and measured Chla. The derived relations are limited to the characteristics of the incorporated dataset and are sensitive to seasonal or reginal variations (Matthews et al., 2010; Ylöstalo et al., 2014). Neural network can provide an alternative solution to overcome the complexity of turbid water bodies with the ability to include the physical information of remote sensing process (Baruah et al., 2001). Four algorithms based on neural network were developed for MERIS sensor to retrieve water leaving reflectance as well as water constituents'

concentrations from MERIS L1b data. The four algorithms are Eutrophic Lake (EUL) (Doerffer and Schiller, 2008), Boreal Lake (BOL) (Doerffer and Schiller, 2008), Case 2 Regional (C2R) (Doerffer and Schiller, 2007) and Free University of Berlin (FUB) (Schroeder et al., 2007). Numerous researches adopted the neural network algorithms to only perform atmospheric correction for MERIS L1B without performing an evaluation for the Chla produced from these algorithms (Bresciani et al., 2011; Jaelani et al., 2013; Majozi et al., 2014; Salem et al., 2017a; Shi et al., 2014).

Researchers compared the Chla retrieval accuracy of the above-mentioned algorithms over different lakes in Europe and Canada. Ruiz-Verdú et al. (2008) performed an evaluation for EUL, BOL and C2R using eleven lakes in Finland, Germany and Spain; whereas Odermatt et al. (2012) compared EUL, C2R and FUB for Greifensee Lake, Swiss. The algorithms compared during the two studies based on neural network and their results revealed that the EUL was the most accurate algorithms. The intercomparison between band height and neural network algorithms showed that the band height algorithms outperformed the neural network as reported by Binding et al. (2011) and Lankester et al. (2015).

No previous studies conducted an intercomparison of the seven algorithms. In addition, the upper limit of Chla concentrations during these studies was less than 70 mg m^{-3} (Binding et al., 2011; Odermatt et al., 2012; Stephanie C.J. Palmer et al., 2015), which does not represent highly turbid water bodies. Thus, this research evaluates the retrieval accuracy of seven Chla algorithms developed for MERIS sensor over a complex water body (i.e., Lake Kasumigaura) which is characterized by varying concentrations of Chla and total suspended matter (TSM). The evaluation is conducted over MERIS lifetime during 2002 - 2012. The aim of the current study is to investigate the performance of the seven algorithms over a wide range of Chl-a concentrations that covers broad trophic status (i.e., mesotrophic to hypertrophic) using 10-year of MERIS archive data.

3.2. In-situ measurements

Since 1977, the National Institute for Environmental Studies (NIES) has performed monthly measurements at ten sites (Fig. 3.1) within its periphery. These monthly in-situ measurements are continuously archived online and are available for free through the database of Lake Kasumigaura (NIES, 2016). The current study conducted a comprehensive evaluation of seven processors developed for the MEdium Resolution Imaging Spectrometer (MERIS) sensor. The corresponding water quality parameters during 2002 – 2012 (i.e., MERIS sensor lifetime) are summarized in Table 3.1. Chla ranged 6.80 − 223.50 mg m^{-3}, while TSM ranged 6.30 − 118.30 g m^{-3}. Chla concentrations revealed that the trophic status of Lake Kasumigaura varied from mesotrophic (i.e., Chla in ranges of 2.5 – 8.0 mg m^{-3}) to hypertrophic (i.e., Chla > 25 mg m^{-3}) (Vollenweider and Kerekes, 1982).

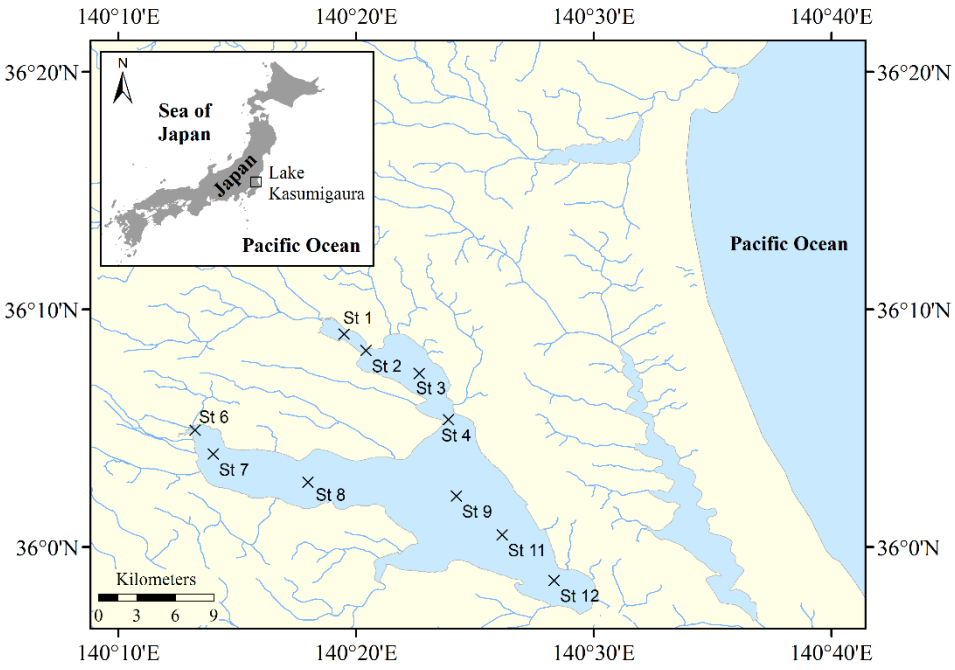

Fig. 3.1. Distribution of the sampling sites in Lake Kasumigaura as defined by the National Institute for Environmental Studies (NIES).

Table 3.1 Descriptive statistics of water quality parameters measured in Lake Kasumigaura. *Monthly campaign* refers to in-situ measurements that were performed every month from May 2002 to May 2012. *Same day* and *1-day difference* datasets represent in-situ measurements that synchronized the acquisition dates of Medium Resolution Imaging Spectrometer (MERIS) images on the same day or with a one-day difference, respectively.

	Min	Max	Mean	Median	SD
Monthly campaign (2002 - 2012) (n = 1210)					
Chla (mg m^{-3})	6.80	223.50	58.73	52.87	31.85
TSM (g m-3)	6.30	118.30	26.80	24.30	12.22
Same day (n = 39)					
Chla (mg m^{-3})	8.10	187.40	72.97	58.90	48.77
TSM (g m-3)	11.60	47.75	24.51	25.00	8.43
1-day difference (n = 73)					
Chla (mg m^{-3})	18.00	164.07	65.72	63.23	31.75
TSM (g m-3)	10.70	71.20	25.71	23.60	11.41

Chla and TSM stand for chlorophyll-a and total suspended matter concentrations; SD denotes standard deviation; and n represents the number of sampling points.

3.3. MERIS chlorophyll-a processors

The MERIS sensor onboard the European Environmental Satellite (ENVISAT) is an ocean color sensor designed to monitor changes in water quality of Case 1 waters (e.g., open ocean) and Case 2 waters (e.g., coastal areas). The mission of MERIS lasted for 10 years (i.e., May 2002 to May 2012). The MERIS sensor provides measurements of reflected sunlight at 15 bands in the spectral range of 412.5-900 nm and with narrow bandwidths (i.e., 3.75-, 7.5-, 10-, 15-, and 20-nm). The products of MERIS have two spatial resolutions: 300 m and 1200 m for the full-resolution (FR) and reduced resolution (RR), respectively. The MERIS sensor is

composed of five cameras sharing a large field of view (68.5°) and a swath of 1150 km with a temporal resolution of three days (Levrini and Delvart, 2011).

Seven algorithms were proposed to retrieve Chla concentrations or Chla-related products (i.e., indices that correlated with Chla concentrations) from MERIS data. Four out of the seven algorithms are based on neural network (NN) (i.e., Eutrophic Lake (EUL), Boreal Lake (BOL), Case 2 Regional (C2R), and Free University of Berlin (FUB)), whereas the other three algorithms rely on band height (i.e., Fluorescence Line Height (FLH), Maximum Chlorophyll Index (MCI), and Maximum Peak Height (MPH)). These algorithms are available as plug-in processors in BEAM V5.0 software (Envisat/Brockman Consult, Hamburg, Germany).

EUL, BOL, and C2R processors have the same structure as they consist of two NNs (i.e., inverse and forward NNs): the inverse NN to execute atmospheric correction and the forward NN to retrieve inherent optical properties (IOPs) and subsequently provide water constituents' concentrations (Doerffer and Schiller, 2008, 2007). The inverse NN requires MERIS L1b top-of-atmosphere (TOA) radiances (i.e., MERIS 15 bands) as well as some ancillary data (e.g., solar flux, sea surface pressure) as input in order to generate atmospherically corrected water-leaving reflectance at 12 bands (i.e., bands 1-10, 12, and 13). Eight out of these 12 atmospherically corrected bands (i.e., MERIS bands 2-7, and 9), as well as three relevant angles (i.e., Sun zenith angle, viewing zenith angle, and azimuth difference angle), are then inputted into the forward NN to generate three IOPs at 443-nm (i.e., absorption coefficient of phytoplankton (a_{pig}), absorption coefficient of CDOM (a_{CDOM}), and particle scattering (b_{tsm})) (Doerffer and Schiller, 2008, 2007). The Chla and TSM concentrations are then estimated from a_{pig}, and b_{tsm}, respectively (Table 3.2).

The difference between the EUL, BOL, and C2R processors are the training datasets that were used to train each processor (Shi et al., 2014). The training datasets of the EUL processor are based on measurements taken from Spanish lakes (Chla of range 1 – 120 mg m^{-3}, TSM of 0.425 – 51 g m^{-3}, and a_{CDOM} (443) of 0.1 – 3 m^{-1}) (Doerffer and Schiller, 2008). The measurements of the BOL processor were collected from Finnish lakes (Chla of 0.5 – 50 mg m^{-3}, TSM of 0.1 – 20 g m^{-3}, and a_{CDOM} (443) of 0.25 – 10 m^{-1}) (Doerffer and Schiller, 2008). The data of C2R were collected from many sites (i.e., North Sea, Baltic Sea, Mediterranean Sea and North Atlantic) with concentrations of 0.016 – 43.181 mg m^{-3}, 0.0087 – 51.9 g m^{-3}, and 0.005 – 5 m^{-1} for Chla, TSM, and a_{CDOM} (443), respectively (Doerffer and Schiller, 2007).

Schroeder et al. (2007) developed the FUB processor to retrieve the concentrations of Chla, TSM, and a_{CDOM}, along with water leaving reflectance at eight bands (i.e., MERIS bands 1-7, and 9), from MERIS L1b TOA radiance using four separate NNs that are run simultaneously. The four NNs models were trained using extensive radiative transfer simulations that cover a wide range of constituents' concentrations, in ranges of 0.05 – 50 mg m^{-3}, 0.05 – 50 g m^{-3}, and 0.005 – 1 m^{-1} for Chla, TSM, and a_{CDOM} (443), respectively. Table 3.2 summarizes the ranges of IOPs and concentrations used to train the NN processors, along with the relationships between the IOPs and concentrations.

Table 3.2 The ranges of inherent optical properties and concentrations used to train the neural network of EUL, BOL, C2R and FUB processors.

	Processors			
	EUL	BOL	C2R	FUB
a_{pig} (443) (m^{-1})	0.0318 – 3.816	0.024 – 0.84	0.001 – 2	
Chla to a_{pig} relation	Chla =31.447*a_{pig}	Chla = 62.6*$a_{pig}^{1.29}$	Chla = 21*$a_{pig}^{1.04}$	
Chla (mg m^{-3})	1 - 120	0.5 - 50	0.016 – 43.181	0.05 - 50
b_{TSM} (443) (m^{-1})	0.25 - 30	0.96 – 19.194	0.005 – 30	
TSM to b_{TSM} relation	TSM = 1.7* b_{TSM}	TSM = 1.042* b_{TSM}	TSM = 1.73* b_{TSM}	
TSM (mg m^{-3})	0.425 – 51	0.1 – 20	0.0087 – 51.9	0.05 – 50
a_{CDOM} (443) (m^{-1})	0.1 – 3	0.25 – 10	0.005 – 5	0.005 – 1
Optical data origin	Spanish lakes	Finnish lakes	North Sea, Baltic Sea, Mediterranean Sea and North Atlantic	
Reference	(Doerffer and Schiller, 2008)	(Doerffer and Schiller, 2008)	(Doerffer and Schiller, 2007)	(Schroeder et al., 2007)

a_{pig} (443), and a_{CDOM} (443) denote the absorption coefficients of phytoplankton and colored dissolved organic matter at 443-nm band; Chla and TSM represent the concentrations of chlorophyll-a and total suspended matter; and b_{TSM} (443) refers to the total scattering coefficient of total suspended matter at 443-nm band.

The sun-induced chlorophyll fluorescence peak at 865-nm is strongly correlated with Chla concentration (Neville and Gower, 1977). Gower et al. (Gower et al., 1999) proposed the FLH algorithm to retrieve Chla concentration from MERIS TOA radiance by measuring the height of radiance at 681-nm (L681) above a linear baseline connecting the radiances at 665-nm (L665) and 709-nm (L709) as follows:

$$\mathrm{FLH} = \mathrm{L}_{681} - k * [\mathrm{L}_{665} + (\mathrm{L}_{709} - \mathrm{L}_{665}) * \frac{(681 - 665)}{(709 - 665)}] \quad \textbf{(3.1)}$$

Where L_{665}, L_{681}, and L_{709} denote MERIS TOA radiances at band 7, 8, and 9, respectively; and k represents a coefficient with a value of 1.005 to reduce the influence of thin cloud. The MERIS band 8 was shifted from the fluorescence peak at 685-nm to 681-nm to avoid the effects of oxygen absorption at 687nm (Gower et al., 1999). Similarly, the MCI algorithm was developed for MERIS data to detect some harmful algal blooms (HABs), such as the red tide, by determining the height of radiance at 709-nm (L_{709}) over the baseline between radiance values at 681-nm (L_{681}) and 754-nm (L_{754}) (Gower et al., 2008b) :

$$\mathrm{MCI} = \mathrm{L}_{709} - k * [\mathrm{L}_{681} + (\mathrm{L}_{754} - \mathrm{L}_{681}) * \frac{(709 - 681)}{(754 - 681)}] \quad (\textbf{3.2})$$

where L_{681}, L_{709}, and L_{754} refer to MERIS TOA radiance at band 8, 9, and 10, respectively. Both FLH and MCI algorithms can also be applied to atmospherically corrected water-leaving reflectance (Gons et al., 2008). MERIS TOA radiance spectra are characterized by high radiance values in the short wavelengths owing to Rayleigh scattering of sunlight in the

atmosphere and a dip in the radiance spectrum at 760-nm due to the oxygen absorption (Fernandez-Jaramillo et al., 2012; Gower et al., 2005) as shown in Fig. 3.2.

Unlike FLH and MCI, both of which have fixed bands, the MPH algorithm searches for the maximum peak height among multiple red and NIR bands (i.e., MERIS band 8, 9, and 10) (Matthews et al., 2012). Bands 7 and 14 are used as a baseline to find the band that has the maximum height. The MPH algorithm requires the bottom of Rayleigh reflectance (BRR) as an input to produce Chla concentrations. Rayleigh correction removes the influence of gaseous absorption (i.e., water vapour (H_2O) and ozone (O_3)) and molecular Rayleigh scattering (not aerosol) from MERIS TOA radiance (Matthews, 2014; Santer et al., 1999). The bottom-of-Rayleigh reflectance processor was used to perform Rayleigh correction. The MPH can be estimated as:

$$\mathrm{MPH} = \rho_{BRR\,max} - \rho_{BRR\,665} - (\rho_{BRR\,885} - \rho_{BRR\,665}) * \frac{(\lambda_{max} - 665)}{(885 - 665)} \qquad (3.3)$$

where $\rho_{BRR\,665}$ and $\rho_{BRR\,885}$ refer to the BRR at 665-nm and 885-nm, respectively; $\rho_{BRR\,max}$ represents the maximum peak height at three candidate bands (i.e., MERIS band 8, 9, and 10) over the linear baseline between MERIS band 7 and band 14; and λ_{max} denotes the wavelength of the $\rho_{BRR\,max}$.

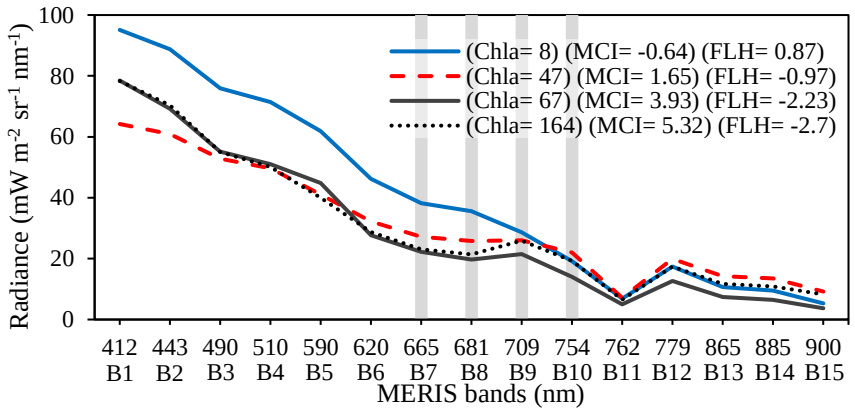

Fig. 3.2. MERIS L1b top-of-atmosphere radiance spectra of Lake Kasumigaura at several chlorophyll-a concentrations with the corresponding values of maximum chlorophyll index (MCI) and fluorescence line height (FLH). The grey columns highlight MERIS bands that are used for FLH and MCI.

3.4. MERIS images processing

A total of 503 MERIS L1b images of 300 m full resolution were available for Lake Kasumigaura between 2002 to 2012 on the European Space Agency (ESA) Earthnet Online (ESA, 2015). However, the clear and partially clear images were found to be 122 out of the 503 images, as summarized in Table 3.3. A synchronization process was executed to match the monthly field campaigns that were performed by NIES during 2002 – 2012 with the 122 images, resulting in five images acquired on the same day as the field campaigns (hereafter, same day) and eight images with one-day difference (hereafter, 1-day difference) (Table 3.4). The 1-day difference images were employed based on the assumption that there are no

significant changes in the Chla concentrations during that day due to stable weather conditions (Table 3.5). Several studies have adopted such a similar assumption, such as Campbell et al. (2011) for MERIS data of Burdekin Falls Dam, Australia. In general, the number of both the clear images (i.e., 122 images) and synchronized images (i.e., 13 images) were relatively few, owing to the high cloud coverage over Japan: the average monthly sunshine ranged 31 – 64 % at Mita station (i.e., the nearest weather station to Lake Kasumigaura) (JMA, 2017) during 2002-2012 (Fig. 3.3).

Table 3.3 Summary of clear and partially clear images of Medium Resolution Imaging Spectrometer (MERIS) sensor over Lake Kasumigaura between 2002 and 2012.

	2002	2003	2004	2005	2006	2007	2008	2009	2010	2011	2012
January				1		3		2	5	2	
February					1	2	4	1	3	1	
March				2	4	3	2	3	1		1
April			2	1	3	2	2	6	1		
May					2	2	4	4	1		
June			2		1	2	2	1			
July			4						1		
August					1	1	1		2	1	
September						1		1			
October			1		1	2	2	3	1		
November					1		3		2		
December		1		1	1	2	2	1	2	4	

Table 3.4 Synchronization between the monthly field measurements and cloud-free images of Medium Resolution Imaging Spectrometer (MERIS) sensor for Lake Kasumigaura during 2002 - 2012.

	2002	2003	2004	2005	2006	2007	2008	2009	2010	2011	2012
January						1*		1*			
February							1*				
March						1					
April								1*			
May							1	1*			
June											
July			1								
August							1*			1*	
September											
October						1					
November									1*		
December										1	

1 represents the images taken at the same day of the in-situ measurements.
1* represents the images with 1-day difference.

Table 3.5 Average wind speed and water surface temperature between MERIS acquisition day and field observation day for the one day difference MERIS images.

	MERIS images Acquisition			Field observation		
	Date	Average wind speed (m / sec)	Water surface Temp. (℃)	date	Average wind speed (m / sec)	Water surface Temp. (℃)
Image (1)	9-Jan-2007	3.9	5.9	10-Jan-2007	2.5	5.7
Image (2)	14-Feb-2008	6.7	4.2	13-Feb-2008	7.3	4.6
Image (3)	7-Aug-2008	2.5	---	6-Aug-2008	3	---
Image (4)	6-Jan-2009	2.5	6.3	7-Jan-2009	3.2	6.4
Image (5)	9-Apr-2009	2.3	15	8-Apr-2009	2.9	14
Image (6)	14-May-2009	5.1	---	13-May-2009	4.5	20.3
Image (7)	9-Nov-2010	4.7	15	10-Nov-2010	4	---
Image (8)	9-Aug-2011	2.5	---	10-Aug-2011	---	---

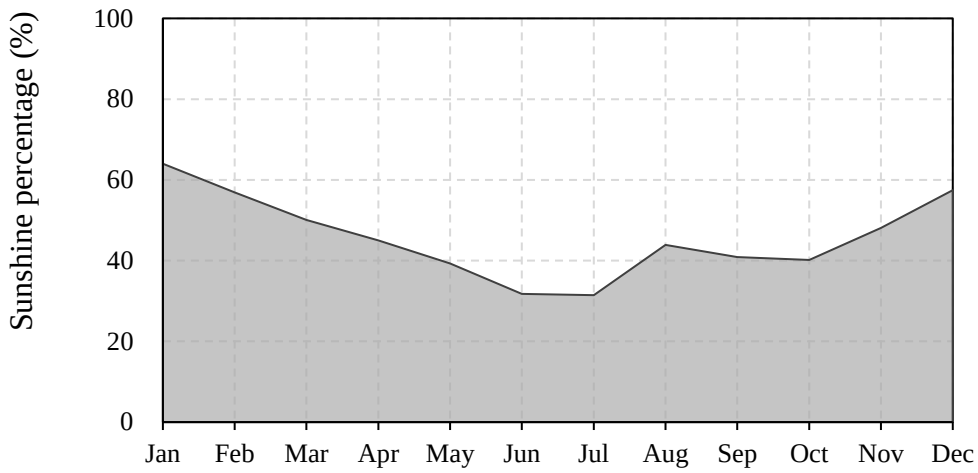

Fig. 3.3. The monthly average of possible sunshine at Mito WMO (World Meteorological Organization) weather station located near Lake Kasumigaura during 2002 − 2012.

The matched-up images were processed using seven processors (i.e., EUL, BOL, C2R, FUB, FLH, MCI, and MPH processors) to retrieve Chla concentrations or Chla indices following the flowchart as illustrated in Fig. 3.4. A smile correction was performed on the MERIS L1b images to adjust the variation of the central wavelength among the pixels of an image for a given band (Levrini and Delvart, 2011). The variation in the central wavelength per pixel can be in the range of 0.1 nm within one camera and within 1.7 nm between the five cameras (ESA, 2012). The land detection expression for EUL, BOL, and C2R processors was modified to be '*toa_reflec_10 > toa_reflec_6 AND toa_reflec_13 > 0.01*' for a better representation of the coastline between the lake and land, as suggested by Binding et al. (Binding et al., 2011). As many of the lakes' pixels were inaccurately masked as land for the FLH, MCI, and MPH processors, the '*l1_flags.LAND_OCEAN*' statement was removed from their default mask expression to make them process all the land and ocean pixels. A shapefile of Lake Kasumigaura, downloaded from the Japanese National Land Numerical Information

(NLNI, 2017), was instead used to mask the land pixels around the lake. Moreover, to remove pixels with strong sunlight, haze or cloud, pixels with radiance at 865nm greater than 15 mW m^{-2} sr^{-1} nm^{-1} were manually flagged and excluded from calculations for FLH and MCI, as reported by Gower et al. (Gower et al., 2008b). Other than these changes, all the other default settings for the seven processors were employed to process MERIS L1b data.

3.5. Results and discussion

3.5.1. Characteristics of the synchronized measurements

The synchronization process between the MERIS data and in-situ measurements at Lake Kasumigaura during 2002-2012 resulted in 130 matchups (i.e., 13 images × 10 sampling stations for each image). Nevertheless, the final number of the matchups varied for each processor based on the flags present in level 1 and level 2. The matchups were 77 for EUL, BOL and C2R, 79 for FUB, 101 for MPH, and 86 for FLH and MCI. Descriptive statistics of water quality parameters for the in-situ measurements of the matchups are summarized in Table 3.1 (some matchup measurements were noted as valid for some processors and invalid for others). The measurements covered a wide range of trophic status for the same day (Chla = 8.1 - 187.4 mg m^{-3}, TSM = 11.6 - 47.75 g m^{-3}) and 1-day difference (Chla = 18.0 – 164.07 mg m^{-3}, TSM = 10.7 – 71.2 g m^{-3}). These measurements confirm the characteristic of Lake Kasumigaura as a complex turbid water body.

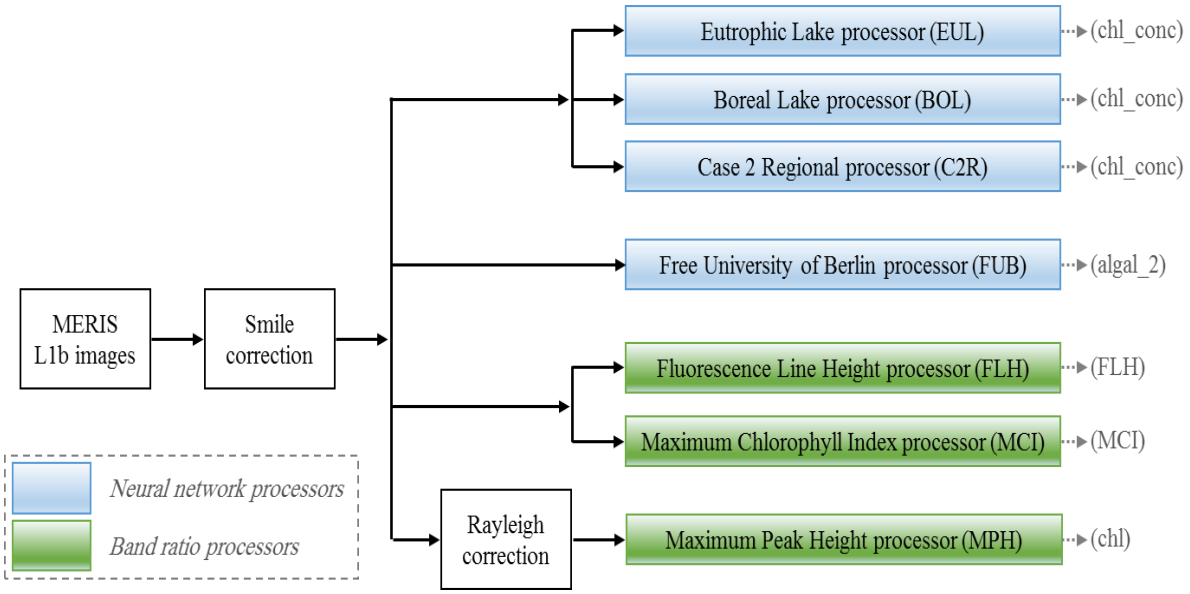

Fig. 3.4. Processing flowchart of Medium Resolution Imaging Spectrometer (MERIS) L1b images to retrieve chlorophyll-a concentrations or indices related to chlorophyll-a concentrations using neural network and band height processors. *chl_conc* indicates the chlorophyll-a (Chla) concentration retrieved from EUL, BOL, and C2R processors; *algal_2*, and *chl* stand for the retrieved Chla of FUB and MPH processors, respectively; and *FLH* and *MCI* denote indices correlated with Chla concentrations.

3.5.2. Evaluation of chlorophyll-a retrieval processors

Five out of the seven processors (i.e., EUL, BOL, C2R, FUB, and MPH) provide Chla concentrations. The retrieved Chla from these processors were compared with the in-situ measurements to evaluate their performances, as shown in Fig. 3.5. In general, the same day and 1-day difference matchups are regularly distributed across different Chla concentrations without any special trend (Fig. 3.5), revealing the applicability of the assumption for one day difference between the in-situ measurements and MERIS data acquisition. EUL, BOL, and C2R considerably underestimated the Chla concentration with an upper limit for the retrieved Chla of 50 mg m^{-3} (Figs. 3.5a, 3.5b, and 3.5c). Although the training dataset of EUL processor used Chla concentrations that ranged 1 – 120 mg m^{-3} (Table 3.2), the processor failed to retrieve Chla concentrations higher than 50 mg m^{-3} (Fig. 3.5a), with retrieval accuracy of 0.42, 55.46 mg m^{-3}, and 61.68 % for coefficient of determination (R^2), RMSE, and MARE, respectively. The BOL processor had the lowest retrieval accuracy with R^2 of 0.26, whereas the C2R outperformed the other processors with R^2, RMSE, MARE of 0.52, 49.38 mg m^{-3}, and 54.34 %, respectively (Figs. 3.5b, and 3.5c). The upper retrieval limit (i.e., 50 mg m^{-3}) for the BOL and C2R processors can be attributed to the training stage of these processors, where Chla concentrations covered ranges of 0.5 – 50 mg m^{-3} and 0.016 – 43 mg m^{-3} for BOL and C2R processors, respectively (Table 3.2).

Although the FUB processor was the second most accurate processor (R^2 = 0.41, RMSE = 34.71 mg m^{-3}, MARE = 69.26 %), it seems that the processor had issues retrieving Chla concentration at 100 mg m^{-3} for many measured matchups in ranges of 25 – 180 mg m^{-3} (Fig. 3.5d). In contrast to the four NN processors (EUL, BOL, C2R, and FUB), the MPH processor overestimated the retrieved Chla up to 390 mg m^{-3} (Fig. 3.5g). As a result, the MPH introduced the highest RMSE and MARE of 106.77 mg m^{-3} and 144.45 %, respectively.

3.5.3. Processors adjustment

As clearly shown in Fig. 3.5, the five processors either underestimated or overestimated the retrieved Chla. The regression approach was therefore used to adjust the inaccurate Chla retrieval, as well as demonstrate the correlation between the measured Chla and the indices that the FLH and MCI processors produced. Salem et al. (2017b) concluded that the differences in retrieval accuracies among linear, quadratic polynomial, and power regression approaches were relatively small for the measured dataset. Therefore, linear regression was adopted during this research. The matchups for each processor were split into a ratio of 70 % : 30 % for calibration and validation datasets, respectively.

The performance of each processor in terms of R^2, as well as the derived relation, are summarized in Table 3.6 for the calibration stage. The MCI_L1 outperformed the other processors (R^2 = 0.65), as shown in Fig. 3.6f. The second tier of processors was the FLH_L1 and C2R with R^2 of 0.55 and 0.52, respectively (Figs. 3.5e and 3.5c). The FLH_L1 provided positive values for Chla concentrations ≤ 10 mg m^{-3}, as the influence of fluorescence at 681-nm is much stronger than the influence of particle scattering at 709-nm. However, the particle scattering significantly increases the radiance at 709-nm for Chla concentrations above 10 mg

m^{-3}, causing negative FLH height values at 681-nm from the baseline between 665-nm and 709-nm (S.C.J. Palmer et al., 2015). Fig. 3.5b illustrates the BOL processor that introduced the lowest retrieval accuracy (R^2 = 0.27). The poor retrieval accuracy for the BOL processor can be attributed to the fact that the Finnish lakes which were used to train the processor are not eutrophic water bodies, resulting in unrealistically low Chla concentrations, as reported by Shi et al. (Shi et al., 2014).

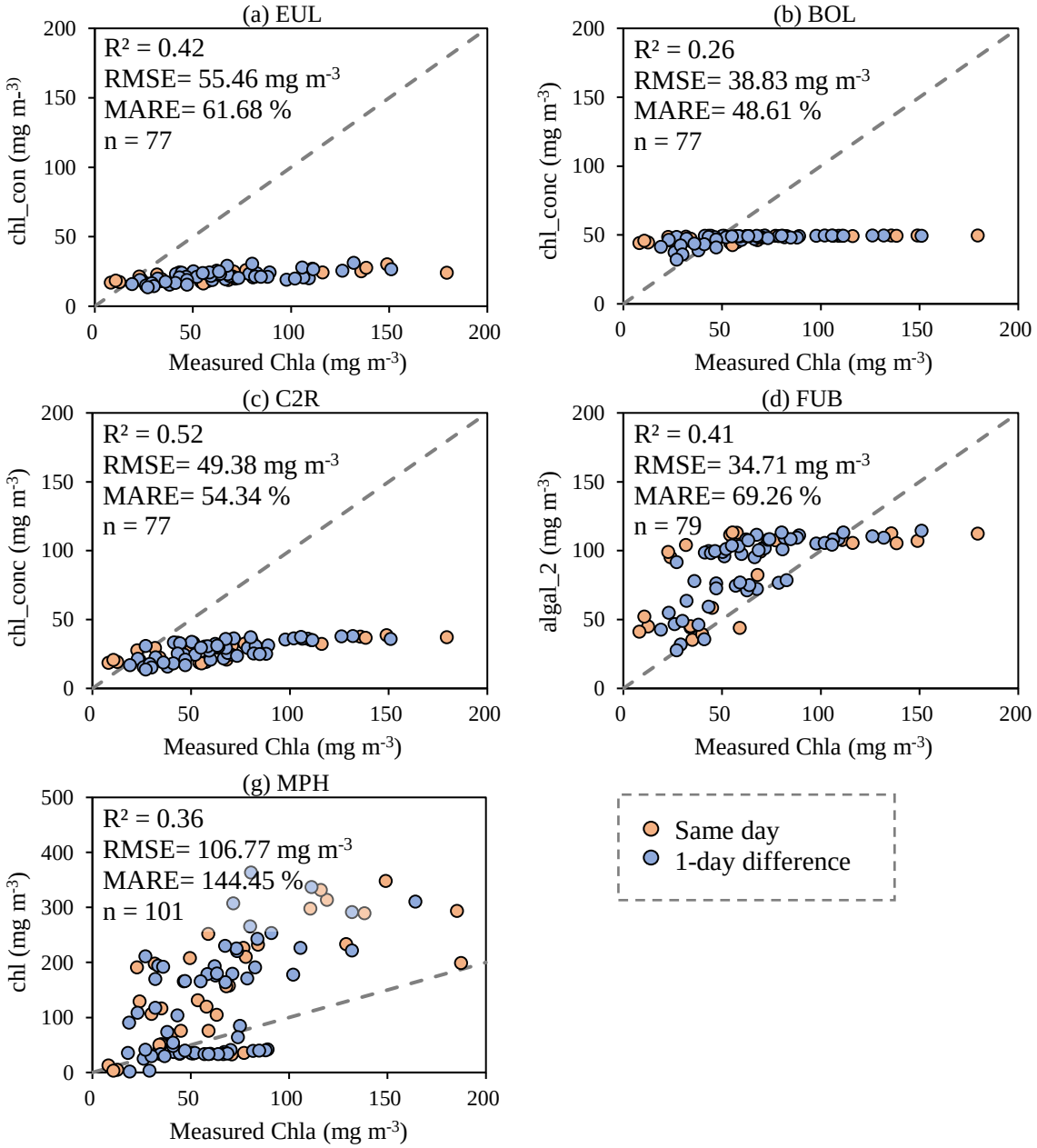

Fig. 3.5. Comparison of the measured and retrieved Chla from (a) EUL, (b) BOL, (c) C2R, (d) FUB, (e) FLH, (f) MCI, and (g) MPH processors. *chl_conc* indicates the chlorophyll-a (Chla) concentration retrieved from EUL, BOL, and C2R processors; *algal_2* and *chl* stand for the retrieved Chla of FUB and MPH processors, respectively; *FLH* and *MCI* denote indices correlated with Chla concentrations; *n* represents the total number of matchups available for each processor.

The seven processors in Fig. 3.6 can be classified into two groups: the first group consists of EUL, C2R, MCI_L1, and FLH_L processors, whereas the other group consists of BOL, FUB, and MPH processors. The first group shows a relatively good agreement between the measured and the retrieved Chla concentrations (Figs. 3.5a, 3.5c, 3.5e, and 3.5f). The common feature of the second group is their failure to retrieve Chla concentrations from MERIS data by producing the same retrieved Chla concentration under different conditions. For example, the BOL processor retrieved Chla concentrations around 50 mg m^{-3} for the measured Chla in a range of 25 – 180 mg m^{-3} for many stations (Fig. 3.6b). Similarly, the FUB retrieved inaccurate Chla concentrations of around 120 mg m^{-3} (Fig. 3.6d). The MPH had a similar trend of around 40 mg m^{-3}; however, this trend was located inside the limits of the retrieved Chla, demonstrating the need for revising the conditions and thresholds of MPH to find the possible cause of this error.

During the validation stage, the Chla concentrations retrieved from each processor were adjusted using the relationship derived from the calibration stage. The MCI_L1 algorithms had the highest R^2 of 0.65 and the lowest RMSE of 22.18 mg m^{-3} among the seven processors (Fig. 3.7f). The second most accurate processors were the FLH_L1 (R^2 = 0.56, RMSE = 25.80 mg m^{-3}, MARE = 34.52 %) and C2R (R^2 = 0.53, RMSE = 26.34 mg m^{-3}, MARE = 48.73 %) as illustrated in Figs. 3.7e and 3.7c, respectively. Although the EUL processor was developed for turbid Case 2 waters and trained with Chla concentrations up to 120 mg m^{-3} (Table 3.2), it showed intermediate retrieval accuracy with R^2, RMSE, and MARE of 0.42, 29.67 mg m^{-3}, and 33.38 %, respectively. The retrieved Chla were close to and consistent with the in-situ measured Chla for EUL, C2R, FLH_L1, and MCI_L1 processors, generally following the 1:1 line for Chla concentrations $\leq$ 100 mg m^{-3}. However, the four processors tended to underestimate the retrieved Chla concentrations > 100 mg m^{-3} (Figs. 3.7a, 3.7c, 3.7e, and 3.7f).

The BOL, FUB, and MPH processors introduced the highest MARE values of 56.20, 57.00, and 59.54 %, respectively. The limitation of the three processors to accurately retrieve Chla concentrations from MERIS data is evident from the data, as shown in Fig. 3.7b (i.e., retrieved Chla around 80 mg m^{-3}), Fig. 3.7d (i.e., retrieved Chla around 80 mg m^{-3}), and Fig. 3.7g (i.e., retrieved Chla around 40 mg m^{-3}), respectively. MCI_L1 and FLH_L1 processors require MERIS L1b radiance as an input, which leads to avoidance of errors arising from atmospheric correction. Furthermore, the MCI_L1 and FLH_L1 processors provided high retrieval accuracy during the calibration and validation stages of the current study, as well as for other studies that compared the NN processors with the band height processors (Table 3.6). Consequently, the MCI_L1 and FLH_L1 processors are recommended for MERIS data.

Table 3.6 the investigated processors' performance during the current study and recent studies.

	Calibration			Validation			
Processors	n	R^2	b	n	R^2	RMSE	MARE
Current study			(Chl-a in ranges of 8.10 – 187.40 mg m^{-3}) (Lake Kasumigaura, Japan)				
EUL	53	0.42	Chla_m = 5.56 * Chl_conc - 55.98	24	0.42	29.67	33.38
BOL	53	0.27	Chla_m = 5.07 * Chl_conc - 171.42	24	0.29	29.41	56.20
C2R	53	0.52	Chla_m = 3.63 * chl_conc - 34.82	24	0.53	26.34	48.73
FUB	55	0.41	Chla_m = 0.80 * algal_2 - 4.46	24	0.42	32.49	57.00
FLH_L1	60	0.55	Chla_m = -31.76 * FLH + 22.50	26	0.56	25.80	34.52
MCI_L1	**60**	**0.65**	**Chla_m = 16.63 * MCI + 19.30**	**26**	**0.65**	**22.18**	**36.88**
MPH	70	0.35	Chla_m = 0.25 * chl + 35.09	31	0.37	29.06	59.54
Ruiz-Verdú et al. (2008)			(Chl-a < 8 mg m^{-3}) (Eleven lakes in Finland, Germany and Spain)				
EUL	16	---	Chla_m = 1.26 * Chl_conc + 0.55	---	0.46	2.54	---
BOL	16	---	Chla_m = 2.65 * Chl_conc – 1.79	---	0.38	6.74	---
C2R	**16**	**---**	**Chla_m = 2.21 * Chl_conc – 1.39**	**---**	**0.57**	**4.21**	**---**
Binding et al. (2011)			(Chl-a in ranges of 1.9 – 70.50 mg m^{-3}) (Lake of the Woods, Canada)				
EUL	16	0.188	Chla_m = -0.129 * Chl_conc + 17.678	12	---	46.24	---
BOL	16	0.207	Chla_m = 0.444 * Chl_conc + 7.566	12	---	11.84	---
C2R	16	0.159	Chla_m = 0.664 * Chl_conc + 7.133	12	---	11.15	---
MCI_L1	**17**	**0.739**	**Chla_m = 6.166 * MCI + 6.347**	**11**	**---**	**5.71**	**---**
Odermatt et al. (2012)			(Chl-a in ranges of 5 – 40 mg m^{-3}) (Greifensee Lake, Swiss)				
EUL	**16**	**0.41**	**Chla_m = 12.20 * Chl_conc – 3.17**	**---**	**---**	**---**	**---**
C2R	16	0.40	Chla_m = 7.87 * Chl_conc – 2.92	---	---	---	---
FUB	16	0.39	Chla_m = 1.27 * algal_2 + 4.70	---	---	---	---
Lankester et al. (2015)			(Chl-a in ranges of 1.50 – 57.00 mg m^{-3}) (Lake Balaton, Hungary)				
EUL	118	0.42	Chla_m = 2.01 * Chl_conc – 0.57	50	0.33	6.85	---
BOL	91	0.46	Chla_m = 0.65 * Chl_conc + 3.25	39	0.48	9.25	---
C2R	116	0.46	Chla_m = 1.63 * Chl_conc + 1.09	50	0.43	7.53	---
FUB	76	0.32	Chla_m = 0.30 * algal_2 + 4.63	32	0.65	3.83	---
FLH_L1	**141**	**0.78**	**Chla_m = -8.08 * FLH + 10.33**	**60**	**0.87**	**4.19**	**---**
MCI_L1	141	0.62	Chla_m = 3.91 * MCI + 11.31	60	0.69	6.62	---

The text highlighted in bold represents the most accurate processor for each study.

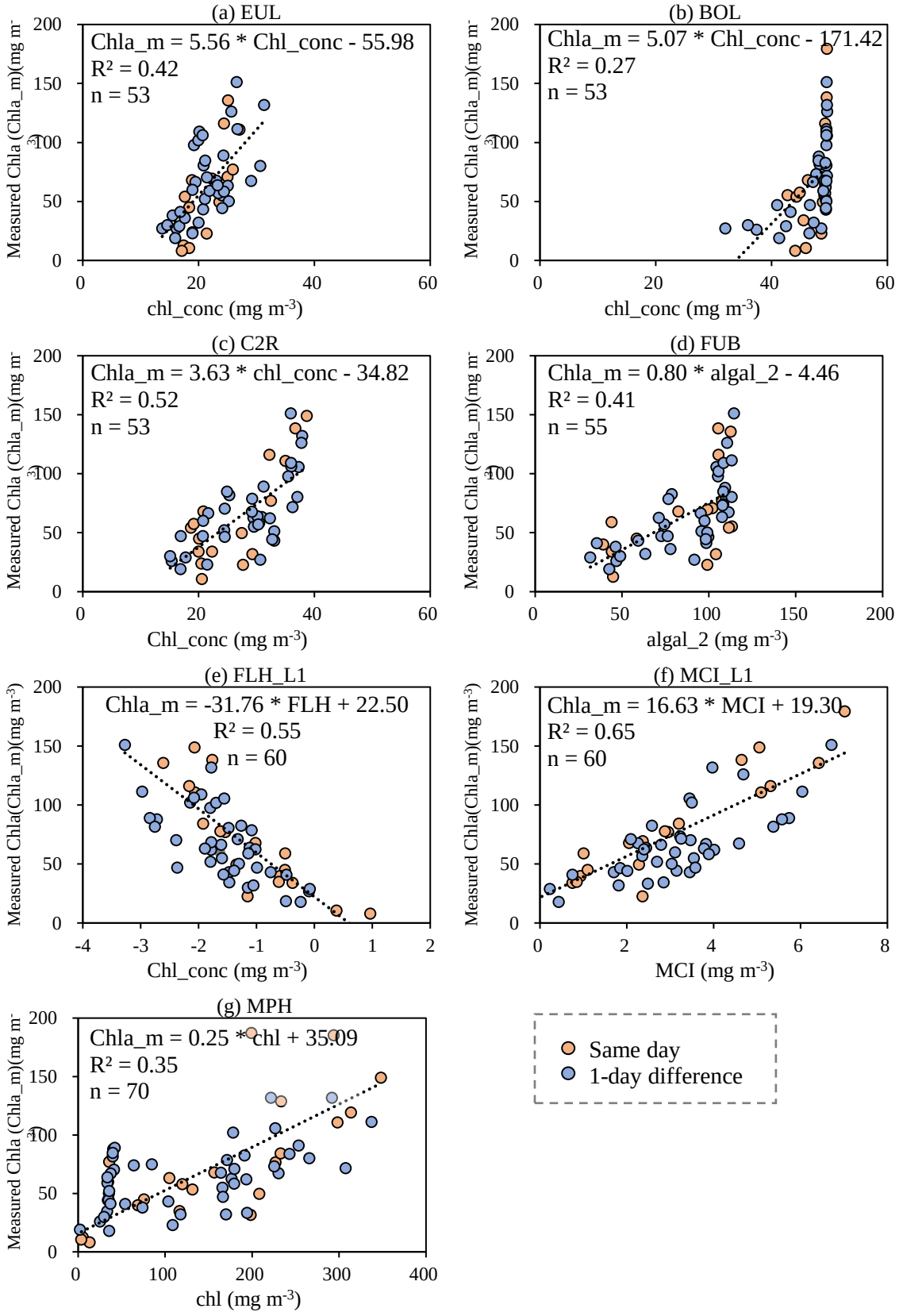

Fig. 3.6. Calibration of (a) EUL, (b) BOL, (c) C2R, (d) FUB, (e) FLH, (f) MCI, and (g) MPH processors. *chl_conc* indicates the chlorophyll-a (Chla) concentration retrieved from EUL, BOL, and C2R processors; *algal_2*, and *chl* stand for the retrieved Chla of FUB and MPH processors, respectively; *FLH* and *MCI* denote indices correlated with Chla concentrations; and *n* symbolizes the number of samples used during the calibration stage (i.e., *n* represents 70 % of total matchups available for each processor).

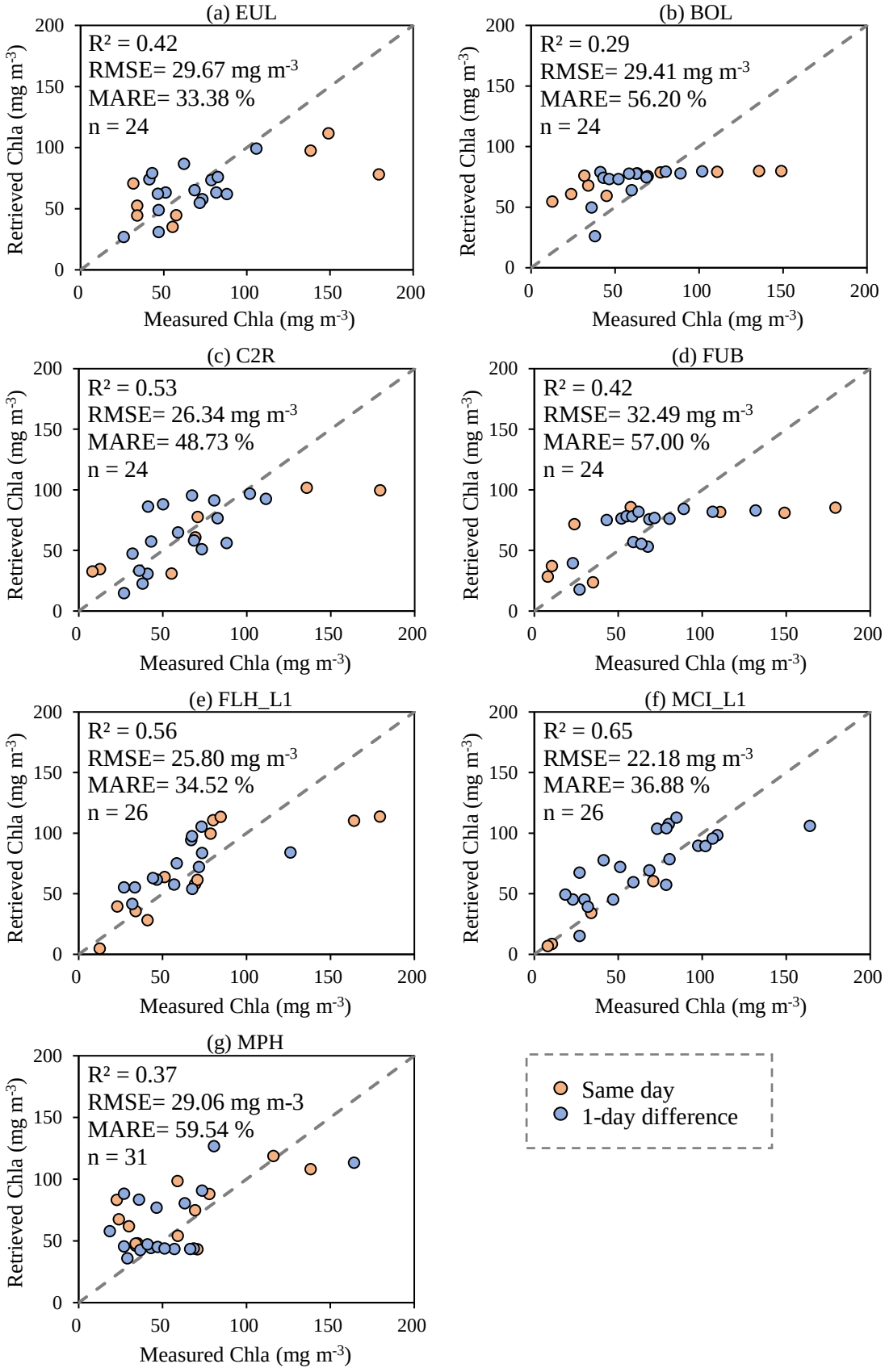

Fig. 3.7. Validation of (a) EUL, (b) BOL, (c) C2R, (d) FUB, (e) FLH, (f) MCI, and (g) MPH processors. *n* denotes the number of samples used during the validation stage (i.e., *n* represents 30 % of total matchups available for each processor).

In order to further investigate the ability of the seven processors to capture the spatial distribution of Chla concentrations throughout Lake Kasumigaura, two MERIS images, one acquired on December 7, 2011 and another on May 14, 2009, were selected to represent moderate and high Chla concentrations, respectively. For each image, Chla concentrations or indices were generated using the seven processors and then the relationships derived during the calibration stage were used to provide the adjusted Chla concentrations, as shown in Figs. 3.8a-g and 3.8i-s. The measured Chla at ten sampling points are illustrated in Figs. 3.8h and 3.8t. Figs. The measured Chla concentrations were interpolated using kriging technique (Hock and Jensen, 1999) via ArcGIS 10.3 to produce the spatial distribution of measured Chla across the lake as shown in Figs. 3.8i and 3.8u.

The measured Chla in Figs. 3.8h and 3.8t indicate that Lake Kasumigaura is y-shaped with relatively high Chla concentrations along both of its branches due to nutrient-rich inflow from rivers near St. 1 (e.g., Sakura and Hanamura River) and St. 6 (e.g., Koise River); however, the remainder of the lake is subjected to relatively moderate Chla concentrations, as shown in Figs. 3.8h and 3.8t. The EUL, C2R, FLH_L1, and MCI_L1 processors introduced relatively accurate trend for Chla distribution comparing with the measured Chla (Figs. 3.8a, 3.8c, 3.8e, 3.8f, 3.8i, 3.8m, 3.8p and 3.8q). The MCI_L1 provided the most accurate image for the moderate Chla concentration on December 2011 (Figs. 3.8h and 3.8i). Whereas the EUL, C2R and FLH produced very similar distributions to the measured concentration for MERIS image on May 2009, particularly the C2R, which showed the closest distribution to the measured concentration (Fig. 3.8c). The MPH processor had a reasonable trend of Chla, with an overestimation of retrieved Chla on December 2011 (Figs. 8g and 8s). Both the BOL and FUB processors failed to capture the Chla distribution for moderate and high concentrations, particularly on May 2009, as they produced almost uniform Chla concentrations of 80 – 90 mg m^{-3}.

The seven processors represent two categories: neural network processors and band height processors. One processor was selected from each category to evaluate their retrieval accuracy over the 10-year MERIS mission. The MCI_L1 and C2R processors were selected because they not only provided the highest R^2 values during the calibration and validation stages, but also represent band height and NN processors, respectively. A total of 122 clear or partially clear MERIS images were first processed using MCI_L1 and C2R processors, following the procedure as shown in Fig. 3.4. Then, the derived relationships during the calibration stage were used to obtain the retrieved adjusted Chla. The Chla concentrations are measured monthly at ten stations of Lake Kasumigaura since 1970s by NIES (NIES, 2016). Figs. 3.9a and 3.9d shows the time series of measured Chla at St. (7) and St. (9), respectively. Additionally, the retrieved adjusted Chla from MCI_L1 and C2R processors are illustrated in Figs. 3.9a and 3.9d.

The visual comparison between the measured and retrieved Chla from MCI_L1 and C2R processors revealed that both processors could follow the seasonal and annual pattern of Chla concentrations during 2002 – 2012 (Figs. 3.93.9a and 3.9d). The retrieved Chla concentrations from MCI_L1 were relatively more accurate than the retrieved Chla concentrations from C2R.

Despite this, the MCI_L1 tended to overestimate the retrieved Chla during the spring seasons of 2004, 2006, 2008, and 2009 (Figs. 3.9a and 3.9d). Diatoms usually bloom in April to June in Lake Kasumigaura (CEBES, 2001), which might have caused this error; however, further investigation is necessary to examine the possible influence of phytoplankton species on the processors' performances.

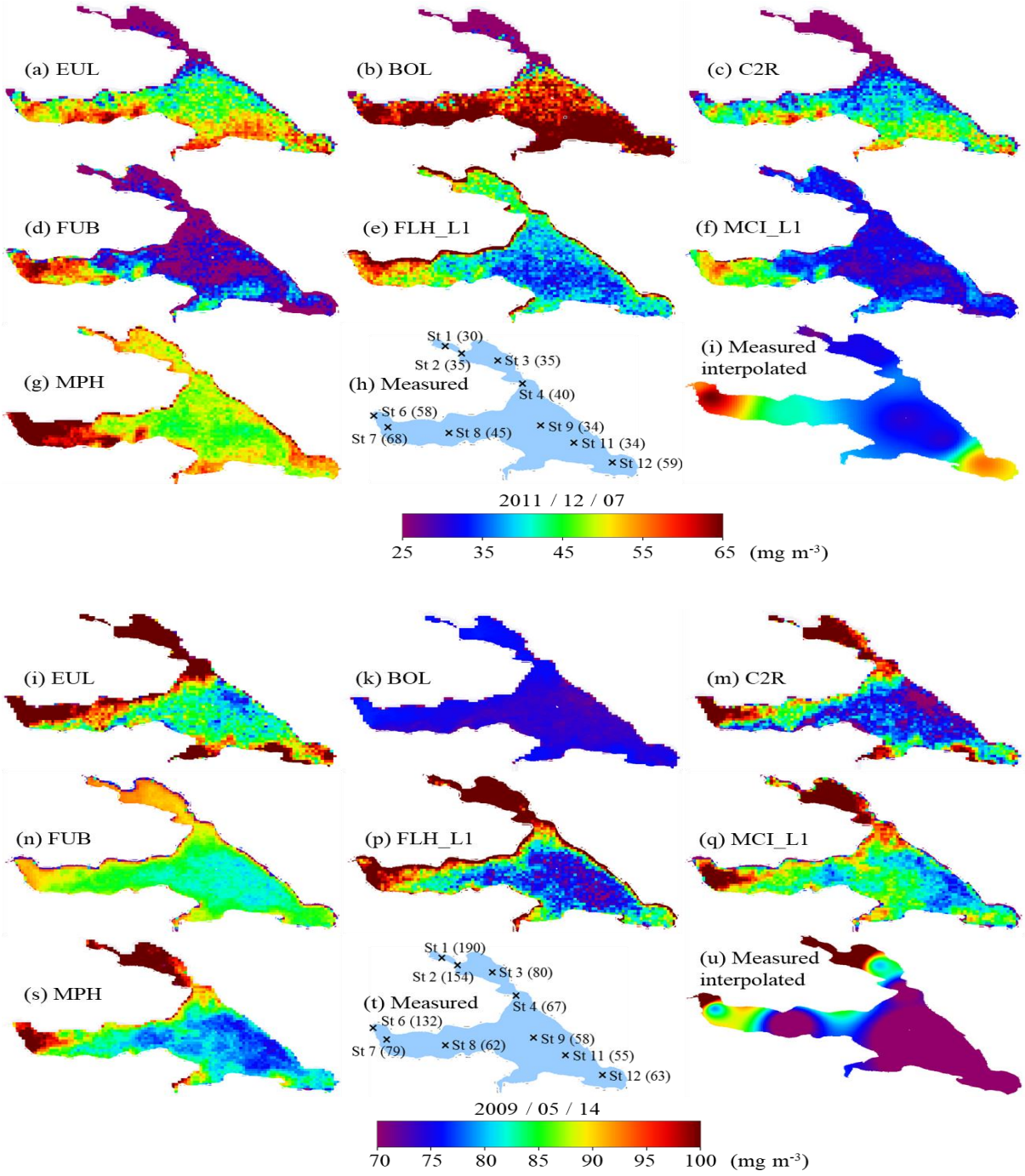

Fig. 3.8. Spatial distribution of chlorophyll-a (Chla) concentration in Lake Kasumigaura on December 7, 2011 (i.e., low Chla concentrations) and May 14, 2009 (i.e., high Chla concentrations) using (a, i) EUL, (b, k) BOL, (c, m) C2R, (d, n) FUB, (e, p) FLH, (f, q) MCI, and (g, s) MPH processors. The measured Chla at the ten stations of NIES shown in (h, t), whereas (i, u) illustrate the interpolated measured Chla. The units of measured and retrieved Chla are in mg m^{-3}.

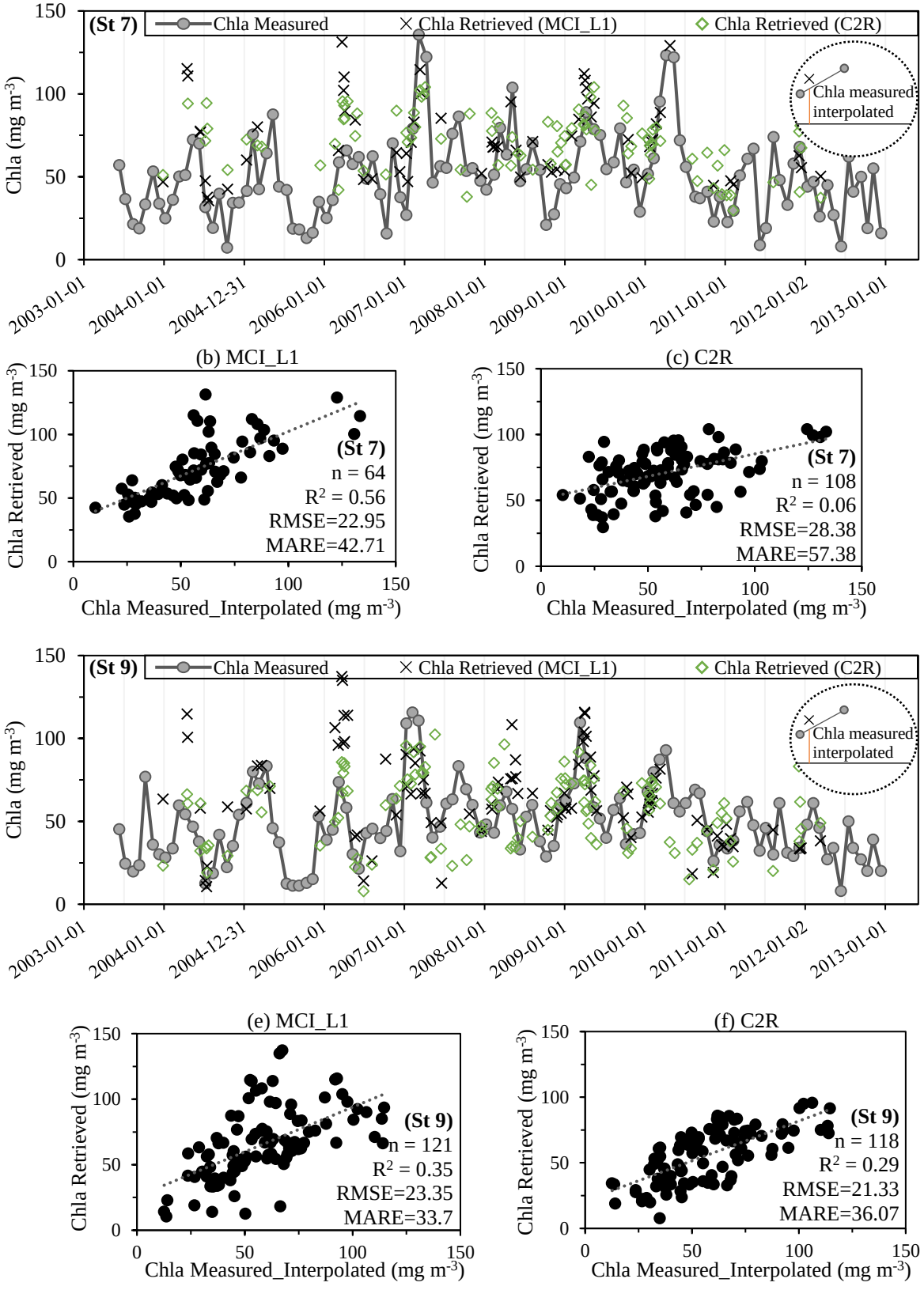

Fig. 3.9. Time series of measured chlorophyll-a (Chla) versus retrieved Chla from MCI_L1 and C2R processors at (a) station 7 (St 7) and (d) station 9 (St 9). Scatter plot of measured interpolated Chla (i.e., linear interpolation was used to estimate measured Chla at the same day of available satellite data) versus retrieved Chla (b) MCI_L1 at St 7; (c) C2R at St 7; (e) (e) MCI_L1 at St 9; and (f) C2R at St 9. *n* stands for the number of matchups. The units of RMSE and MARE are in mg m^{-3} and %, respectively.

The main limitation of performing a quantitative evaluation of the retrieved Chla from MCI_L1 and C2R processors is that there are only 13 out of the 122 images that synchronized the in-situ measurements with only one-day difference. In order to overcome this limitation, the measured Chla were linearly interpolated to match the dates of MERIS images. The comparison between the measured interpolated Chla and the retrieved Chla demonstrated that the MCI_L1 provide better retrieval accuracy than C2R in terms of R^2 at St. 7 (R^2 = 0.56) and St. 9 (R^2 = 0.35), as shown in Figs. 3.9b and 3.9e, respectively.

3.6. Conclusions

Seven Chla retrieval processors developed for MERIS data were evaluated throughout the 10-year MERIS lifetime. An evaluation of five out of the seven processors that provide direct Chla concentrations reveal that these processors tend to underestimate (i.e., EUL, BOL, C2R, and FUB) or overestimate (i.e., MPH) the retrieved Chla. These results emphasize the importance of performing local calibration for the retrieved Chla. The MCI_L1 processor outperforms the seven processors during the calibration (R^2 = 0.65) and validation stages (R^2 = 0.65), in spite of the fact that the MCI processor was not developed for low Chla concentrations. Although the EUL, C2R, MCI_L1, and FLH_L1 provide acceptable accuracies for the validation stage, they underestimate the retrieved Chla for Chla concentrations > 100 mg m^{-3}. Thus, these results reveal the limitation of band height algorithms to eliminate the influence of other constituents, particularly with high concentrations as reported by (Matsushita et al., 2016) and emphasize the importance of including high Chla concentration during the training stage of NN processors, particularly before incorporating these processors with the OLCI sensor. The ability of the seven processors to capture the spatial distribution of Chla across the lake were investigated for moderate and high concentrations in 2011 and 2009, respectively. EUL, C2R, FLH_L1 and MCI_L1 generally could capture the trend of Chla across the lake for moderate and high concentrations. MCI was accurate for moderate Chla, whereas C2R estimated an accurate trend for high Chla. The BOL and FUB processors failed to capture the Chla distribution across the lake for both moderate and high Chla. In addition, the comparison between MCI_L1 and C2R processors versus the 10-years of measured Chla show that both processors could follow the seasonal and annual pattern of Chla concentrations as a whole. However, the MCI_L1 provided better retrieval accuracy than C2R with a slight overestimation of retrieved Chla during the springtime. In general, the performance of band height processors (i.e., MCI_L1 and FLH_L1) outperformed the neural network processors as shown in our results and the previous studies that reported during this research. These results can be attributed to two reasons; (1) the band height processors incorporated MERIS TOA radiance, which leads to avoidance of errors arising from atmospheric correction, in contrast to the NN processors which performing atmospheric correction; and (2) the simulated datasets that used to trained the NN processors could not represent the various trophic statuses of Case 2 water.

The findings of this study highlight the limitation of the seven processors developed for MERIS sensor and demonstrate the need to incorporate regression approach. The neural

network should be retrained using wider ranges of constituents' concentration. The band height algorithms could provide a solution to avoid errors arising from atmospheric correction. The retrieval of numerous semi-analytical algorithms will be evaluated during chapter 4.

CHAPTER 4

Evaluation of current chlorophyll-a retrieval algorithms

4.1. Introduction

Monitoring the water quality of water bodies is an essential tool to determine and control pollution-prone areas to conserve our planet. In particular, inland lakes and coastal areas should be continuously and accurately monitored. The former contains approximately 90 % of the global freshwater that supports human activities (Zhou and Zhao, 2011). The latter provide most of the dissolved organic carbon (DOC), which is a vital link in the global carbon cycle(Mannino et al., 2008). Water constituents' concentrations are used as indicators to assess water quality. These constituents include chlorophyll-a (Chla), total suspended solids (TSS), non-algal particles (NAP), colored dissolved organic matter (CDOM) and nutrients (Schroeder et al., 2007; Usali and Ismail, 2010). Chla is an important pigment in phytoplankton that acts as an indicator for trophic status, water clarity and phytoplankton biomass (Boyer et al., 2009). Indeed, in-situ and laboratory measurements are accurate for sampling points but do not provide the spatial or temporal distribution of the water constituents to monitor water quality. Remote sensing techniques provide spatial relationship for entire water bodies with repetitive coverage and historical records (Dekker et al., 2011).

Water bodies can be classified into Case 1 waters (e.g., open oceans) and Case 2 waters (e.g., coastal regions and inland waters) (Morel and Prieur, 1977). The optical properties of Case 1 waters are dominated by phytoplankton (Gordon and Morel, 1983). The blue and green spectrum regions are used to retrieve Chla concentrations by detecting the blue absorption peak of Chla, considering the strong signal-to-noise ratio (SNR) at these wavelengths (Gordon et al., 1988; O'Reilly et al., 1998). In contrast, absorption at the blue and green wavelengths in Case 2 waters depends not only on phytoplankton but also on NAP and CDOM (Gitelson et al., 2008; Gons, 1999). Hence, Chla retrieval in Case 2 waters shifts from blue and green wavelengths to red and near-infrared (NIR) wavelengths to detect the red absorption peak of Chla, where the absorption is dominated by Chla (Dall'Olmo et al., 2003; Oki and Yasuoka, 1996). In addition, the presence of suspended particles increases backscattering, resulting in good SNRs in the red-NIR wavelengths (Gons et al., 2008).

During the last two decades, researchers have proposed a number of algorithms to retrieve Chla from the remote sensing reflectance (R_{rs}) (Matthews, 2011). NASA's ocean color (OC4E)

algorithm (O'Reilly et al., 1998), quasi-analytical algorithm (QAA) (Lee et al., 2002; Loisel et al., 2017), and Garver-Siegel-Maritorena (GSM) semi-analytical algorithm (Garver and Siegel, 1997) were proposed for Case 1 waters. Applying Case 1 algorithms to retrieve Chla in turbid water provided significant errors, as reported by Werdell et al. (2009). The two-band ratio (Gons, 1999; Ha et al., 2013; Oki, 2010; Oki et al., 2001), three-band algorithm (Dall'Olmo et al., 2003; El-Alem et al., 2012; Watanabe et al., 2015), four-band algorithm (Le et al., 2009), normalized difference chlorophyll index (Augusto-Silva et al., 2014; Mishra and Mishra, 2012), maximum chlorophyll index (Gower et al., 2005) and synthetic chlorophyll index (Shen et al., 2010) were developed for Case 2 waters. These algorithms have been applied in numerous study areas (Dall'Olmo and Gitelson, 2006; Le et al., 2013; Lyu et al., 2015; Xu et al., 2009; Yang et al., 2011a; Yu et al., 2014). The optimal bands that were used in each algorithm varied among studies; for instance, Le et al. (2013) used the 681-, 709-, and 754-nm MERIS central bands with the maximum chlorophyll index algorithm, while Matsushita et al. (2015) employed the 665-, 709-, and 754-nm bands. Huang et al. (2014) also illustrated the various bands used with the three-band algorithm at different inland waters in the USA and China.

The proper selection of algorithms is limited by the absence of clear criteria for algorithm selection based on water constituents' concentrations. To the best of our knowledge, the abovementioned algorithms were mainly evaluated based on limited in-situ observations, which has been reported in previous research (e.g., Le et al. (2013); Zhang et al. (2015)). Thus, a comparison of these algorithms with a huge dataset that covers a broad range of trophic statuses is required, particularly when the optimal bands and regression model are considered. In this study, three simulated datasets of 500,000 reflectance spectra each, along with measured dataset were used to achieve the following objectives: 1) assess the performance of seven Chla retrieval algorithms over wide ranges of Chla, NAP and CDOM concentrations; 2) evaluate the effect of different band combinations and regression approaches on the Chla retrieval accuracy; and 3) provide a reference for algorithm selection based on the concentrations of Chla and NAP, which can be a base for developing a classification scheme.

4.2. Candidate Chla algorithms and band selection

Various algorithms were introduced based upon the bio-optical model with various assumptions. Gons (1999) outlined the first two-band ratio to retrieve the Chla concentration, which replaced the blue and green wavelengths with red and NIR wavelengths:

$$Chla \propto R_{rs}(\lambda_2) / R_{rs}(\lambda_1) \approx \left(a_{ph}(\lambda_1)+a_W(\lambda_1)\right) / a_w(\lambda_2) \quad (\mathbf{4.1})$$

where λ_1 and λ_2 are the red and NIR wavelengths, respectively. Three assumptions govern this algorithm: 1) the absorption at (λ_1) is dominated by phytoplankton; 2) the absorption at (λ_2) is dominated by water; and 3) the backscattering is independent of λ between λ_1 and λ_2. The normalized difference chlorophyll index (NDCI) is a modified version of the two-band ratio (Mishra and Mishra, 2012). The NDCI was proposed to reduce any uncertainties from seasonal solar azimuth differences and atmospheric contributions at those wavelengths by taking the difference in the numerator and the sum in the denominator for $R_{rs}(\lambda_1)$ and $R_{rs}(\lambda_2)$. The NDCI was originally developed to retrieve the Chla concentration from MERIS products and can be expressed as follows:

$$Chla \propto \left(R_{rs}(\lambda_2)-R_{rs}(\lambda_1)\right) / \left(R_{rs}(\lambda_2)+R_{rs}(\lambda_1)\right) \quad (\mathbf{4.2})$$

Both the two-band ratio and NDCI neglect the absorption of NAP and CDOM, which is no longer valid with increasing turbidity, where the absorption of both NAP and CDOM are significant. Therefore, the three-band algorithm was introduced (Dall'Olmo et al., 2003):

$$Chla \propto \left(R_{rs}^{-1}(\lambda_1)-R_{rs}^{-1}(\lambda_2)\right) * R_{rs}(\lambda_3) \approx \left(a_{ph}(\lambda_1)+a_W(\lambda_1)-a_w(\lambda_2)\right) / a_w(\lambda_3) \quad (\mathbf{4.3})$$

where λ_1 is the red wavelength, and λ_2 and λ_3 are the NIR wavelengths. The assumptions of the three-band algorithm are 1) the Chla absorption at (λ_1) >> that at (λ_2); 2) the absorption at (λ_3) is dominated by water; 3) the backscattering is independent of λ between λ_1 and λ_2; and 4) the absorption of NAP and CDOM at λ_1 and λ_2 is close and the difference between λ_1 and λ_2 eliminates their effect. In highly turbid water, the previous assumptions of the three-band algorithm become invalid because of increasing TSS concentration, which causes significant absorption and backscattering in the NIR region (Zimba and Gitelson, 2006). A four-band algorithm was proposed by Le et al. (2009) to improve the three-band algorithm in highly turbid water by considering the absorption and backscattering of suspended solids and pure water. $R_{rs}(\lambda_3)$ was replaced by ($R_{rs}^{-1}(\lambda_4)-R_{rs}^{-1}(\lambda_3)$) to reduce the absorption of pure water, as well as the absorption and backscattering of suspended solids. The four-band algorithm is expressed as

$$Chla \propto \left(R_{rs}^{-1}(\lambda_1)-R_{rs}^{-1}(\lambda_2)\right) / \left(R_{rs}^{-1}(\lambda_4)-R_{rs}^{-1}(\lambda_3)\right) \approx \left(a_{ph}(\lambda_1)+a_W(\lambda_1)-a_w(\lambda_2)\right) / \left(a_w(\lambda_4)-a_w(\lambda_3)\right) \quad (\mathbf{4.4})$$

Gower et al. (2005) adopted the maximum chlorophyll index (MCI) for MERIS sensor to detect the maximum reflectance at 709 nm from baseline wavelengths of 685 nm and 754 nm. To distinguish the water pixels of MERIS level 1 products from others (i.e., land, cloud and sun glint pixels), the MCI applied for pixels that the radiance values at 865 nm were less than 15 mW m^{-2} sr^{-1} nm^{-1} (Gower et al., 2008b). The MCI is as follows:

$$MCI = R_{rs}(\lambda_2) - R_{rs}(\lambda_1)\left[\frac{\lambda_2 - \lambda_1}{\lambda_3 - \lambda_1} R_{rs}(\lambda_3) - R_{rs}(\lambda_1)\right] \quad (\mathbf{4.5})$$

where λ_1, λ_2 and λ_3 refer to the 681-, 709- and 754-nm wavelengths. The synthetic chlorophyll index (SCI) was also developed for MERIS sensor to detect the reflectance trough (H_{chl}) at 665 nm from baseline wavelengths at 620 nm and 681 nm because of the maximum absorption of phytoplankton (Shen et al., 2010). A correction factor (H_{Δ}) was introduced to eliminate backscattering from high suspended solids. The absorption of CDOM for wavelengths larger than 555 nm was assumed to be negligible, and the SCI is expressed as

$$H_{chl} = \left[R_{rs}(\lambda_4) + \frac{\lambda_4 - \lambda_3}{\lambda_4 - \lambda_2}\left(R_{rs}(\lambda_2) - R_{rs}(\lambda_4)\right)\right] - R_{rs}(\lambda_3) \quad (\mathbf{4.6})$$

$$H_{\Delta} = R_{rs}(\lambda_2) - \left[R_{rs}(\lambda_4) - \frac{\lambda_4 - \lambda_2}{\lambda_4 - \lambda_1}\left(R_{rs}(\lambda_1) - R_{rs}(\lambda_4)\right)\right] \quad (\mathbf{4.7})$$

$$SCI = H_{chl} - H_{\Delta} \quad (\mathbf{4.8})$$

where λ_1, λ_2, λ_3 and λ_4 are the wavelengths 560, 620, 665 and 681 nm, respectively. While all the aforementioned algorithms were developed for Case 2 waters, the ocean color V4 (OC4) (O'Reilly et al., 1998) algorithm, which was established for Case 1 waters and MERIS sensor, was also assessed for Chla concentrations less than 20 mg m^{-3}. OC4 is expressed as

$$Chla = 10^{\left(0.3255 - 2.7677x + 2.4409x^2 - 1.1288x^3 - 0.499x^4\right)} \quad (\mathbf{4.9})$$

$$x = \log_{10}\left(R_{rs}^1 / R_{rs}^2\right) \quad (\mathbf{4.10})$$

$$R_{rs}^1 / R_{rs}^2 = \max\left(\frac{Rrs(\lambda_1)}{Rrs(\lambda_4)}, \frac{Rrs(\lambda_2)}{Rrs(\lambda_4)}, \frac{Rrs(\lambda_3)}{Rrs(\lambda_4)}\right) \quad (\mathbf{4.11})$$

where λ_1, λ_2, λ_3 and λ_4 denote the wavelengths 443, 490, 510 and 555 nm, respectively. The coefficients were derived from a huge dataset (2804 station) with wide ranges of Chla

concentrations (0.01 - 64 mg m^{-3}), while the majority of Chla concentrations were less than 10 mg m^{-3} (O'Reilly et al., 2000a).

The aforementioned algorithms are general expressions that can be applied to various band combinations of multispectral and hyperspectral data. All the possible band combinations for each algorithm were examined, resulting in 15 algorithms (Table 4.1). The proposed bands were the same as MERIS's central bands. Although the MERIS mission ended in 2012, the Ocean and Land Colour Instrument (OLCI) sensor on board of Sentinel-3 satellite was recently launched with similar configurations to MERIS and additional bands to improve atmospheric correction. The 665-nm and 680-nm bands were selected for three reasons. First, these two bands exist in most ocean color sensors (e.g., the spectral bands of the MEdium Resolution Imaging Spectrometer (MERIS) and MODerate resolution Imaging Spectro-radiometer (MODIS) sensors). Second, these two wavelengths are interchangeable for Case 2 water algorithms; for instance, Le et al. (2013) and Matsushita et al. (2015) used the 680-nm and 665-nm bands with the MCI algorithms, respectively. Finally, these two bands are correlated with chlorophyll-a because the 665-nm band is located near the red Chla absorption maximum in the spectral curves, while the 680-nm band is closer to the maximum fluorescence of Chla. The band tuning approach was applied to the three- and four-band algorithms to find the optimal band, as proposed by Sun et al. (2013) (details are mentioned in section 4.3).

All 15 algorithms, except for OC4_V6, provided indices that could be related to the measured constituents through the regression process. Researchers considered linear (Huang et al., 2010; Xu et al., 2009) , polynomial (Le et al., 2011; Mishra and Mishra, 2012; O'Reilly et al., 2000b; Zhang et al., 2015) and power (Gilerson et al., 2010; O'Reilly et al., 1998) regression techniques. Consequently, 14 out of the 15 proposed algorithms, excluding OC4E, were assessed with linear, quadratic polynomial and power regression approaches. Thus, this study proposed 43 algorithms to be evaluated. The linear, polynomial and power regressions were as follows:

$$Chla = a * a\lg_r + b \quad \textbf{(4.12)}$$

$$Chla = a * a\lg_r + b * (a\lg_r)^2 + c \quad \textbf{(4.13)}$$

$$Chla = (a * a\lg_r + b)^c \quad \textbf{(4.14)}$$

where $a\lg_r$ denotes the indices from each algorithm; and a, b and c are the regression coefficients. The selected power regression varies from the standard power regression

expression ($Chla = a * (a\lg_r)^b$) because this standard expression causes an error for negative values of $a\lg_r$. The proposed power model was also employed by Matsushita et al. (Matsushita et al., 2015).

Table 4.1 Investigated algorithms with the proposed bands for each algorithm combination.

No.	Investigated Algorithms	Algorithms' abbreviation	Proposed Bands				References
			λ_1	λ_2	λ_3	λ_4	
1	Ocean Color 4	OC4E	443	490	510	560	O'Reilly et al., (O'Reilly et al., 1998)
2	Two-band ratio	2b_665	665	709			Gons (Gons, 1999)
3		2b_680	680	709			
4		2b_max_min	Min (660-690)	Max (690-710)			
5	Three-band algorithm	3b_665	665	709	754		Dall'Olmo et al., (Dall'Olmo et al., 2003)
6		3b_680	680	709	754		
7		3b_tuning	Band tuning				
8	Four-band algorithm	4b_tuning	Band tuning				Le et al. (Le et al., 2009)
9	Maximum chlorophyll index	MCI_665	665	709	754		Gower et al. (Gower et al., 2005)
10		MCI_680	680	709	754		
11	Normalized difference chlorophyll index	NDCI_665	665	709			Mishra et al., (Mishra and Mishra, 2012)
12		NDCI_680	680	709			
13		NDCI_max_min	Min (660-690)	Max (690-710)			
14	Synthetic chlorophyll index	SCI_4b	560	620	665	681	Shen et al., (Shen et al., 2010)
15		SCI_max_min	Max (540-590)	Max (630-650)	Min (660-690)	Max (690-710)	

4.3. Band tuning selection

One of the potential combinations of the three-band and the four-band algorithms relied on the band tuning approach (Zimba and Gitelson, 2006) to find the optimal bands. In order to find the optimal band for the three-band algorithm, firstly, λ_2 and λ_3 were assigned to 700 and 750 nm, respectively. The correlation coefficient was estimated between $\left(R_{rs}^{-1}(\lambda_1) - R_{rs}^{-1}(700)\right) * R_{rs}(750))$ and reference Chla concertation for each value of λ_1 in the range 400 – 800 nm (Fig. 4.1a) as proposed by Sun et al. (2013). The highest correlation coefficient achieved at 662 nm which was specified for λ_1 (Fig. 4.1). In the second iteration, λ_2 tested from 400 to 800 nm with λ_1 at 662 nm from the first step and λ_3 at 750 nm. The maximum correlation coefficient was at 700 nm between $\left(R_{rs}^{-1}(662) - R_{rs}^{-1}(\lambda_2)\right) * R_{rs}(750))$ and Chla (Fig. 4.1b). For determination of the optimal wavelength of λ_3, both λ_1 and λ_2 were fixed at 662 and 700 nm respectively and the correlation coefficients were estimated for

$\left(R_{rs}^{-1}(662) - R_{rs}^{-1}(700)\right) * R_{rs}(\lambda_3)$) vs. Chla for each value of $\lambda_3$in the range 400 to 800 nm. The correlation coefficients were maximum in range 748 and 800 nm (Fig. 4.1c). λ_3 was selected at 748 nm.

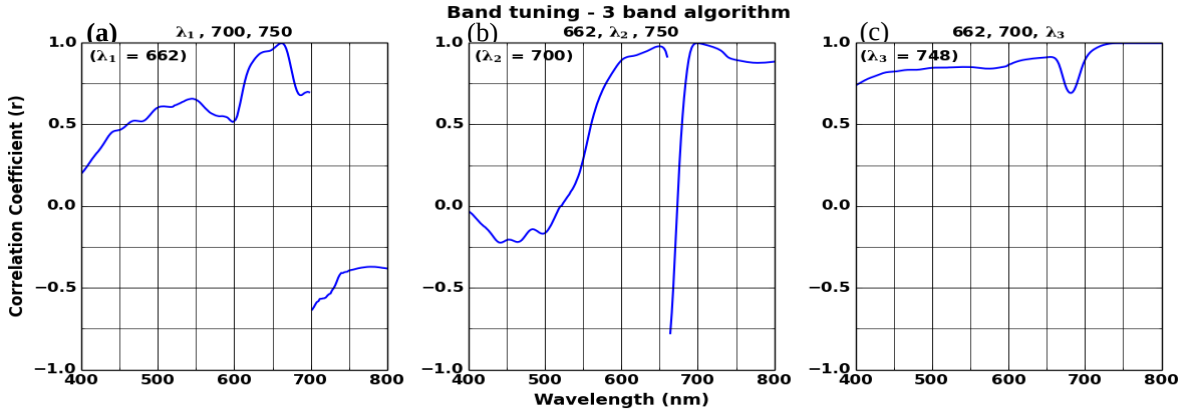

Fig. 4.1. Optimal wavelength positions of the three-band algorithms as determined through optimization for local parameterization scenario. The correlation coefficients between the algorithm ratio and the reference known Chla were estimated at each wavelength.

Similarly, the four-band algorithm was tuned to find the optimal wavelengths for λ_1, λ_2, λ_3 and λ_4. Firstly, λ_2, λ_3, and λ_4 were assigned to 700, 720 and 750 nm, respectively. The correlation coefficient was estimated between $\left[\left(R_{rs}^{-1}(\lambda_1) - R_{rs}^{-1}(700)\right) / \left(R_{rs}^{-1}(750) - R_{rs}^{-1}(720)\right)\right]$ and Chla concertation for each value of λ_1 in the range 400 – 800 nm (Fig. 4.2a). The highest correlation coefficient achieved at 660 nm which was specified for λ_1. In the second iteration, λ_2 tested from 400 to 800 nm with λ_1 at 660 nm, λ_3 at 720 nm, and λ_4 at 750 nm. The correlation coefficient between $\left[\left(R_{rs}^{-1}(660) - R_{rs}^{-1}(\lambda_2)\right) / \left(R_{rs}^{-1}(750) - R_{rs}^{-1}(720)\right)\right]$ and Chla revealed that λ_2 achieved maximum correlation at 696 nm (Fig. 4.2b). For determination of the optimal wavelength of λ_3, both λ_1, λ_2 and λ_4 were fixed at 660, 696 and 750 nm, respectively, and the correlation coefficients were estimated for $\left[\left(R_{rs}^{-1}(660) - R_{rs}^{-1}(696)\right) / \left(R_{rs}^{-1}(750) - R_{rs}^{-1}(\lambda_3)\right)\right]$ vs. Chla in the range 400 to 800 nm and the correlation coefficients were maximum was at 728 nm (Fig. 4.2c). In the fourth iteration, λ_1, λ_2 and λ_3 were fixed at 660, 696 and 728 nm, respectively, and the value of λ_4 was tuned from 400 to 800 nm. The correlation between $\left[\left(R_{rs}^{-1}(660) - R_{rs}^{-1}(696)\right) / \left(R_{rs}^{-1}(\lambda_4) - R_{rs}^{-1}(728)\right)\right]$ and Chla (Fig. 4.2d) resulted in λ_4 at 738 nm. Table 2.1Table 4.2 summarizes the optimal band of the three- and four-band algorithms for local simulation, wide range simulation and in-situ measurements (Dataset 1).

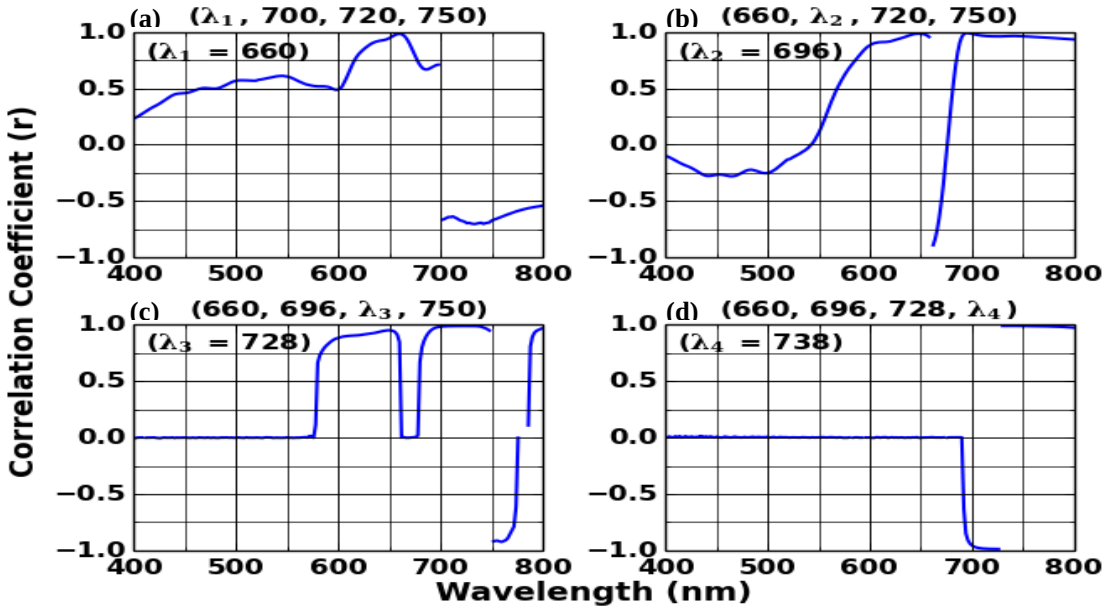

Fig. 4.2. Optimal wavelength positions of the four-band algorithms as determined through optimization for local parameterization scenario. The correlation coefficients between the algorithm ratio and the reference known Chla were estimated at each wavelength.

Table 4.2. The optimal band of the three-and four-band algorithms from the bund tuning process for local simulation scenario, wide range simulation scenario, and in-situ measurements (Dataset 1).

	Three-band algorithm*			Four-band algorithm**		
	Local simulation	Wide simulation	In-situ Dataset1	Local simulation	Wide simulation	In-situ Dataset1
λ_1	662	690	666	660	688	668
λ_2	700	700	706	696	694	706
λ_3	748	764	738	728	732	712
λ_4				738	742	738

* The formula of the three-band algorithm is $\left[R_{rs}^{-1}(\lambda_1)-R_{rs}^{-1}(\lambda_2)\right]*R_{rs}(\lambda 3)$

** The formula of the four-band algorithm is $\left[\left(R_{rs}^{-1}(\lambda_1)-R_{rs}^{-1}(\lambda_2)\right)/\left(R_{rs}^{-1}(\lambda_4)-R_{rs}^{-1}(\lambda_3)\right)\right]$

4.4. Generating Simulated dataset

A simulated reflectance dataset is required to assess the proposed algorithms for waters that range from low to highly turbid waters. Bio-optical modeling is used to connect remote sensing reflectance with Chla, Nap, and CDOM concentrations. Changing any of these three constituents will change the remote sensing reflectance. Remote sensing reflectance spectra were generated based on a bio-optical model. Two scenarios for generating simulated reflectance were employed: (1) local parameterization scenario that used Specific inherent optical properties (SIOPs) from Tokyo bay, and (2) wide range scenario with SIOPs values based on IOCCG database (IOCCG, 2006). SIOPs for the wide range scenario were randomly

changed during the simulation process. Table 2.4 summarizes the SIOPs values for both scenarios). The concentrations of Chla (hereafter called the reference Chla), NAP, and CDOM (the CDOM concentration refers to the absorption of CDOM at 440 nm) were changed in range of 1-200 (mg m^{-3}), 1-200 (g m^{-3}) and 0.1-10 (m^{-1}), respectively. Increments of 2 (mg m^{-3}), 2 (g m^{-3}) and 0.2 (m^{-1}) were used for Chla, NAP and CDOM, respectively.

Two simulated datasets for local parameterization and wide range scenarios were generated with 500,000 reflectance spectra (i.e., 100*50*100) for each dataset. These two datasets were used in the calibration stage. A dependent dataset based on wide range parameters was generated to validate the algorithms. Fig. 4.3 illustrates a comparison between the measured and simulated reflectance spectra at two stations. The simulated reflectance spectra for these two stations were generated by using the bio-optical model and IOPs measured at these two stations. This comparison revealed that the simulated reflectance spectra were similar to the measured reflectance in terms of both the spectral shape and spectral magnitude, especially in the red-NIR region, which is mainly used to substitute for Case 2 water algorithms. Fig. 4.4 illustrates the comparison between measured and simulated reflectance for the 12 sites that had IOPs measurements. Fig. 4.5 demonstrates the simulated reflectance for different Chla concentrations of 1-200 mg m^{-3} and CDOM concentration of 5.1 m^{-1} for two groups of data. While the NAP was 5.1 g m^{-3} (Fig. 4.5a) and 61 g m^{-3} b (Fig. 4.5b). Based on these evaluations, the simulated reflectance could be a reliable dataset to assess the performance of Chla algorithms over wide ranges of Chla, NAP and CDOM concentrations.

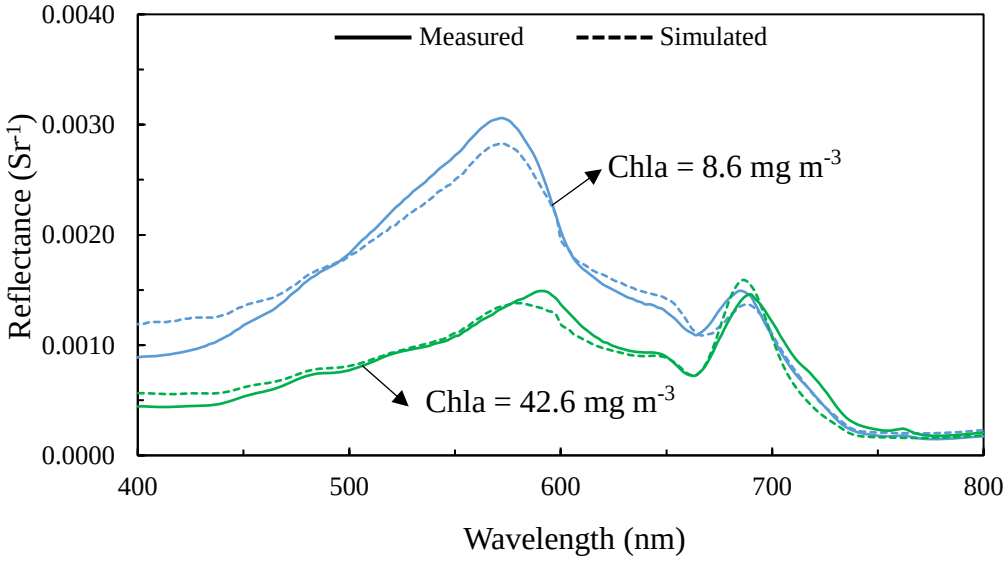

Fig. 4.3. Measured versus simulated remote sensing reflectance spectra at two stations with Chla of 8.6 and 42.6 mg m^{-3}. The solid and dashed lines represent the measured and simulated reflectance, respectively.

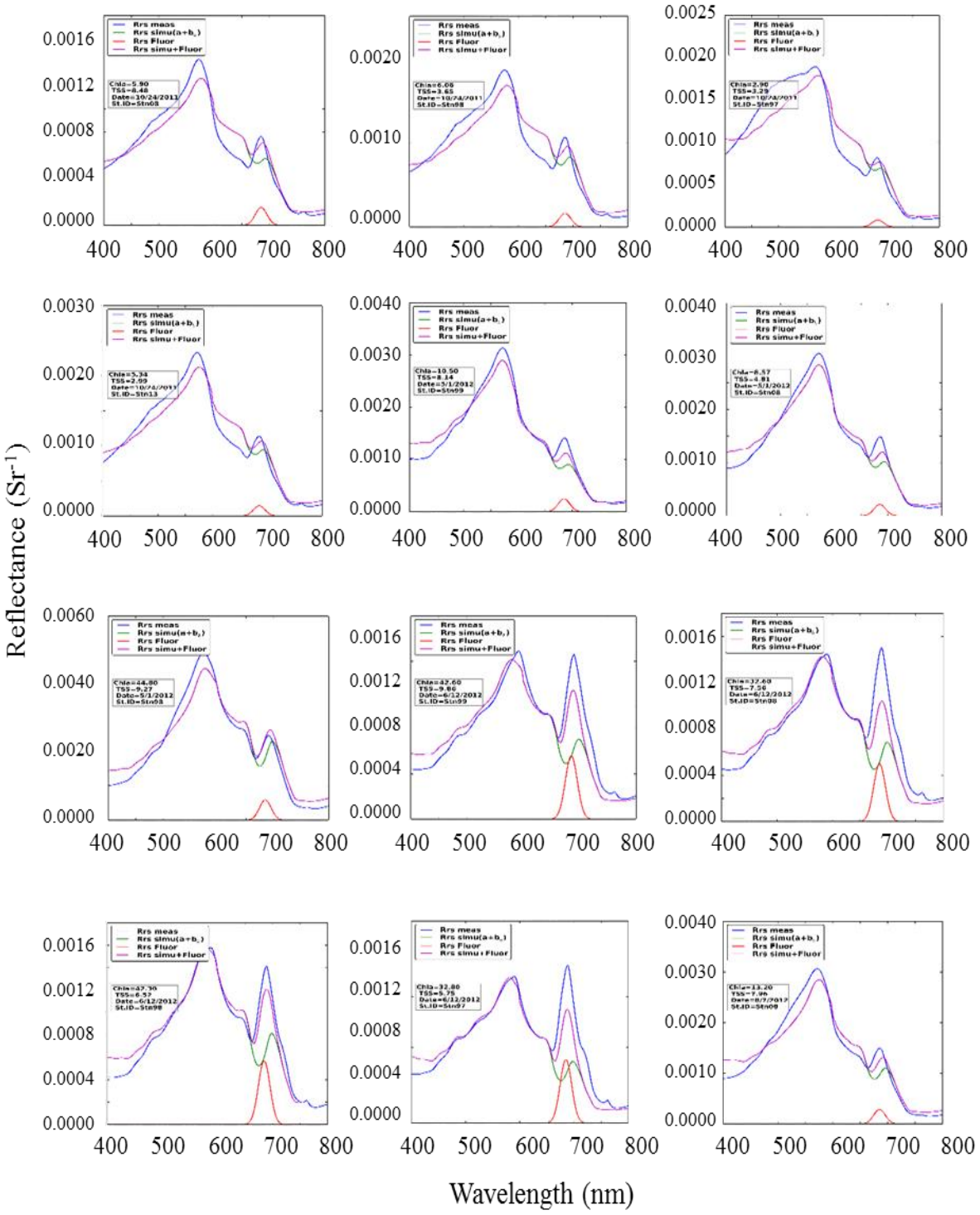

Fig. 4.4. Measured versus simulated remote sensing reflectance spectra at all stations with IOPs measurements. The blue and purple lines represent measured and simulated reflectance. The simulated reflectance spectrum is the summation of elastic reflectance (green line) and fluorescence reflectance (red line). Elastic reflectance refers to generating simulated reflectance by considering only total absorption and total backscattering without fluorescence reflectance.

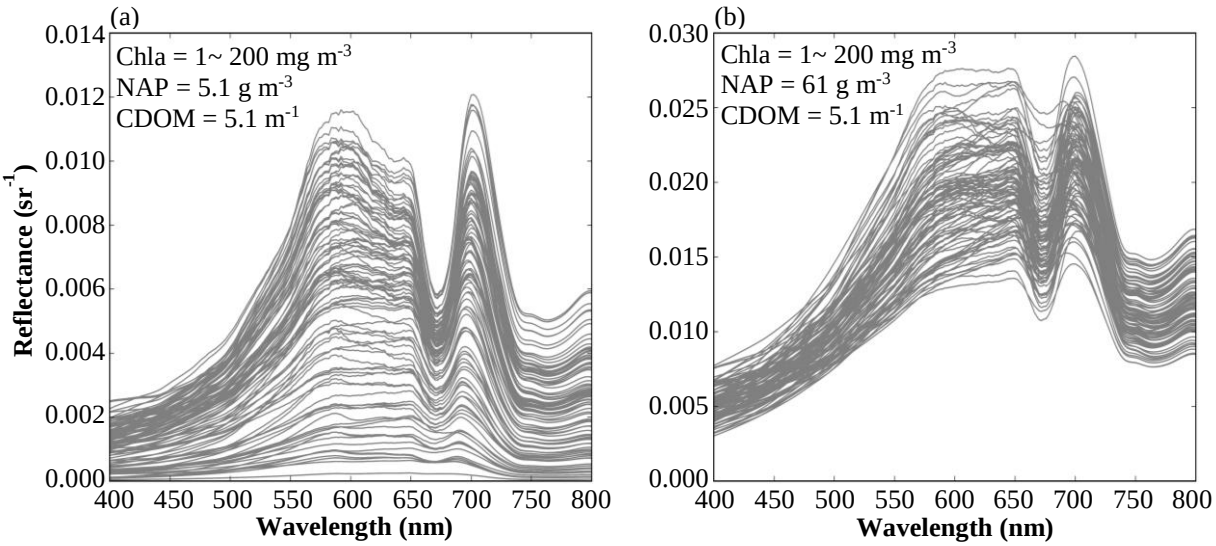

Fig. 4.5. Examples for simulated reflectance spectra of the wide range scenario. Both panels show simulated reflectance spectra for Chla in range of 1 ~ 200 mg m^{-3} and CDOM of 5.1 m^{-1}: (a) reflectance spectra at low NAP (5.1 g m^{-3}), and (b) reflectance spectra at high NAP (61.0 g m^{-3}).

During the calibration stage, algorithms' indices were estimated using the local parameterization and wide range calibration datasets. The algorithms' indices were then related with the reference Chla to obtain the regression coefficients of linear, quadratic polynomial and power regression approaches and coefficient of determination (R^2) values were summarized in Table 4.3. The regression coefficients of linear, quadratic polynomial and power approaches generated during the calibration process for both local and wide range scenarios were summarized in Table 4.4.Fig. 4.6 and Fig. 4.7 show scatterplots of reference Chla versus algorithms' indices for the wide range and local parameterization scenarios, respectively. The R^2 values for the local parameterization scenario in the calibration stage were higher than that of the wide range, because of the fact that the local parameterization dataset is a noise-free simulation data (Yang et al., 2011a). The 4b_tuning, 3b_tuning, and 3b_665 revealed a relatively high correlation with reference Chla for both scenarios with R^2 ranged from 0.89 to 0.99. The algorithms incorporated 680 nm band introduced a higher correlation in the wide range scenario than the local parameterization scenario. The MCI_665, MCI_680, and SCI_4b introduced the lowest correlation with reference Chla, particularly for local parameterization scenario with $R^2 < 0.2$. For the validation stage, the Chla concentrations were retrieved using regression coefficient estimated during the calibration stage and simulated reflectance of the validation dataset. In the next sections, an evaluation of the retrieved Chla will be conducted.

Table 4.3 Algorithms evaluation during the calibrations and validation stages for all algorithms using simulated datasets. The calibration datasets for local parameterization and wide ranges scenarios were generated based on IOPs from Tokyo bay and IOCCG database, respectively. A new dependent dataset was generated based on IOPs ranges of IOCCG database to validate both scenarios.

	Local Parameterization				Wide Range			
	Calibration	Validation			Calibration	Validation		
Algorithms	R^2	R^2	RMSE	MARE	R^2	R^2	RMSE	MARE
OC4E	0.00	---	**6.83**	176.93	0.05	---	**9.89**	191.79
2b_665_LN	0.96	0.77	67.80	75.07	0.77	0.77	27.50	81.86
2b_665_QP	0.96	0.75	69.55	70.11	0.75	0.75	29.08	81.23
2b_665_PW	0.96	---	69.42	74.52	0.72	---	30.66	98.62
2b_680_LN	0.50	0.78	40.77	113.28	0.78	0.78	27.33	70.58
2b_680_QP	0.54	0.75	42.07	110.72	0.75	0.75	29.15	73.82
2b_680_PW	0.58	0.67	45.81	116.06	0.72	0.72	30.85	96.34
2b_max_min_LN	0.78	0.58	68.47	**55.53**	0.58	0.58	37.39	104.33
2b_max_min_QP	0.71	0.54	65.84	84.99	0.53	0.53	39.44	126.63
2b_max_min_PW	0.78	0.59	68.21	**54.04**	0.63	0.63	34.98	61.85
3b_665_LN	0.95	**0.90**	53.58	62.35	0.89	0.90	18.71	59.50
3b_665_QP	0.95	**0.90**	53.67	62.04	0.89	0.90	18.71	58.93
3b_665_PW	0.95	---	55.31	59.91	0.88	---	19.80	57.97
3b_680_LN	0.51	**0.93**	**32.15**	105.50	**0.93**	**0.93**	15.62	46.11
3b_680_QP	0.53	0.89	35.87	128.68	**0.93**	**0.93**	15.58	48.82
3b_680_PW	0.53	**0.90**	34.90	121.13	0.91	---	17.55	48.40
3b_tuning_LN	**0.99**	0.87	59.55	69.68	**0.93**	**0.93**	15.09	**45.31**
3b_tuning_QP	**0.99**	0.87	60.39	64.83	**0.93**	**0.93**	**15.05**	46.90
3b_tuning_PW	**0.99**	---	61.39	61.68	0.91	---	17.46	58.79
4b_tuning_LN	**0.98**	0.70	**34.09**	66.38	**0.94**	**0.93**	**14.73**	**40.10**
4b_tuning_QP	**0.98**	0.70	34.11	66.29	**0.94**	**0.94**	25.61	118.63
4b_tuning_PW	**0.98**	---	35.47	57.21	0.82	0.81	25.61	118.63
MCI_665_LN	0.17	0.38	112.51	406.49	0.38	0.38	45.45	154.44
MCI_665_QP	0.18	0.40	196.38	510.71	0.40	0.40	44.83	152.70
MCI_665_PW	0.19	0.39	356.58	633.04	0.40	0.40	44.77	155.56
MCI_680_LN	0.15	0.50	98.57	343.19	0.50	0.50	40.88	115.11
MCI_680_QP	0.17	0.50	182.70	418.79	0.50	0.50	40.76	123.71
MCI_680_PW	0.17	0.46	299.45	484.54	0.50	0.50	40.67	116.69
NDCI_665_LN	0.92	0.78	63.39	94.71	0.78	0.78	27.18	93.75
NDCI_665_QP	0.97	0.74	70.75	67.58	0.78	0.78	26.90	83.78
NDCI_665_PW	0.97	---	70.18	69.38	0.71	---	---	---
NDCI_680_LN	0.42	0.79	40.65	126.07	0.79	0.79	26.56	80.09
NDCI_680_QP	0.58	0.71	44.56	110.26	0.79	0.79	26.49	75.50
NDCI_680_PW	0.49	0.79	113.29	95.39	0.77	---	---	---
NDCI_max_min_LN	0.82	0.63	69.58	94.91	0.63	0.63	34.98	76.17
NDCI_max_min_QP	0.79	0.55	69.55	62.13	0.70	0.70	31.71	60.07
NDCI_max_min_PW	0.81	0.58	69.69	**57.00**	0.65	0.65	34.02	57.33
SCI_4b_LN	0.20	0.07	165.67	228.68	0.07	0.07	55.53	223.13
SCI_4b_QP	0.23	0.07	532.09	769.97	0.07	0.07	55.59	226.13
SCI_4b_PW	0.23	---	65.82	922.62	0.08	---	55.52	222.66
SCI_max_min_LN	0.56	0.75	150.49	183.90	0.75	0.75	28.85	**41.88**
SCI_max_min_QP	0.56	0.75	99.60	184.22	0.77	0.77	27.98	52.44
SCI_max_min_PW	0.56	---	157.97	140.44	0.74	0.74	29.58	56.79

The highest three performance algorithms were highlighted in bold.
The lowest three performance algorithms were single underlined.

Table 4.4 Linear, quadratic polynomial and power regression coefficients during calibration process for local parameterization and wide range IOPs scenarios.

	Local Parameterization			Wide Range		
Algorithms	a	b	c	a	b	c
2b_665_LN	155.46	-141.31	---	304.32	-261.24	---
2b_665_QP	42.14	27.45	-49.71	110.24	30.51	-94.57
2b_665_PW	13.20	-6.95	1.74	16.46	-8.21	1.88
2b_680_LN	142.68	-86.12	---	295.80	-254.96	---
2b_680_QP	47.46	30.67	-24.75	104.92	29.94	-90.03
2b_680_PW	0.01	1.01	246.47	14.63	-6.79	1.92
2b_max_min_LN	128.49	-124.90	---	213.29	-182.64	---
2b_max_min_QP	27.60	21.77	-26.74	62.12	25.42	-45.29
2b_max_min_PW	175.72	-175.72	0.94	2002.34	-2002.34	0.72
3b_665_LN	350.29	17.50	---	626.91	31.19	---
3b_665_QP	7.82	346.66	17.72	30.27	620.36	31.31
3b_665_PW	108.07	11.88	1.26	66.33	9.32	1.62
3b_680_LN	**320.97**	**55.08**	---	624.45	27.70	---
3b_680_QP	524.46	171.45	57.06	-109.79	650.00	27.09
3b_680_PW	2.84	2.85	3.85	63.28	8.92	1.63
3b_tuning_LN	442.64	1.14	---	1931.03	34.98	---
3b_tuning_QP	125.88	387.85	4.97	-1121.35	2007.35	34.61
3b_tuning_PW	109.32	6.49	1.33	137.36	7.98	1.79
4b_tuning_LN	126.40	-0.80	---	**1315.75**	**1252.01**	---
4b_tuning_QP	0.18	126.11	-0.72	41.99	-37.02	32.41
`4b_tuning_PW	47.16	5.94	1.21	-0.03	0.96	-291.39
MCI_665_LN	28361.04	39.12	---	19068.81	-9.17	---
MCI_665_QP	4020694.75	14728.90	46.94	1208885.88	6474.20	19.05
MCI_665_PW	1.71	1.02	205.42	62.74	1.63	6.63
MCI_680_LN	25473.12	54.47	---	20525.57	-8.56	---
MCI_680_QP	3871337.50	15875.36	56.07	1296821.88	7055.46	21.35
MCI_680_PW	1.67	1.02	191.98	3201.62	4.90	1.48
NDCI_665_LN	453.89	9.57	---	724.11	41.93	---
NDCI_665_QP	804.20	200.28	16.26	462.70	661.01	41.73
NDCI_665_PW	8.82	2.74	2.97	3.88	1.30	3.61
NDCI_680_LN	311.45	63.43	---	720.36	38.49	---
NDCI_680_QP	1138.25	186.80	45.97	229.99	684.93	38.68
NDCI_680_PW	2.48	1.26	2.04	3.53	1.29	2.53
NDCI_max_min_LN	476.68	-22.66	---	635.72	15.15	---
NDCI_max_min_QP	647.10	160.16	8.40	-2220.14	1309.20	-23.60
NDCI_max_min_PW	122.84	0.00	1.32	1819.05	0.22	0.84
SCI_4b_LN	62498.71	105.65	---	-16818.44	61.55	---
SCI_4b_QP	-47629108.00	73981.28	115.30	798889.88	-12357.51	66.96
SCI_4b_PW	1625298437.87	1045700.74	0.34	-39036.16	112.38	0.87
SCI_max_min_LN	49359.57	15.73	---	18622.68	21.93	---
SCI_max_min_QP	-2852058.25	58402.75	10.80	-824219.81	25764.77	12.42
SCI_max_min_PW	40328.45	15.65	1.04	6639.74	15.67	1.22

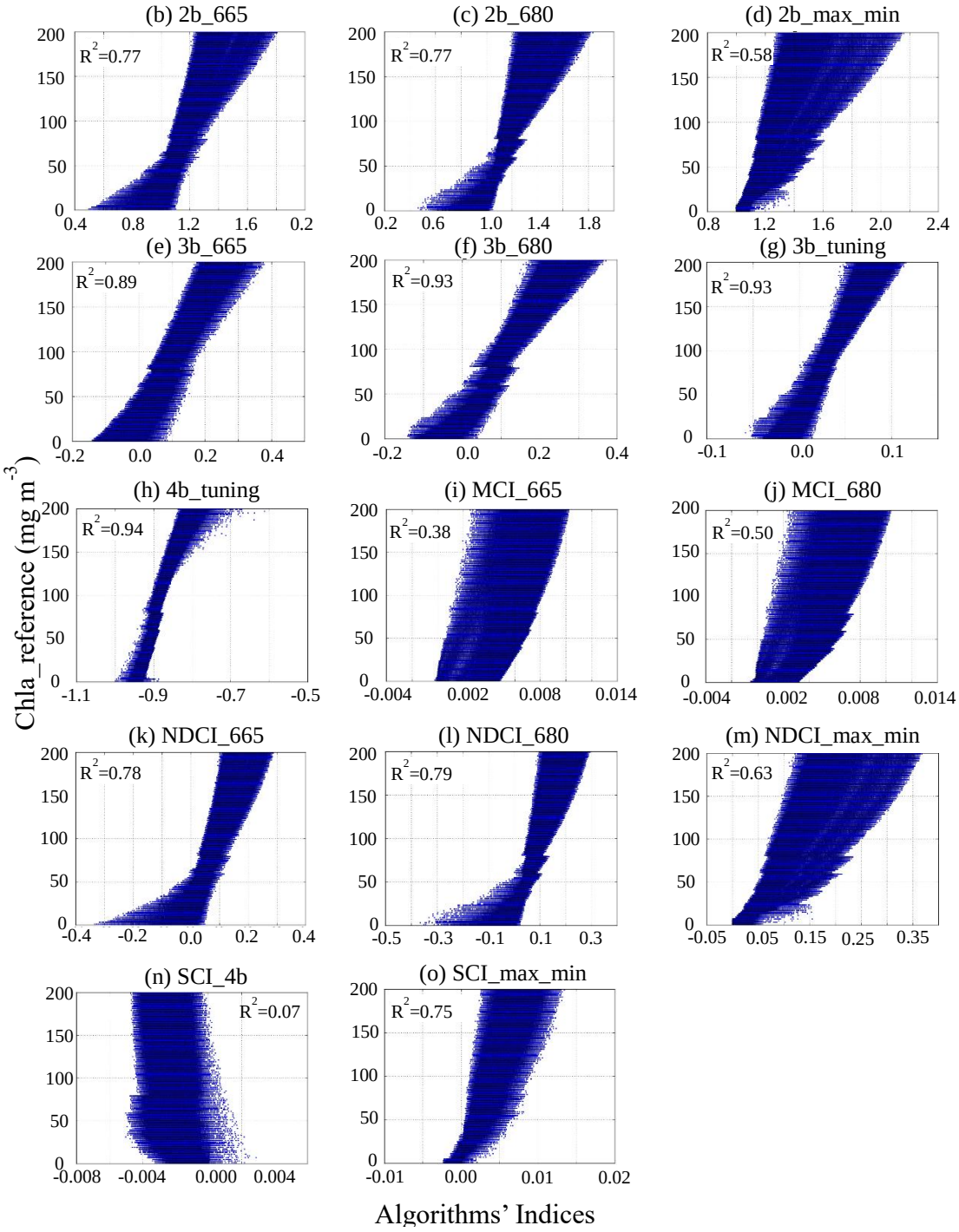

Fig. 4.6. Reference reflectance versus algorithms' ratio for the calibration dataset of wide range scenario.

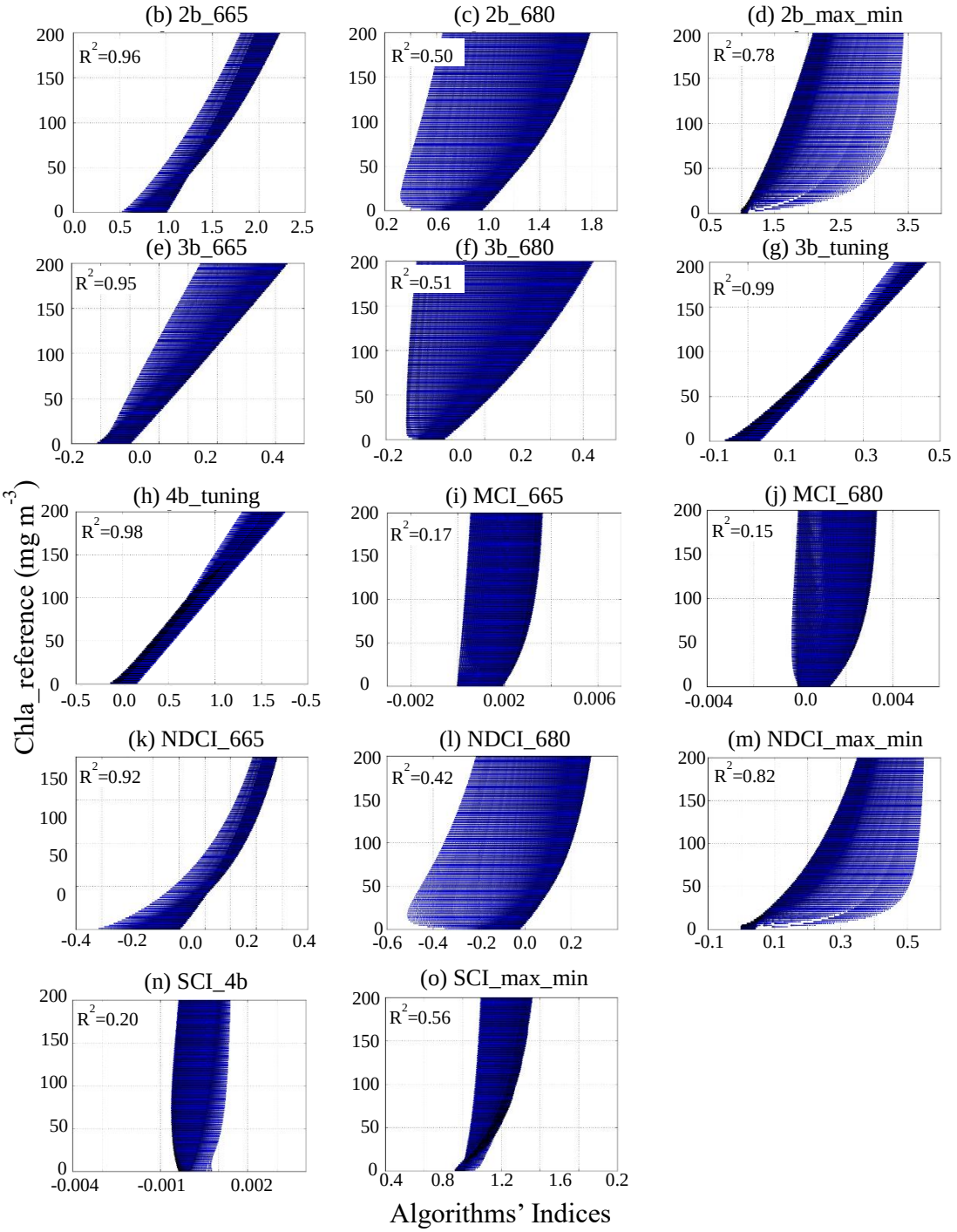

Fig. 4.7. Reference reflectance versus algorithms' ratio for the calibration dataset of local parameterization scenario.

4.5. Results and Discussion

4.5.1. Algorithms' assessment using simulated reflectance dataset

The overall retrieval accuracy of the 43 algorithm combinations was compared in terms of the RMSE and MARE (Table 4.5). Although both scenarios introduced almost same R^2 during the validation stage, the retrieval accuracies of the wide range scenario were higher than the local scenario in terms of RMSE and MARE. The average RMSE and MARE of all algorithms

were (RMSE = 95.92 mg m^{-3}, MARE = 182.81 %) and (RMSE = 30.10 mg m^{-3}, MARE = 95.20 %) for local and wide scenarios, respectively. This result mainly because of both the calibration and validation datasets of the wide range scenario based on wide ranges of IOPs values, which enabled the optimized algorithms to accurately retrieve Chla concentrations. Across all algorithm combinations, the 3b_680_LN and 4b_tuning_LN algorithms outperformed the other algorithms for local (RMSE = 32.15 mg m^{-3}) and wide range (R MSE = 14.73 mg m^{-3}) scenarios, respectively.

The comparison of the three-regression approach (i.e., linear, quadratic polynomial and power regression) among each algorithm revealed that their retrieval accuracies were comparable. Consequently, the RMSE and MARE values were averaged for the three-regression approach within each algorithm (Fig. 4.8). The most three accurate algorithms for local scenario were 3b_680 (RMSE = 34.31 mg m^{-3}), 4b_tuning (RMSE = 34.56 mg m^{-3}), and 2b_680 (RMSE = 42.88 mg m^{-3}). For the wide scenario, the 3b_tuning (RMSE = 15.87 mg m^{-3}), 3b_680 (RMSE = 16.25 mg m^{-3}), and 3b_665 (RMSE = 19.05 mg m^{-3}) outperformed other algorithms. In contrast, the MCI_665, MCI_680, and SCI_4b algorithms showed the highest error for both scenarios, with RMSE > 100.0 mg m^{-3} and > 40.0 mg m^{-3} for local and wide range scenarios, respectively.

The results from the SCI_4b and SCI_max_min revealed that the SCI_max_min provided less error in terms of RMSE which decreased from 254.53 mg m^{-3} to 136.01 mg m^{-3} for local scenario and from 55.55 mg m^{-3} to 28.80 mg m^{-3} for wide ranges scenarios. These result can be attributed to the selected bands because SCI_4b did not contain the 709-nm band, which is significant to Chla retrieval, which is consistent with the results of Gower et al. (2005).

The OC4E algorithm was evaluated using relatively low Chla and NAP concentrations in ranges of 1-20 mg m^{-3} and 1-20 g m^{-3}, respectively. Although the OC4E algorithm was trained using a huge dataset (2804 station) with wide ranges of Chla concentrations (0.01 - 64 mg m^{-3}) (O'Reilly et al., 2000a), it introduced relatively high error for local scenario (RMSE = 6.83 mg m^{-3}, MARE = 176.96 %), and wide range scenario (RMSE = 9.89 mg m^{-3}, MARE = 191.79 %). The MARE of OC4E was very high because the MARE is a relative error, which assesses the Chla retrieval over a small range of Chla values ($\leq$ 20 mg m^{-3}); thus, any small difference between the reference and retrieved Chla concentrations would cause a high relative error. These results reveal the importance of executing an optimization process to determine the coefficients of OC4E with a calibration dataset to improve retrieval accuracy.

Table 4.5 Algorithms evaluation during the calibrations and validation stages for all algorithms using simulated datasets. The calibration datasets for local parameterization and wide ranges scenarios were generated based on IOPs from Tokyo bay and IOCCG database, respectively. A new dependent dataset was generated based on IOPs ranges of IOCCG database to validate both scenarios.

	Local Parameterization				Wide Range			
	Calibration	Validation			Calibration	Validation		
Algorithms	R^2	R^2	RMSE	MARE	R^2	R^2	RMSE	MARE
OC4E	0.00	---	**6.83**	176.93	0.05	---	**9.89**	191.79
2b_665_LN	0.96	0.77	67.80	75.07	0.77	0.77	27.50	81.86
2b_665_QP	0.96	0.75	69.55	70.11	0.75	0.75	29.08	81.23
2b_665_PW	0.96	---	69.42	74.52	0.72	---	30.66	98.62
2b_680_LN	0.50	0.78	40.77	113.28	0.78	0.78	27.33	70.58
2b_680_QP	0.54	0.75	42.07	110.72	0.75	0.75	29.15	73.82
2b_680_PW	0.58	0.67	45.81	116.06	0.72	0.72	30.85	96.34
2b_max_min_LN	0.78	0.58	68.47	**55.53**	0.58	0.58	37.39	104.33
2b_max_min_QP	0.71	0.54	65.84	84.99	0.53	0.53	39.44	126.63
2b_max_min_PW	0.78	0.59	68.21	**54.04**	0.63	0.63	34.98	61.85
3b_665_LN	0.95	**0.90**	53.58	62.35	0.89	0.90	18.71	59.50
3b_665_QP	0.95	**0.90**	53.67	62.04	0.89	0.90	18.71	58.93
3b_665_PW	0.95	---	55.31	59.91	0.88	---	19.80	57.97
3b_680_LN	0.51	**0.93**	**32.15**	105.50	**0.93**	**0.93**	15.62	46.11
3b_680_QP	0.53	0.89	35.87	128.68	**0.93**	**0.93**	15.58	48.82
3b_680_PW	0.53	**0.90**	34.90	121.13	0.91	---	17.55	48.40
3b_tuning_LN	**0.99**	0.87	59.55	69.68	**0.93**	**0.93**	15.09	**45.31**
3b_tuning_QP	**0.99**	0.87	60.39	64.83	**0.93**	**0.93**	**15.05**	46.90
3b_tuning_PW	**0.99**	---	61.39	61.68	0.91	---	17.46	58.79
4b_tuning_LN	**0.98**	0.70	**34.09**	66.38	**0.94**	**0.93**	**14.73**	**40.10**
4b_tuning_QP	**0.98**	0.70	34.11	66.29	**0.94**	**0.94**	25.61	118.63
4b_tuning_PW	**0.98**	---	35.47	57.21	0.82	0.81	25.61	118.63
MCI_665_LN	0.17	0.38	112.51	406.49	0.38	0.38	45.45	154.44
MCI_665_QP	0.18	0.40	196.38	510.71	0.40	0.40	44.83	152.70
MCI_665_PW	0.19	0.39	356.58	633.04	0.40	0.40	44.77	155.56
MCI_680_LN	0.15	0.50	98.57	343.19	0.50	0.50	40.88	115.11
MCI_680_QP	0.17	0.50	182.70	418.79	0.50	0.50	40.76	123.71
MCI_680_PW	0.17	0.46	299.45	484.54	0.50	0.50	40.67	116.69
NDCI_665_LN	0.92	0.78	63.39	94.71	0.78	0.78	27.18	93.75
NDCI_665_QP	0.97	0.74	70.75	67.58	0.78	0.78	26.90	83.78
NDCI_665_PW	0.97	---	70.18	69.38	0.71	---	---	---
NDCI_680_LN	0.42	0.79	40.65	126.07	0.79	0.79	26.56	80.09
NDCI_680_QP	0.58	0.71	44.56	110.26	0.79	0.79	26.49	75.50
NDCI_680_PW	0.49	0.79	113.29	95.39	0.77	---	---	---
NDCI_max_min_LN	0.82	0.63	69.58	94.91	0.63	0.63	34.98	76.17
NDCI_max_min_QP	0.79	0.55	69.55	62.13	0.70	0.70	31.71	60.07
NDCI_max_min_PW	0.81	0.58	69.69	**57.00**	0.65	0.65	34.02	57.33
SCI_4b_LN	0.20	0.07	165.67	228.68	0.07	0.07	55.53	223.13
SCI_4b_QP	0.23	0.07	532.09	769.97	0.07	0.07	55.59	226.13
SCI_4b_PW	0.23	---	65.82	922.62	0.08	---	55.52	222.66
SCI_max_min_LN	0.56	0.75	150.49	183.90	0.75	0.75	28.85	**41.88**
SCI_max_min_QP	0.56	0.75	99.60	184.22	0.77	0.77	27.98	52.44
SCI_max_min_PW	0.56	---	157.97	140.44	0.74	0.74	29.58	56.79

The highest three-performance algorithms were highlighted in bold.

The lowest three-performance algorithms were single underlined.

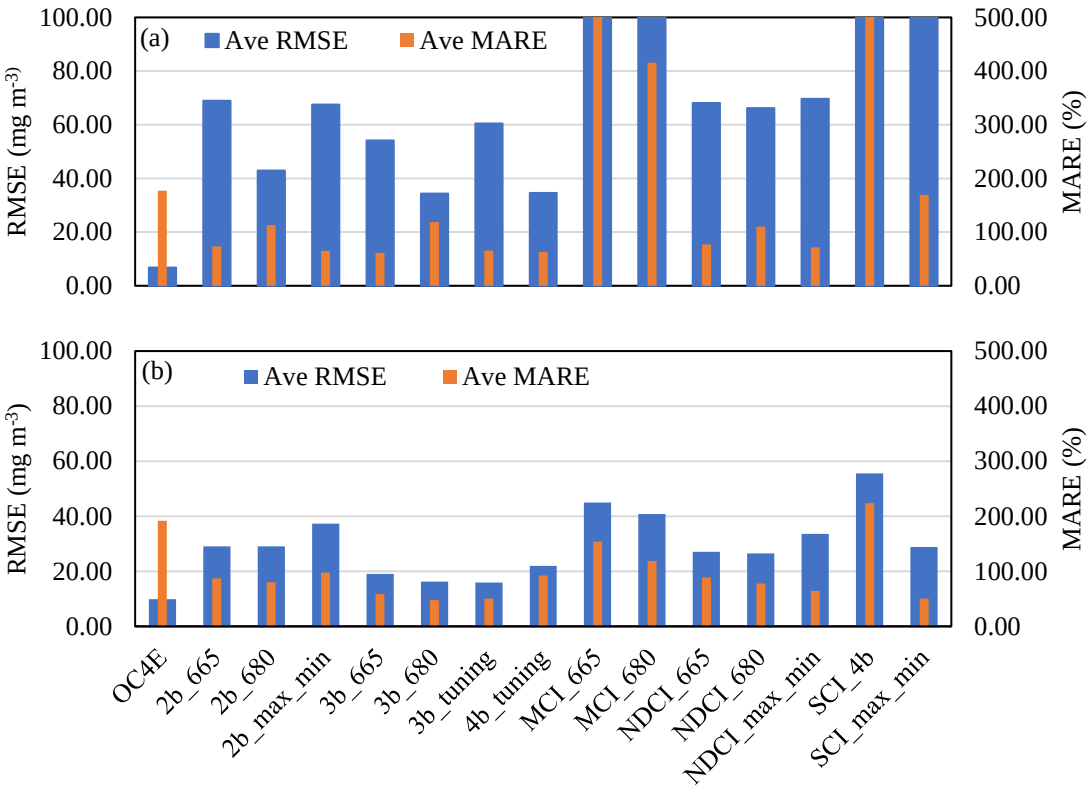

Fig. 4.8. Overall assessment of the 15 algorithms in terms of RMSE and MARE. The values for RMSE and MARE were averaged for the three regression approaches of each algorithm (e.g., the RMSE and MARE of 2b_665_LN, 2b_665_QP, and 2b_665_PW were averaged as 2b_665).

4.5.2. Algorithm performance by considering Chla and NAP.

As explained, the bio-optical model links the remote sensing reflectance with IOPs (i.e., total absorption and total backscattering). The CDOM only contributes to the total absorption, while the Chla and NAP are fractions of both the absorption and backscattering. The CDOM absorption is very high in the blue wavelengths and exponentially decreases with increasing wavelength. Thus, its contribution to the total absorption in the red-NIR wavelengths is very low compared to that of phytoplankton, which has a relatively high absorption in the red-NIR wavelengths (Dogliotti et al., 2015). In addition, increasing the NAP increases the total backscattering and the backscattering in the NIR wavelengths. The reflectance spectra were compared for two groups of simulated reflectance to reveal the influence of changing CDOM concentrations on the simulated reflectance for blue-green and red-NIR regions for wide and local parameterization scenarios as shown in Fig. 4.9 and Fig. 4.10, respectively. Within each group, the concentrations of Chla and NAP were fixed, while the CDOM was examined at three concentrations: low (0.1 m^{-1}), moderate (2.5 m^{-1}) and high (9.9 m^{-1}). For both groups, the influence of changing CDOM concentrations was relatively higher in the blue-green region than in the red-NIR region. Case 2 waters' algorithms mainly use the reflectance spectra in the

red-NIR region. Accordingly, the algorithms' retrieval accuracy was assessed for various combinations of Chla and NAP.

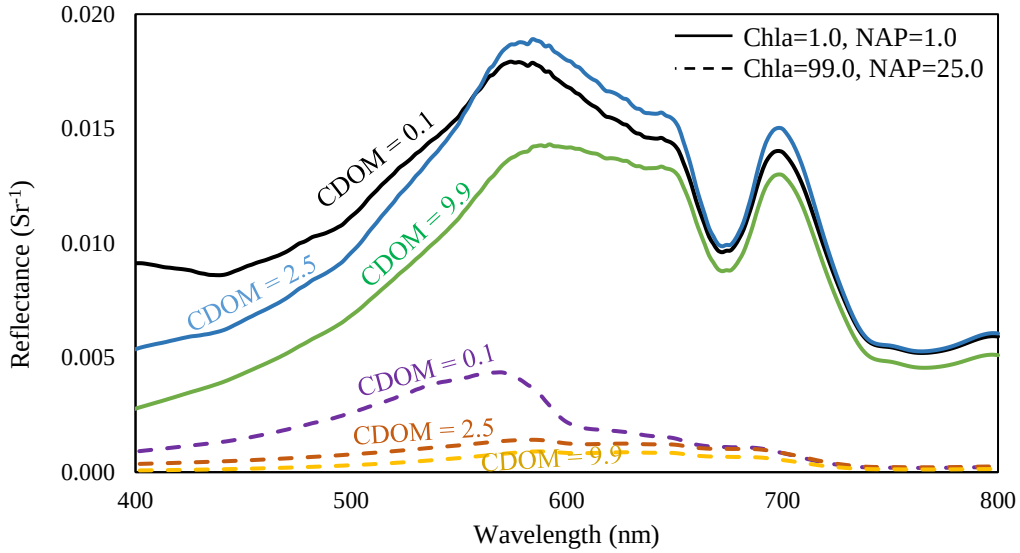

Fig. 4.9. Comparing the influence of changing CDOM concentrations on the simulated reflectance spectra of wide range scenario within the blue-green and red-NIR regions. The CDOM concentrations were 0.1, 2.5 and 9.9 m^{-1}. The solid lines indicate Chla and NAP concentrations of 1.0 mg m^{-3} and 1.0 g m^{-3}, respectively. The dashed lines indicate a Chla of 99 mg m^{-3} and NAP of 25 g m^{-3}.

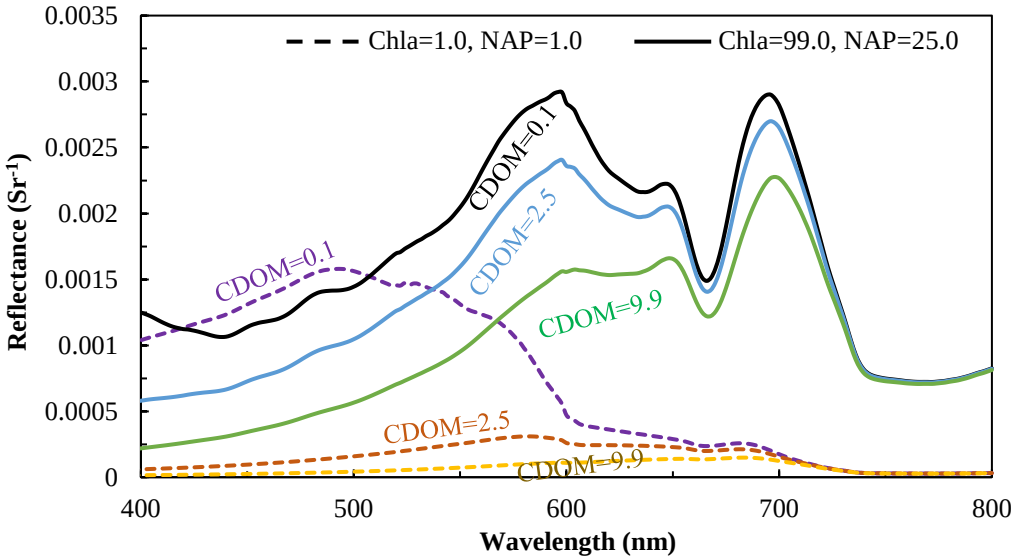

Fig. 4.10. Comparing the influence of changing CDOM concentrations on the simulated reflectance spectra of local scenario within the blue-green and red-NIR regions. The CDOM concentrations were 0.1, 2.5 and 9.9 m^{-1}. The solid lines indicate Chla and NAP concentrations of 1.0 mg m^{-3} and 1.0 g m^{-3}, respectively. The dashed lines indicate a Chla of 99 mg m^{-3} and NAP of 25 g m^{-3}.

The RMSE of the 43 algorithms were estimated between the reference and retrieved Chla for each Chla and NAP combination at local (Fig. 4.11) and wide range scenarios (Fig. 4.12). The red colors indicate low error, whereas the blue colors indicate high error with an upper limit of 40 mg m^{-3} for RMSE. The overall comparison among the two scenarios revealed that the wide range scenario provided higher retrieval accuracy than local scenario. These results achieved because the algorithms were calibrated and validated with wide range of IOPs to simulate reflectance, in contrast to local scenario that was calibrated with local IOPs and validated with wide range of IOPs.

For the wide range scenario, twelve out of the 43 combinations (3b_665, 3b_680, 3b_tuning and 4b_tuning with linear, quadratic polynomial and power models) introduced less error for different concentrations' combinations of Chla and NAP (Fig. 4.12). The second-tier of algorithms resulted in acceptable accuracies at the wide range scenario were (2b_665, 2b_680, 2b_max_min, NDCI_665, NDCI_680, and NDCI_max_min with linear, quadratic polynomial and power models. The second-tier algorithms were accurate with moderate Chla and NAP concentrations (Fig. 4.12). The MCI and SCI algorithms with different combinations showed the lowest retrieval accuracies. The performance of SCI_Max_min was higher than SCI_4b, because of using the maximum and minimum technique to find the optimal band enabled SCI_Max_min to correlate with Chla concentration.

For the local parameterization scenario, the two-, three-band, and NDCI algorithms incorporated 665-nm band or band tuning technique introduced high retrieval accuracy for Chla < 50 mg m^{-3}, while same algorithms incorporated 680-nm band provided high accuracy for Chla from 50 mg m^{-3} to 80 mg m^{-3}. These results can be attributed to the phytoplankton absorption and fluorescence because the maximum phytoplankton absorption in the red region of spectrum is located near 665-nm and the maximum fluorescence is located near 680-nm. Therefore, the algorithms incorporated bands correlated with absorption could be more accurate to capture Chla concentration less than 50 mg m^{-3}. While the fluorescence will be a significant factor to retrieve Chla concentration with increasing Chla concentration more than 50 mg m^{-3}.

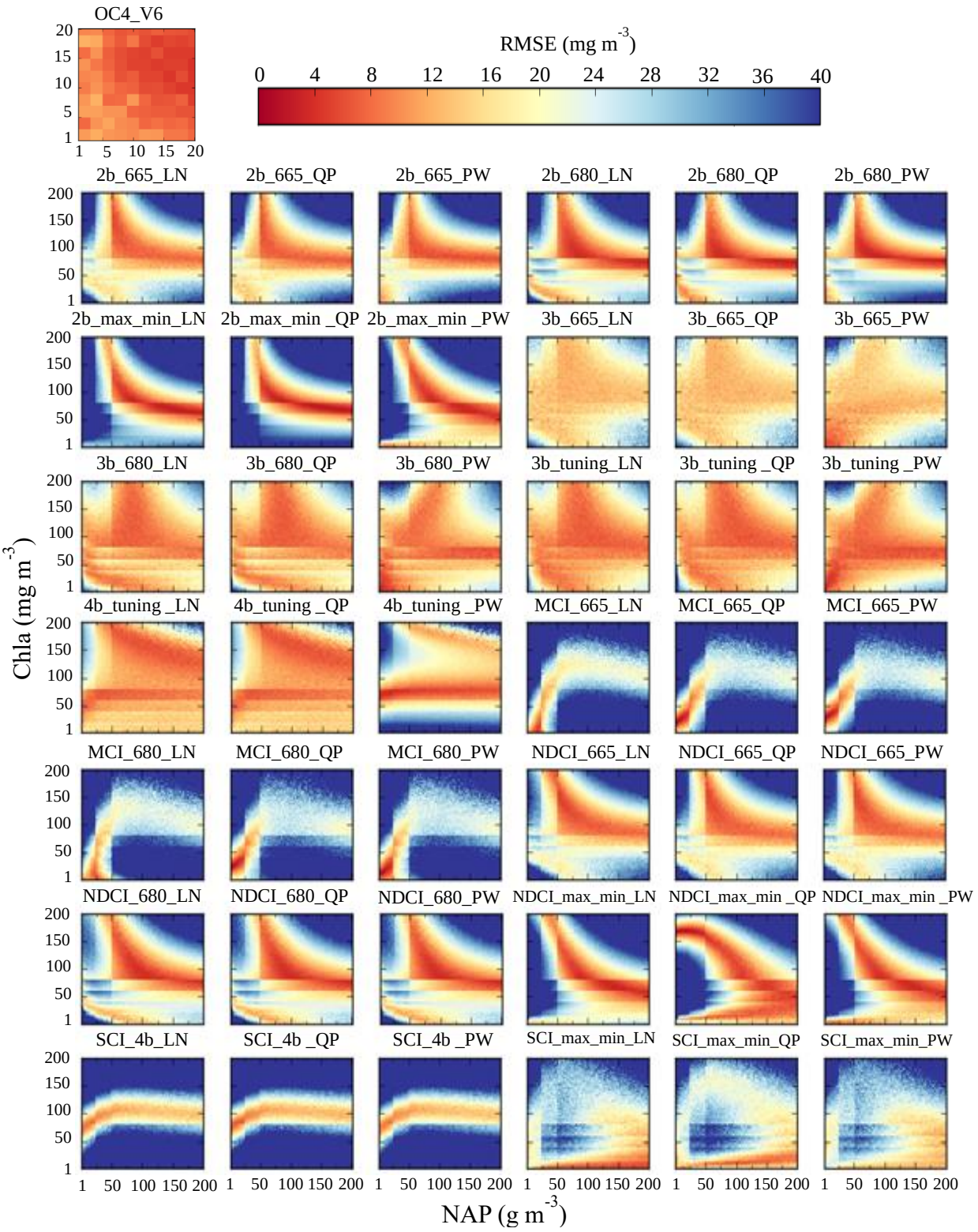

Fig. 4.11. RMSEs of the 43 algorithms between the reference and retrieved Chla for each Chla and NAP combination in case of wide range simulated reflectance.

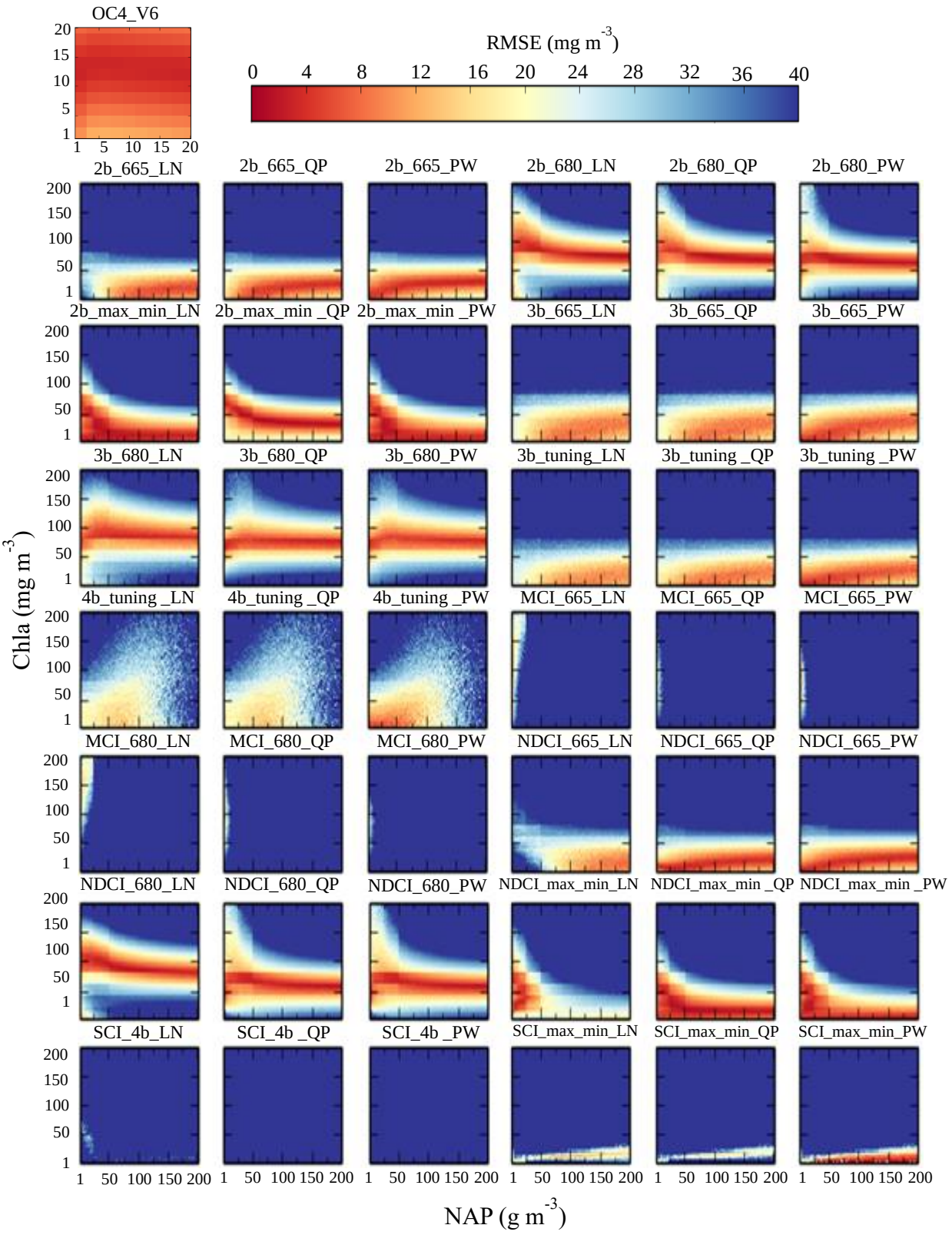

Fig. 4.12. RMSEs of the 43 algorithms between the reference and retrieved Chla for each Chla and NAP combination in case of local parameterized simulated reflectance.

The Chla retrieval accuracy of OC4E in terms of RMSE was about 8.0 mg m^{-3} for various combinations of Chla and NAP at both scenarios (Figs. 4.11 and 4.12). However, this retrieval

accuracy can be considered as a low accuracy, due to the fact that the OC4E was investigated in low ranges of Chla and NAP. This result can be attributed to two reasons; (1) the coefficients of OC4E need to be optimized with calibration dataset to improve the retrieval accuracy, and (2) high absorbance of NAP and CDOM along with Chla in the blue-green wavelengths could affect the accuracy of OC4E to precisely retrieve Chla.

4.5.3. The most accurate algorithms among Chla and NAP combinations.

The retrieval accuracies by using linear, quadratic polynomial and power regression were comparable as concluded in section 3.1.1. Thus, the quadratic polynomial regression approaches along with OC4E were compared to find the most accurate algorithms among Chla and NAP combinations, resulting in 15 algorithms listed in Table 4.6. A total of 10,000 combinations of Chla and NAP concentrations existed. The lowest RMSE values were selected among the 15 algorithms to find the most accurate algorithm for each combination of Chla and NAP. Table 4.6 summarizes the frequency of producing the minimum error for each algorithm. The 3b_680_QP and 3b_tuning outperformed other algorithms in terms of frequency for local (27.78 %) and wide range (33.19 %) scenario, respectively. In addition, the ten algorithms that required only multispectral data (i.e., OC4E and the nine multi-band algorithms and excluding all algorithms that required band tuning) were also examined. The 3b_680_QP also introduced the outstanding accuracy for being the most frequent algorithm among the ten multi-band algorithms for both local (50.66 %) and wide range (60.52 %) scenarios.

Table 4.6 Frequency of each algorithm to achieve the minimum RMSE of the 10,000 combinations of Chla and NAP concentrations. The evaluation executed among OC4E and quadratic polynomial algorithms only.

	Frequency			
	All 15 algorithms		Multi-band algorithms only	
Algorithms	local parameterization	Wide Range	local parameterization	Wide Range
OC4E	43	63	63	76
2b_665_QP	133	49	764	212
2b_680_QP	1257	355	**1259**	**1208**
2b_max_min_QP	904	535	---	---
3b_665_QP	3	145	218	**880**
3b_680_QP	**2778**	1143	**5066**	**6052**
3b_tuning_QP	24	**3319**	---	---
4b_tuning_QP	**2291**	**1304**	---	---
MCI_665_QP	2	87	2	164
MCI_680_QP	3	92	3	116
NDCI_665_QP	194	154	878	403
NDCI_680_QP	**1264**	458	**1747**	724
NDCI_max_min_QP	1103	**1875**	---	---
SCI_4b_QP	0	102	0	165
SCI_max_min_QP	1	19	---	---

The best three algorithms in terms of frequency were highlighted in bold.

Fig. 4.13 illustrates the spatial distribution of the best three algorithms by considering all 15 algorithms and the ten multi-band algorithms for both scenarios. In general, the 3b_680_QP was the most accurate in three out of the four cases, especially with high Chla concentration (Fig. 4.13). This result was observed because the 3b_680_QP is correlated with maximum phytoplankton fluorescence at 680-nm, which could be a dominant factor to retrieve high Chla concentration. The band tuning algorithms were more accurate than other algorithms by considering all 15 algorithms for wide range scenario (Fig. 4.13c). Overall, there was a complex interaction between the spatial distribution of the most accurate algorithms in wide range scenario (Fig. 4.13c and Fig. 4.13d) in comparison with local scenario (Fig. 4.13a and Fig. 4.13b). This is mostly because of the fact that the local parameterization dataset is a noise-free simulated data (Yang et al., 2011a). Clearly, no single algorithm can provide outstanding accuracy for Chla retrieval, and multi-algorithms should be included to reduce the error. This finding is consistent with those of recently published results (Lyu et al., 2015; Moore et al., 2014). In addition, the two-, three-, four-band and NDCI algorithms were more accurate when retrieving the Chla concentration than the other algorithms.

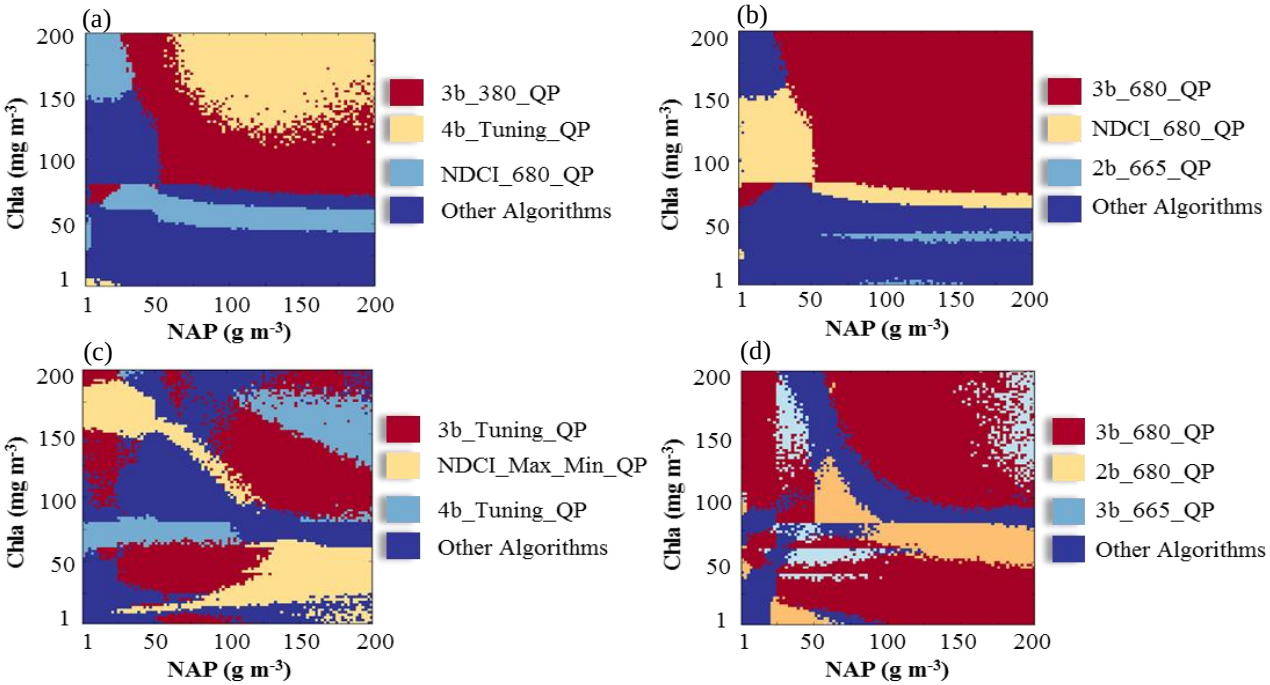

Fig. 4.13. Colors illustrate the most accurate algorithms with the lowest RMSE by considering the Chla and NAP concentrations. The OC3E and quadratic polynomial algorithms were only compared (i.e., 15 algorithm combinations). Top panels represent local parameterization scenario: (a) top 3 algorithms of the 15 algorithm combinations; (b) top 3 algorithms of 10 multi-band algorithm combinations (i.e., excluding the algorithm combinations that relied on hyperspectral data, such as algorithms with the maximum and minimum). Lower panels denote

wide range scenario: (c) top 3 algorithms of the 15 algorithm combinations (d) top 3 algorithms of 10 multi-band algorithm combinations.

4.5.4. Algorithms' assessment using field measurements

The 43 algorithms were evaluated based on five measured datasets to address the similarities and differences in performances from the simulated datasets. The first dataset comprised all the measured samples at Tokyo Bay (i.e., 70 samples with full water quality parameters and water surface reflectance values). The second dataset included 12 out of the 70 samples that had IOP measurements in addition to the water quality parameters and water surface reflectance. The other three datasets (i.e., datasets 3, 4 and 5) were obtained by classifying the 70 samples depending on their trophic status into mesotrophic, eutrophic and hypertrophic datasets (Vollenweider and Kerekes, 1982). The Chla retrieval accuracy for the 43 algorithms was assessed, as shown in Table 4.7. The regression coefficients of linear, quadratic polynomial and power approaches generated during the calibration process for the first dataset were summarized in Table 4.8.The retrieval accuracy of the five datasets was compared, and the most accurate algorithm varied among these datasets. The MCI_665_QP, 4b_tuning_QP, and 3b_tuning_QP algorithms outperformed the others for dataset 1 (RMSE = 13.46 mg m^{-3}), dataset 2 (RMSE = 3.73 mg m^{-3}), and dataset 3 (RMSE = 14.34mg m^{-3}), respectively (Table 4.7). However, NDCI_665_QP outperformed the others for both datasets 3 and 4, displaying low RMSEs of 1.44 and 3.04 mg m^{-3}, respectively.

The best three algorithms in terms of RMSE for the five datasets were highlighted in bold (Table 4.7). Eleven algorithms achieved the highest retrieval accuracy among the five datasets. 3b_tuning_QP and NDCI_665_QP were among the highest algorithms in multiple datasets. In contrast to the result from simulated dataset, none of the eleven algorithms incorporated the 680-nm band. Furthermore, eight out of the eleven algorithms employed the quadratic polynomial regression model.

OC4E introduced the lowest retrieval accuracy in terms of RMSE for all the datasets, even for dataset 3 (Chla < 8.0 mg m^{-3}). This result was observed because OC4E was proposed for applications in open oceans, where the optical properties are dominated by the Chla concentrations. In contrast, the optical properties of Tokyo Bay are influenced not only by Chla but also by NAP and CDOM, especially in the blue and green wavelengths, which are used to substitute for the OC4E algorithm. Therefore, the coefficients of the OC4E should be calculated first in calibration process to improve the retrieval accuracy.

Table 4.7 Algorithm evaluations for different datasets (i.e., sample number and trophic status) using in situ dataset.

	Dataset 1			Dataset 2	Dataset 3	Dataset 4	Dataset 5
	All samples			Stations with IOPs	Chla		
					< 8.0	8.0 - 25.0	> 25.0
	R^2	RMSE	MARE	RMSE	RMSE	RMSE	RMSE
Algorithms	n = 70			n = 12	n = 23	n = 24	n = 23
OC4_V6	- - -	23.02	**53.55**	18.40	3.51	7.63	39.27
2b_665_LN	0.53	14.68	91.53	4.92	1.75	3.46	15.13
2b_665_QP	**0.56**	14.21	83.33	4.78	**1.51**	3.20	15.07
2b_665_PW	0.54	14.51	83.79	4.77	1.55	3.42	15.13
2b_680_LN	0.43	16.06	131.16	7.50	1.90	4.01	15.08
2b_680_QP	0.50	15.10	107.37	6.40	1.52	3.85	14.96
2b_680_PW	0.45	15.80	129.13	6.65	1.81	4.01	15.08
2b_max_min_LN	0.41	16.35	96.25	6.20	1.67	3.40	15.35
2b_max_min_QP	0.41	16.33	94.92	5.90	1.58	**3.08**	14.92
2b_max_min_PW	0.41	16.34	95.26	6.14	1.51	3.37	15.35
3b_665_LN	0.52	14.76	95.18	4.36	1.82	3.35	15.23
3b_665_QP	**0.56**	14.19	85.86	4.34	1.79	3.30	15.22
3b_665_PW	0.53	14.55	90.75	**4.32**	1.79	3.33	15.23
3b_680_LN	0.46	15.62	130.91	7.45	1.93	3.90	15.11
3b_680_QP	0.55	14.29	126.67	6.72	1.92	3.86	14.91
3b_680_PW	0.48	15.38	131.58	6.75	1.93	3.90	15.12
3b_tuning_LN	**0.56**	14.06	89.88	4.09	1.62	3.16	14.79
3b_tuning_QP	**0.57**	**13.99**	85.21	4.00	**1.45**	3.15	**14.34**
3b_tuning_PW	0.57	14.02	86.98	3.97	1.51	3.13	14.75
4b_tuning_LN	0.57	14.02	97.70	**3.99**	1.66	3.10	14.76
4b_tuning_QP	0.57	13.92	94.45	**3.73**	1.61	3.10	14.75
4b_tuning_PW	0.57	**13.97**	97.50	- - -	1.60	3.10	14.77
MCI_665_LN	0.53	14.60	96.81	5.19	1.79	3.80	15.16
MCI_665_QP	**0.60**	**13.46**	88.12	5.02	1.59	3.33	14.77
MCI_665_PW	0.55	14.24	81.72	4.99	1.81	3.77	15.18
MCI_680_LN	0.48	15.43	132.82	8.19	1.93	3.99	15.10
MCI_680_QP	0.55	14.22	110.32	6.85	1.69	3.91	14.78
MCI_680_PW	0.50	15.12	131.33	13.08	1.93	4.01	15.11
NDCI_665_LN	0.54	14.41	90.39	5.19	1.72	3.53	15.23
NDCI_665_QP	0.55	14.33	**79.52**	4.64	**1.44**	**3.04**	**14.61**
NDCI_665_PW	0.55	14.30	**76.48**	4.74	1.55	3.48	15.22
NDCI_680_LN	0.47	15.46	114.45	7.90	1.89	4.01	15.04
NDCI_680_QP	0.48	15.41	111.65	6.05	1.51	3.78	15.04
NDCI_680_PW	0.47	15.46	113.41	6.61	1.81	4.01	15.04
NDCI_max_min_LN	0.41	16.42	108.19	6.06	1.63	3.28	15.37
NDCI_max_min_QP	0.41	16.33	94.05	6.06	1.55	**3.04**	14.79
NDCI_max_min_PW	0.41	16.33	94.19	6.06	1.51	3.13	15.37
SCI_4b_LN	0.15	19.68	172.47	7.52	1.81	3.80	15.32
SCI_4b_QP	0.15	19.63	178.04	7.52	1.73	3.62	15.30
SCI_4b_PW	0.15	19.64	180.32	7.50	1.83	3.79	15.32
SCI_max_min_LN	0.41	16.37	146.24	13.90	1.91	3.86	15.11
SCI_max_min_QP	0.42	16.28	149.21	11.07	1.91	3.58	**14.63**
SCI_max_min_PW	0.41	16.43	145.96	13.44	1.91	3.84	15.011

The highest three performance algorithms were highlighted in bold.

The lowest three performance algorithms were single underlined.

The variable "N" refers to the number of samples within each dataset.

Table 4.8 Linear, quadratic polynomial and power regression coefficients for in-situ measurements.

	Dataset 1 (All Samples)		
Algorithms	a0	a1	a2
2b_665_LN	38.41	-17.06	---
2b_665_QP	-15.56	79.83	-40.72
2b_665_PW	96.81	-52.85	0.82
2b_680_LN	65.33	-23.62	---
2b_680_QP	-63.38	183.41	-72.52
2b_680_PW	225.52	-99.18	0.77
2b_max_min_LN	31.60	-28.72	---
2b_max_min_QP	-4.24	46.52	-40.98
2b_max_min_PW	49.83	-48.23	0.90
3b_665_LN	133.80	20.74	---
3b_665_QP	-242.01	179.74	23.35
3b_665_PW	368.68	45.61	0.81
3b_680_LN	248.76	42.46	---
3b_680_QP	-1009.03	209.38	49.18
3b_680_PW	466.77	73.77	0.87
3b_tuning_LN	131.38	17.32	---
3b_tuning_QP	-73.30	148.44	17.84
3b_tuning_PW	251.19	27.74	0.87
4b_tuning_LN	89.63	18.18	---
4b_tuning_QP	-41.60	103.64	18.92
4b_tuning_PW	172.46	29.59	0.87
MCI_665_LN	39975.86	6.69	---
MCI_665_QP	-32482174.00	84559.31	-1.01
MCI_665_PW	151496.57	4.64	0.76
MCI_680_LN	52741.51	19.36	---
MCI_680_QP	-57163884.00	89261.59	21.78
MCI_680_PW	260829.07	64.31	0.73
NDCI_665_LN	93.32	24.13	---
NDCI_665_QP	46.44	90.27	22.75
NDCI_665_PW	31.61	10.32	1.34
NDCI_680_LN	117.68	44.57	---
NDCI_680_QP	-52.46	105.45	44.93
NDCI_680_PW	99.14	38.12	1.04
NDCI_max_min_LN	112.02	-1.83	---
NDCI_max_min_QP	111.01	61.89	2.19
NDCI_max_min_PW	24.28	1.78	1.56
SCI_4b_LN	12981.87	16.59	---
SCI_4b_QP	2409751.50	9115.53	16.91
SCI_4b_PW	30.11	1.16	18.89
SCI_max_min_LN	30439.76	-14.35	---
SCI_max_min_QP	-6459144.50	49664.88	-26.88
SCI_max_min_PW	16389.72	-5.38	1.16

The SCI_4b algorithm with linear, quadratic polynomial, and power regression models also introduced poor performances. For instance, SCI_4b_PW produced the highest MARE of 180.32 % and lowest R^2 of 0.15 for dataset 1. In contrast, SCI_max_min_QP was one of the best of the eleven algorithms, which can be attributed to the band selection because SCI_max_min incorporated the reflectance peak at 709 nm, while SCI_4b did not. These results reveal the importance of incorporating the 709-nm wavelength to retrieve Chla with adequate accuracy.

The Chla retrieval accuracies of the ten algorithms with the lowest RMSE for dataset 1 were evaluated by comparing the measured and retrieved Chla (Fig. 4.14a) and by calculating $Error_{log}$ between the measured and retrieved Chla (Fig. 4.14b). A common trend existed among these algorithms, which overestimated low Chla concentrations (Chla $\leq$ 6.0 mg m^{-3}) with $Error_{log} > 0.1$ and underestimated high Chla concentrations (Chla > 50.0 mg m^{-3}) with $Error_{log} < - 0.08$, as shown in Figs. 4.14a and 4.14b. No bias occurred for Chla concentrations from 7.0 to 50 mg m^{-3}. The values of the retrieved Chla from 43 algorithm combinations at 12 stations with dataset 2 were plotted as a box-whisker plot as a comparison with the measured Chla (Fig. 4.15). The results indicated that the retrieved Chla was overestimated for Chla $\leq$ 10.50 mg m^{-3} (i.e., stations 1 to 6), whereas all the algorithms considerably underestimated the retrieved Chla, as can be seen at station 10, which had a measured Chla of 42.30 mg m^{-3}. The results from datasets 1 and 2 revealed the limitation of the investigated algorithms to accurately retrieve low and high Chla concentrations, which implies the importance of developing new algorithms that can reduce the influence of NAP and CDOM to accurately retrieve the Chla concentrations in turbid water.

4.5.5. Comparing the algorithms' performance for in-situ and simulated datasets

Comparing the results of both the measured and simulated datasets revealed similarities and differences among the performances of the 43 algorithms. The 3b_tuning and 4b_tuning with the three regression models, provided high performance for the in situ and simulated datasets. The lowest accuracy was obtained by the SCI_4b algorithms, with average RMSEs of 763.58 mg m^{-3}, 55.55 mg m^{-3} and 19.65 mg m^{-3} for the local simulated, wide range simulated, and in situ dataset 1, respectively. This result can be attributed to the bands that were used for SCI_4b, which did not incorporate the 709-nm band.

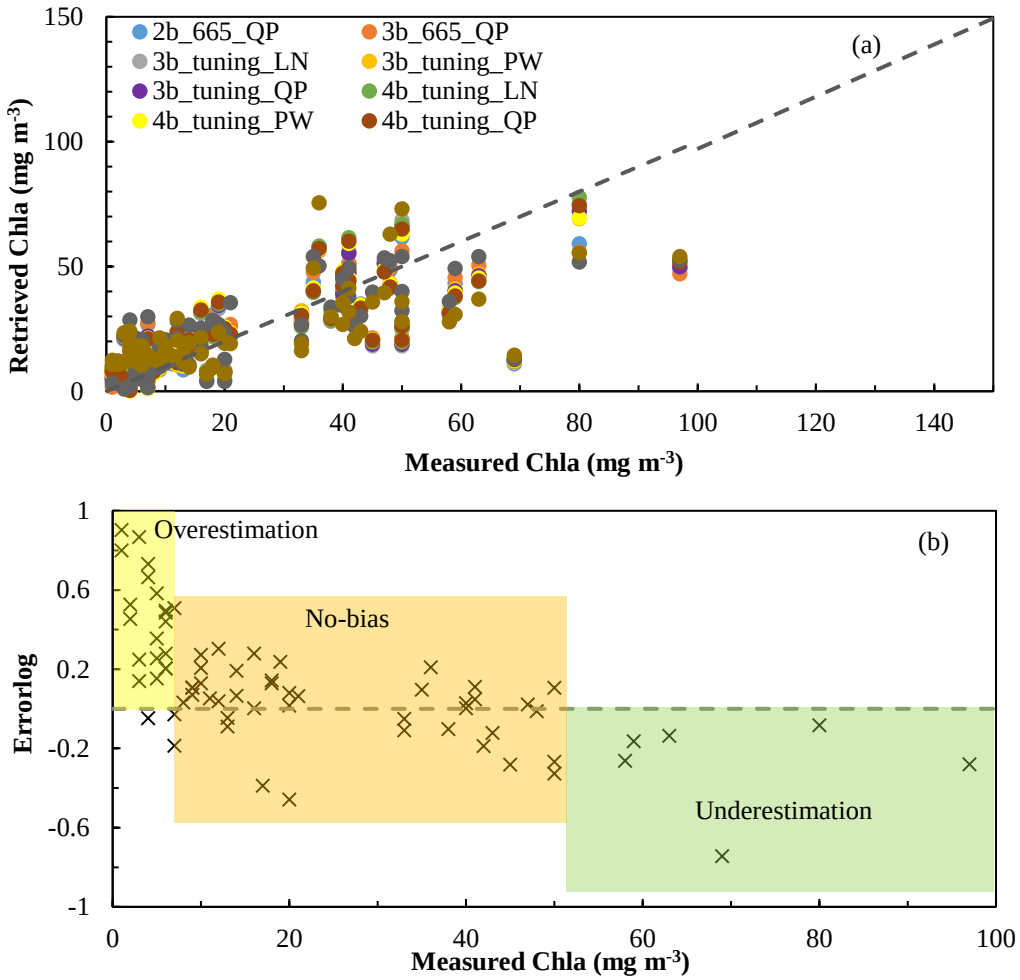

Fig. 4.14. Assessment of the best 10 algorithms for dataset 1. (a) Measured versus retrieved Chla. (b) Errors versus the measured Chla, where the errors were estimated between the measured and mean retrieved Chla of the 10 algorithms.

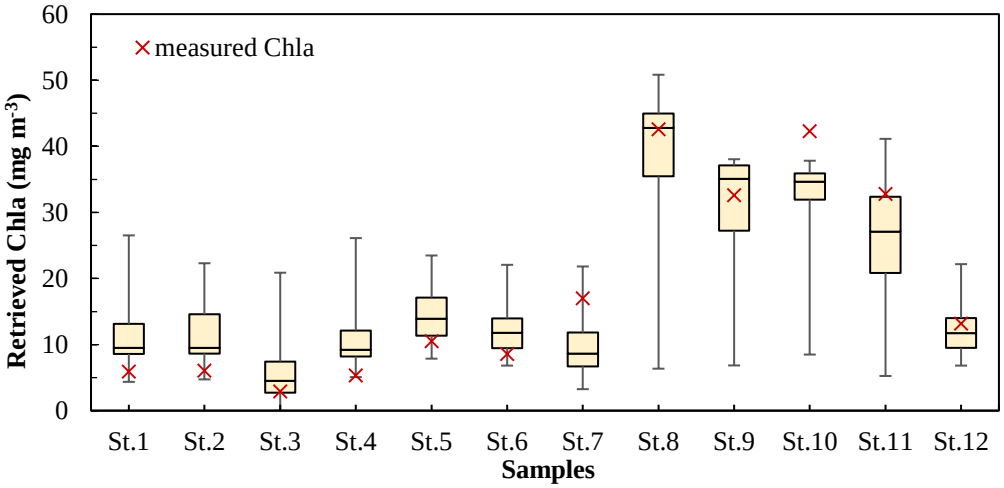

Fig. 4.15. Measured versus retrieved Chla for 12 stations with dataset 2. The box-whisker plots show the retrieved minimum, 25 %, 50 %, 75 %, and maximum from 43 algorithm combinations.

The overall retrieval accuracy of the band selection (e.g., algorithms with the 665-nm or band tuning) and regression models (i.e., linear, quadratic polynomial, and power models) were compared for the measured (i.e., dataset 1, which included the 70 samples), local simulated and wide simulated datasets (Fig. 4.16). Except for OC4E, the other 42 of the 43 algorithms were classified into four groups: algorithms with the 665-nm band (665_algs), algorithms with the 680-nm band (680_algs), algorithms that incorporated band tuning (Tuning_algs), and algorithms included the maximum and minimum approach (Max_min_algs). The retrieval accuracy in terms of the RMSE for all the algorithms in each group was averaged (Fig. 4.16a). The Tuning_algs algorithms outperformed the other three groups, with RMSE of 14.00 mg m^{-3}, 47.50 mg m^{-3} and 25.05 mg m^{-3} for the in-situ, local simulated and wide range simulated datasets, respectively. The second most accurate group varied among the three datasets, the 665_algs, 680_algs, and Max_Min_algs were the second accurate for in-situ (RMSE = 14.35 mg m^{-3}), local simulated (RMSE = 84.23 mg m^{-3}), and wide range simulated (RMSE = 33.21 mg m^{-3}) datasets, respectively. The 665_algs algorithm had the lowest retrieval accuracy for the both simulated dataset with RMSE of 103.26 mg m^{-3} and 36.84 mg m^{-3} for local and wide range simulated scenarios. While the Max_Min_algs provided the worst performance for the in-situ dataset.

Similarly, 42 of the 43 algorithms, excluding the OC4E algorithm, were classified into three groups, namely, LN_algs, QP_algs, and PW_algs, which were estimated by averaging the Chla retrieval accuracy for all the algorithms with the linear, quadratic polynomial and power regression models, respectively (Fig. 4.16b). In general, the regression approach (i.e., LN, QP, and PW) had more influence on the simulated datasets than the measured dataset due to the fact that the variation of the remote sensing reflectance among the simulated dataset was very huge as shown in Fig. 4.5a, comparing with measured reflectance (Fig. 2.3). Thus, the impact of these approaches to relate the algorithms' ratio with reference Chla was significant based on their ability to represent the data scattering. The LN_algs provide the most retrieval accuracy for local simulated (RMSE = 68.58 mg m^{-3}) and wide range (RMSE = 27.71 mg m^{-3}) simulated dataset. Whereas the QP_algs revealed the highest retrieval accuracy in terms of RMSE of 14.77 mg m^{-3}. The PW_algs algorithm introduced the lowest accuracy for in-situ (RMSE = 15.44 mg m^{-3}), local simulated (RMSE = 78.85 mg m^{-3}) and wide simulated (RMSE = 42.03 mg m^{-3}) datasets.

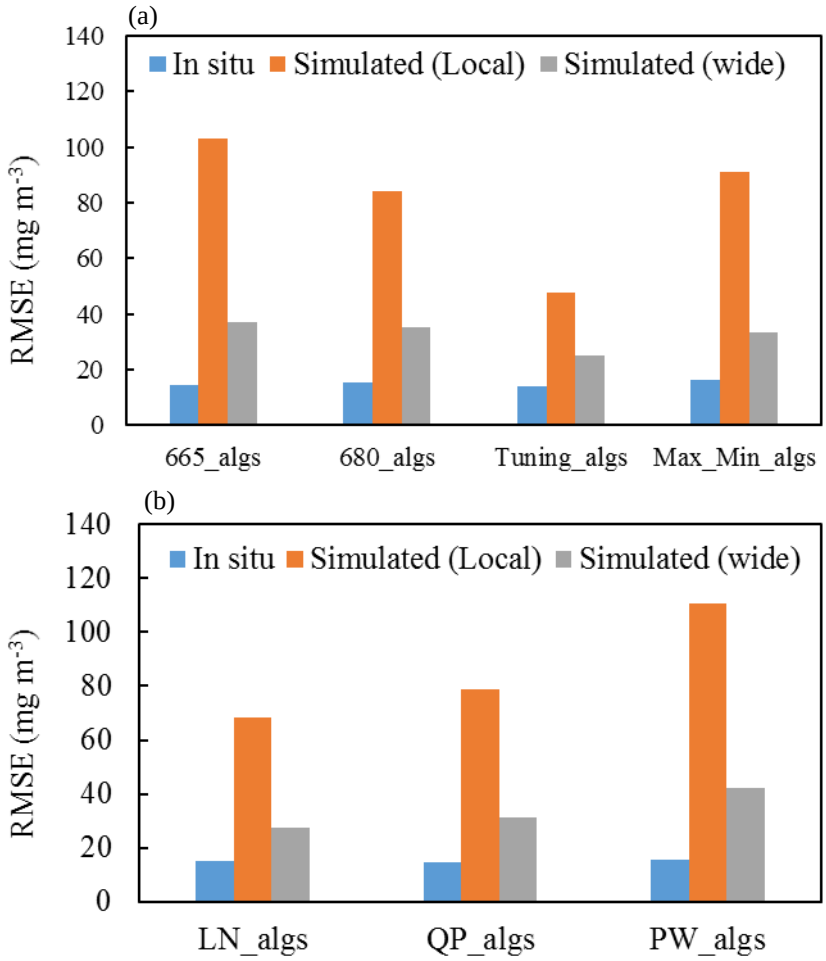

Fig. 4.16. Comparison of the average retrieval accuracy of the in-situ and simulated datasets in terms of RMSE. Both local parameterization and wide range scenarios were evaluated. (a) 665_algs, 680_algs, tuning_algs, and Max_Min_algs denote the average retrieval for all the algorithms that included the 665-nm band, 680-nm band, band tuning and maximum and minimum, respectively. (b) LN_algs, QP_algs, and PW_algs represent the average of all the algorithms with linear, quadratic polynomial, and power regression models, respectively.

4.6. Conclusions

In this study, the performances of seven Chla algorithms were investigated with all possible band combinations and three regression models (i.e., linear, quadratic polynomial and power regression models). In total, 43 algorithms were assessed based on in-situ and simulated datasets. Two simulation scenarios based on local IOPs from Tokyo bay and wide range IOPs from IOCCG database were used to generate simulated reflectance for calibration stage. A simulated dataset based on wide range IOPs was also generated to validate the 43 algorithms. The three simulated datasets coved wide ranges of Chla (1-200 mg m^{-3}), NAP (1-200 g m^{-3}),

and CDOM (0.1-10 m^{-1}), resulting in 500,000 reflectance spectra each. Having a large pool of simulated reflectance enabled us to thoroughly evaluate the Chla algorithms.

The wide range IOPs scenario provided less error comparing with local IOPs with an average RMSE and MARE of all algorithms of (RMSE = 30.10 mg m^{-3}, MARE = 95.20 %) and (RMSE = 95.92 mg m^{-3}, MARE = 182.81 %) for wide and local scenarios, respectively. This can be attributed to the calibration and validation datasets of wide range scenario that incorporated wide IOPs values to generate simulated reflectance, which enabled the tuned algorithms to accurately retrieve Chla concentrations. Across all algorithm combinations, the 3b_680_LN and 4b_tuning_LN algorithms outperformed the other algorithms for local (RMSE = 32.15 mg m^{-3}) and wide range (RMSE = 14.73 mg m^{-3}) scenarios, respectively. The MCI and SCI algorithms showed the highest error for both scenarios, with average RMSE of 201.49 mg m^{-3} and 42.53 mg m^{-3}, respectively. The spatial distribution of the most accurate algorithms for the 10,000 combinations of Chla, and NAP revealed that the 3b_680_QP and 3b_tuning_QP outperformed other algorithms in terms of minimum RMSE frequency for local (27.78 %) and wide range (33.19 %) scenario, respectively. In addition, the spatial distribution highlighted the importance of incorporating multi-algorithms to improve retrieval accuracy.

The 43 algorithms were evaluated by using five datasets of in-situ observations, which revealed that 3b_tuning_QP and NDCI_665_QP were the most accurate algorithms for three of the five datasets with RMSE $\leq$ 14.34 mg m^{-3} and 14.61 mg m^{-3}, respectively. The assessment of these algorithms with measured datasets indicates that the currently available algorithms do not have enough dynamic range: these algorithms overestimate low Chla concentrations (Chla $\leq$ 6.0 mg m^{-3}) and underestimate high Chla concentrations (Chla > 50.0 mg m^{-3}).

Comparing the results of both the measured and simulated datasets revealed that the 3b_tuning and 4b_tuning outperformed other algorithms with RMSE of 14.00 mg m^{-3}, 47.50 mg m^{-3}, and 25.05 mg m^{-3} for measure, local, and wide range scenarios. The two-, three-, four-band, and NDCI algorithms tend to provide acceptable accuracy among measured and simulated dataset, while some other algorithms provide high error (i.e., SCI algorithms). Overall, the regression approach has more influence on simulated datasets than measured dataset, because of the wide range of simulated datasets magnified the influence of fitting process. Linear and quadratic polynomial provided high retrieval accuracy for measured and simulated datasets. Whereas the power algorithm introduced the lowest accuracy in terms of average RMSE for in-situ (RMSE = 15.44 mg m^{-3}), local simulated (RMSE = 78.85 mg m^{-3}) and wide simulated (RMSE = 42.03 mg m^{-3}) datasets.

The results of this study demonstrate the strength and limitation of 43 algorithms' combination. In addition, the findings highlight the complexity of Case 2 waters and additional technique such as classification scheme or look-up table should be combined with semi-analytical algorithms to achieve better retrieval accuracy. Thus, chapter 5 introduce a novel technique that combine multi-algorithms with look-up table for better performance.

CHAPTER 5

Developing a novel technique for chlorophyll-a retrieval in turbid water bodies

5.1. Introduction

Several approaches were developed to retrieve chlorophyll-a (Chla) for Case 1 waters such as quasi-analytical algorithm (QAA) (Lee et al., 2002), the Garver-Siegel-Maritorena (GSM) algorithm (Garver and Siegel, 1997), and band ratio in the blue-green wavelengths as ocean color V4 (OC4E) algorithm (O'Reilly et al., 1998). Both QAA and GMS derive inherent optical properties of open oceans, while the difference between them is that GMS requires the absorption spectral shape of water constituents, while QAA does not require these data (Li et al., 2013). Chla retrieval accuracy for Case 2 waters using in-situ or satellite data is a challenging problem due to the complex interaction between Chla, non-algal particles (NAP), and colored dissolved organic matter (CDOM) (Song et al., 2013; Sun et al., 2013; Yang et al., 2011b). Numerous approaches have been developed to overcome that complexity as described in the following statements. Empirical and semi-analytical algorithms provide indices which are correlated with Chla concentration (Oki, 2010; Oki and Yasuoka, 2002; Shen et al., 2010; Zhang et al., 2015). The retrieval of Chla concentration from algorithm's indices is achieved through regression process using linear (Carder et al., 1999; Huang et al., 2010; Shi et al., 2013; Zhou et al., 2014), polynomial (Gurlin et al., 2011; Matsushita et al., 2015; Shen et al., 2010), and power regression approaches (Kutser et al., 2006; O'Reilly et al., 1998). Matthews (2011) reviewed the retrieval accuracy of many algorithms for different sites, revealing the ability of tuned algorithms to retrieve Chla concentration. However, the main limitation associated with the empirical and semi-analytical algorithms is that the derived relationship may not be applicable to other locations with different water composition (Yang et al., 2011a).

Lee et al. (1998) developed a semi-analytical inversion model for shallow water to derive water depth, and water column properties (i.e., absorption and backscattering coefficients) of the water column by optimizing the difference between measured reflectance (Rrs) and simulated Rrs. Many researchers upgraded the model of Lee et al. Lee et al. (1998) to involve many bottom types instead of sand-bottom type (Giardino et al., 2007; Klonowski et al., 2007) and to retrieve Chla, NAP, and CDOM concentrations (Brando et al., 2009). These inversion models were mainly applied to shallow, and relatively clear water with high CDOM concentrations in the Bahamas and Moreton Bay in eastern Australia using airborne

hyperspectral data with a high spatial resolution (Dekker et al., 2011; Lee et al., 2001; Lyons et al., 2011; Schueler et al., 2011). The airborne hyperspectral data is much more expensive with small area coverage comparing with multispectral satellite date which is freely available for many satellites with routine global coverage (Dalponte et al., 2012). Regarding spectrum matching approach, a matchup process is performed between the measured Rrs and a library of simulated Rrs covering different water conditions to find the closest simulated Rrs with its known properties (Lesser and Mobley, 2007). Similarly, spectrum matching approach requires hyperspectral data to perform matching process.

Accordingly, a new technique is required to combine the advantages of semi-analytical algorithms (i.e., providing indices correlated with Chla concentration) with the merits of look-up table (i.e., providing dataset corresponding to various water properties) and applicable to multispectral data. The current study proposed multi-algorithm indices and look-up table technique. The aim of this study is to 1) develop a new technique for Chla retrieval based on algorithms' indices and look-up table; 2) select the proper combination of algorithms for the proposed technique; and 3) evaluate the performance of proposed technique using in-situ measurements and MERIS satellite data over turbid and highly turbid water bodies.

5.2. MERIS images processing

MERIS L1b product of 300 m full resolution from European Space Agency (ESA) Earthnet Online (http://earth.esa.int/) was processed using BEAM V5.0 software (Envisat/ Brockman Consult). All clear and partially clear MERIS images that contain Lake Kasumigaura and matched the monthly field observations from 2002 till 2012 were extracted. The matchup process included all the images acquired at the same day or one day difference from field observations. It was assumed that the changes in Chla concentrations within one day would not be significant, due to the stability of weather conditions (e.g., wind speed) during that day as shown in Table 5.1. The matchup process resulted in a total of 13 images (i.e., 5 images at the same day and 8 images within one-day difference).

Table 5.1 Average wind speed and water surface temperature between MERIS acquisition day and field observation day for the one day difference MERIS images.

	MERIS images Acquisition			**Field observation**		
	Date	Average wind speed (m / sec)	Water surface Temp. (°C)	date	Average wind speed (m / sec)	Water surface Temp. (°C)
Image (1)	9-Jan-2007	3.9	5.9	10-Jan-2007	2.5	5.7
Image (2)	14-Feb-2008	6.7	4.2	13-Feb-2008	7.3	4.6
Image (3)	7-Aug-2008	2.5	---	6-Aug-2008	3	---
Image (4)	6-Jan-2009	2.5	6.3	7-Jan-2009	3.2	6.4
Image (5)	9-Apr-2009	2.3	15	8-Apr-2009	2.9	14
Image (6)	14-May-2009	5.1	---	13-May-2009	4.5	20.3
Image (7)	9-Nov-2010	4.7	15	10-Nov-2010	4	---
Image (8)	9-Aug-2011	2.5	---	10-Aug-2011	---	---

All images were pre-processed using Smile Correction processor to adjust the variations in the spectral wavelengths among MERIS's five cameras and within the same camera (Binding et al., 2011). In order to convert MERIS L1b top-of-atmosphere radiances to water-leaving reflectance, the Case-2 Regional (C2R), the Eutrophic Lake (EUL) and Boreal Lake (BL) processors are neural network modules for performing atmospheric correction in Case 2 waters (Doerffer and Schiller, 2008, 2007). The three processors share the same neural network atmospheric correction module, while the difference among them is the training data that used to trained inverse and forward coupled neural network to retrieve the IOPs and constituents concentrations from the atmospherically corrected reflectance (Doerffer and Schiller, 2008, 2007). During this study, the water-leaving reflectance is only needed from MERIS data, while the Chla concentrations will be taken from the matched field observations, not from the neural network modules. Thus, EUL processor was employed to perform atmospheric correction (Doerffer and Schiller, 2008). The final number of matched stations decreased from 130 to 77 stations due to quality control flags in L1b product (e.g., invalid, bright, suspect, land, or glint risk) or during the atmospheric correction process. Fig. 5.1 shows the water leaving reflectance of the 77 stations resulting from the matching process over Lake Kasumigaura.

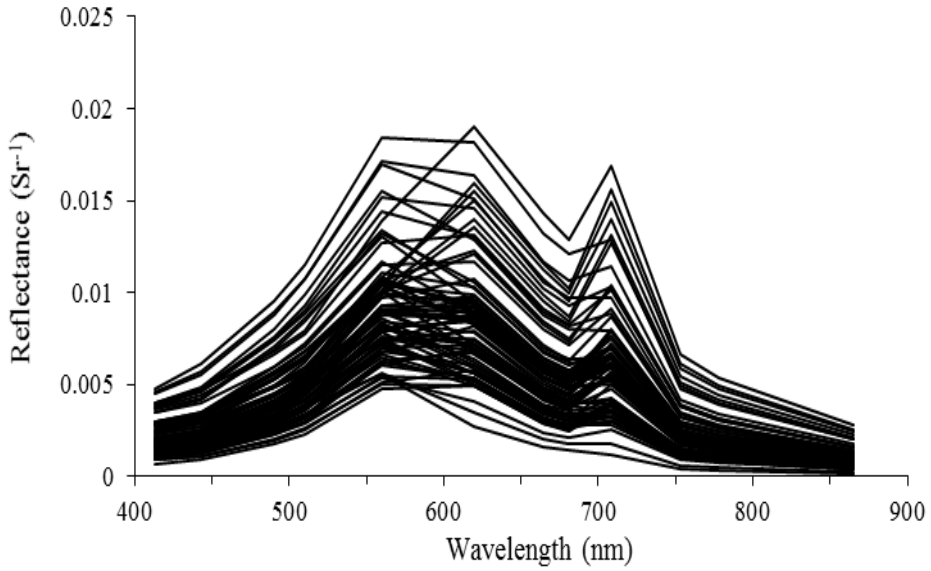

Fig. 5.1. Atmospheric corrected remote sensing reflectance spectra for 77 stations matched the field observation in Lake Kasumigaura from 2002 to 2012.

5.3. Construction of the Multi-Algorithm Indices and Look-Up Table (MAIN-LUT)

The proposed technique relies on creating a library of simulated reflectance dataset covering wide ranges of Chla, NAP and CDOM concentrations. The simulated reflectance dataset was generated based on the bio-optical model and specific inherent optical properties (SIOPs) from Tokyo Bay (sections 2.2 and 2.3). The bio-optical modeling is used to link remote sensing reflectance with optically active constituents in the water column (i.e., Chla, NAP, and CDOM). By changing the concentration of any of these three constituents, remote sensing reflectance will change. Consequent, a simulated dataset of 500,000 Rrs spectra were generated covering wide ranges of Chla (1 – 200 mg m^{-3}) (hereafter, reference Chla), NAP (1 – 200 g m^{-3}), and CDOM (1 – 10 m^{-1}) concentrations. Increment of 2.0 mg m^{-3}, 2.0 g m^{-3}, and 2.0 m^{-1} were used for Chla, NAP and CDOM concentrations, respectively. Each of the generated Rrs spectra was tagged with the Chla, NAP, and CDOM concentrations which used during the generation of simulated Rrs spectra.

The major limitation to perform spectral matching with multi-spectral data is associated with the limited number of available bands, particularly when the bands of the blue spectrum excluded due to difficulties in atmospheric correction for that part of spectrum (Le et al., 2013). On the other hand, there was no relation between the reference Chla and individual bands of the multi-spectral data (e.g., 665-nm band) as shown in Fig. 5.2. Many algorithms have been proposed to retrieve Chla concentration in Case 2 waters (Dall'Olmo et al., 2003; Gons, 1999; Le et al., 2009; Mishra and Mishra, 2012). These algorithms provide indices correlated with

Chla concentration (Zhang et al., 2015). Four algorithms were proposed for the proposed technique (i.e., 2-band ratio (Eq. 5.1), 3-band algorithm (Eq. 5.2), maximum chlorophyll index (Eq. 5.3) and normalized difference chlorophyll index (Eq. 5.4)).

$$Chla \propto R_{rs}(\lambda_2) / R_{rs}(\lambda_1) \quad (\mathbf{5.1})$$

$$Chla \propto \left(R_{rs}^{-1}(\lambda_1) - R_{rs}^{-1}(\lambda_2)\right) * R_{rs}(\lambda_3) \quad (\mathbf{5.2})$$

$$MCI = R_{rs}(\lambda_2) - R_{rs}(\lambda_1)\left[\frac{\lambda_2 - \lambda_1}{\lambda_3 - \lambda_1} R_{rs}(\lambda_3) - R_{rs}(\lambda_1)\right] \quad (\mathbf{5.3})$$

$$Chla \propto \left(R_{rs}(\lambda_2) - R_{rs}(\lambda_1)\right) / \left(R_{rs}(\lambda_2) + R_{rs}(\lambda_1)\right) \quad (\mathbf{5.4})$$

The wavelengths incorporated with each algorithm were summarized in Table 4.1. Scatter plots between the reference Chla and the above-mentioned algorithms with different wavelengths were performed (Fig. 5.2). Investigated algorithms provided correlation with reference Chla: high correlation (e.g., 2b-[665, 709]), moderated correlation (e.g., 3b-[680, 709, 754]), and low correlation (e.g., MCI [680, 709, 754]) (Fig. 5.3). Thus, the index of these algorithms could be used to retrieve Chla concentration of measured Rrs by comparing the index of measured Rrs with the indices of simulated Rrs to extract the simulated Rrs with the same index. The problem is that there are many simulated Rrs that have same measured index during the matchup process. Thus, multi-algorithms indices should be used to obtain the simulated Rrs which is close to the measured Rrs.

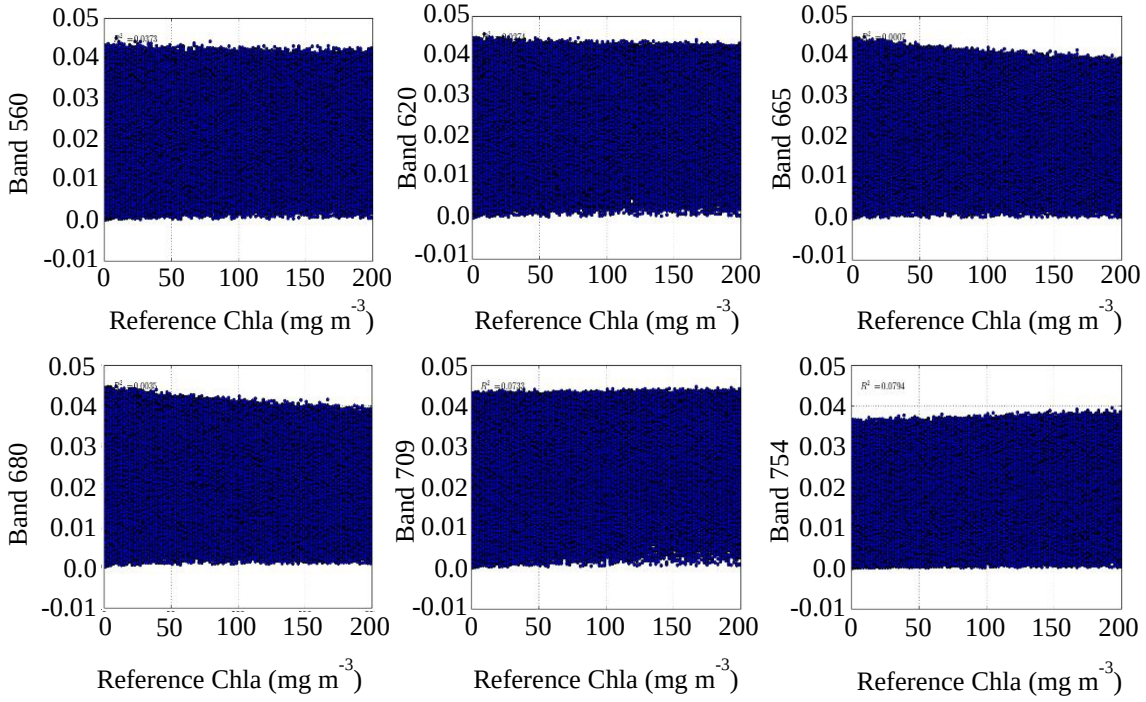

Fig. 5.2. Scatter plots of reference Chla versus individual bands.

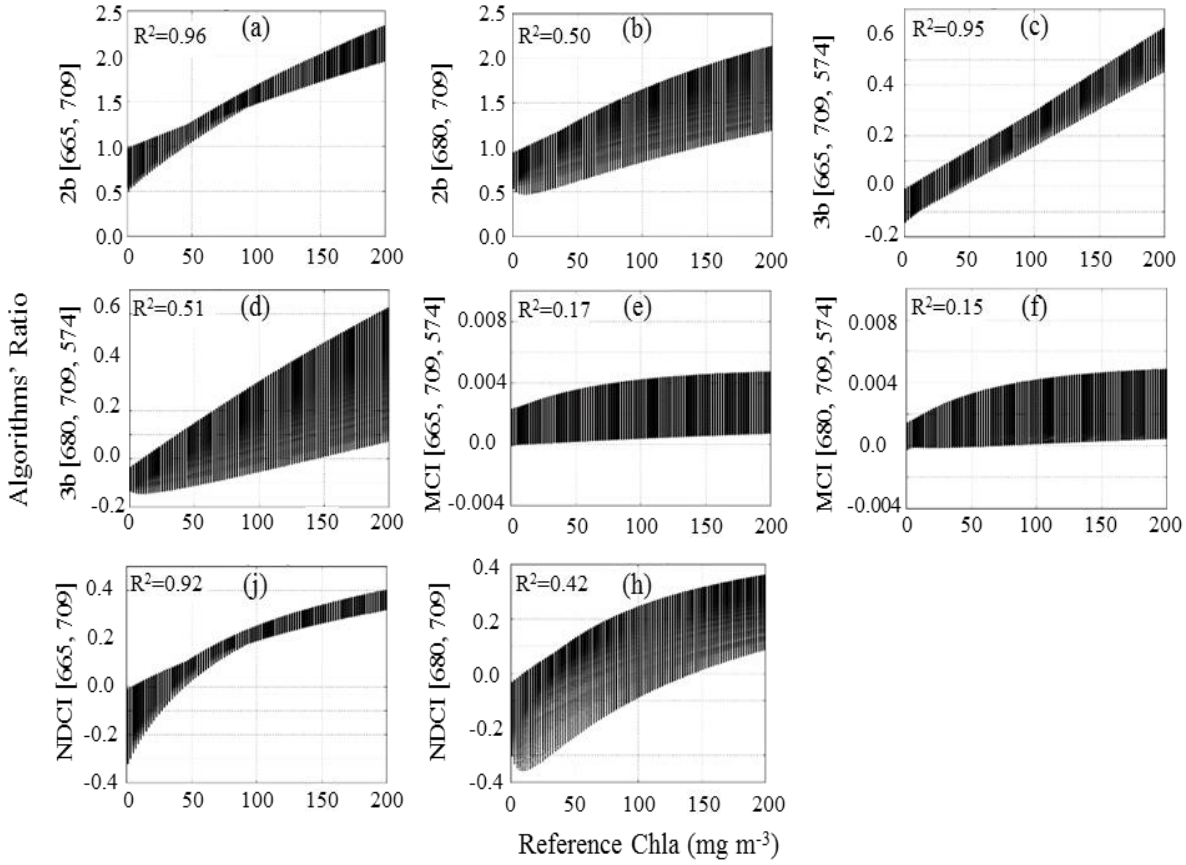

Fig. 5.3. Scatter plots of reference Chla versus algorithms indices for the 500,000 simulated reflectance spectra.

Table 5.2 Algorithms' combination investigated with MAIN-LUT.

Algorithms* / Algorithms' combinations	2b [665, 709]	2b [680, 709]	3b [665,709,754]	3b [680,709,754]	MCI [665,709,754]	MCI [680,709,754]	NDCI [665,709]	NDCI [680,709]
8-indices	✓	✓	✓	✓	✓	✓	✓	✓
6-indices	✓	✓	✓	✓			✓	✓
4-indices-[2b & 3b]	✓	✓	✓	✓				
4-indices-[665]	✓		✓		✓		✓	
3-indices-[665]	✓		✓				✓	
2-indices-[665]	✓		✓					
4-indices-[680]		✓		✓		✓		✓
3-indices-[680]		✓		✓				✓

* Wavelengths incorporated with each algorithm were summarized in .

Different combinations of these four algorithms were examined with the MAIN-LUT technique to find the best combination. Table 5.2 summarizes eight combinations which were investigated. The flowchart in Fig. 5.4 illustrates the concept of MAIN-LUT using the 2-indices-[665] combination as an example, whereas the major steps of the MAIN-LUT as follows:

Step (0): two things should be prepared and selected before using MAIN-LUT: (1) a library of simulated Rrs should be provided through a look-up table; and (2) one combination of algorithms should be selected from Table 5.2. The selected combination is hereafter called Sample Combination through the coming steps.

Step (1): calculating algorithms indices for the measured reflectance using Eqs. (**5.1**) – (**5.4**). The number of required indices relies on the selection of the Sample Combination in Step (0). For example, the 2-indices-[665] combination was selected in the flowchart (Fig. 5.4). As a result, the indices of 2b-[665, 709] and 3b-[665, 709, 754] algorithms were estimated as $\left(2b_{665}^{meas} = R_{rs}(709)/R_{rs}(665)\right)$ and $\left(3b_{665}^{meas} = [1/R_{rs}(665) - 1/R_{rs}(665)] * R_{rs}(754)\right)$ as shown in Fig. 5.4.

Step (2): for each measured index estimated in Step (1), simulated reflectance spectra from a look-up table (LUT) that have the same index should be extracted. Of course, many simulated reflectance spectra with different tagged Chla will be extracted from this matching process. For example, the simulated reflectance ($Rrs_{rs,200}^{simu}$, $Rrs_{rs,1520}^{simu}$) were extracted because they matched the $3b_{665}^{meas}$. The 200 and 1520 represent the tagged numbers of simulated reflectance for a certain combination of Chla, NAP, and CDOM and these tagged numbers range from 1 to 500,000.

Step (3): grouping of simulated reflectance extracted from Step (2), which generated from the matching process of each measured index.

Step (4): estimating algorithm indices for each of simulated reflectance grouped in Step (3). The number of required indices based on the Sample Combination selected in step (0).

Step (5): The RMSE is used to compare the indices of measured reflectance with simulated indices of each extracted reflectance in Step (3) as follows:

$$RMSE = \sqrt{\frac{\sum_{i=1}^{n}\left(Index_{i,meas} - Index_{i,simu}^{j}\right)^2}{n}} \qquad (19)$$

where $Index_{i,meas}$ denote measured indices (i.e., $2b_{665}^{meas}$ and $3b_{665}^{meas}$ for 2b-indices-[665] combination); $Index_{i,simu}^{j}$ refer to simulated indices calculated for each simulated Rrs spectrum (i.e., $\left(2b_{665}^{simu}\right)^{j}$ and $\left(3b_{665}^{simu}\right)^{j}$ for 2b-indices-[665] combination), j is an index for simulated reflectance grouped in Step (3); and n represents the number of indices in the Sample Combination (i.e., n = 2 for 2b-indices-[665] combination). The minimum RMSE value represents the closest simulated spectrum from the measured spectrum. As a result, the tagged Chla for that simulated Rrs will be the retrieved Chla concentration of the measured Rrs.

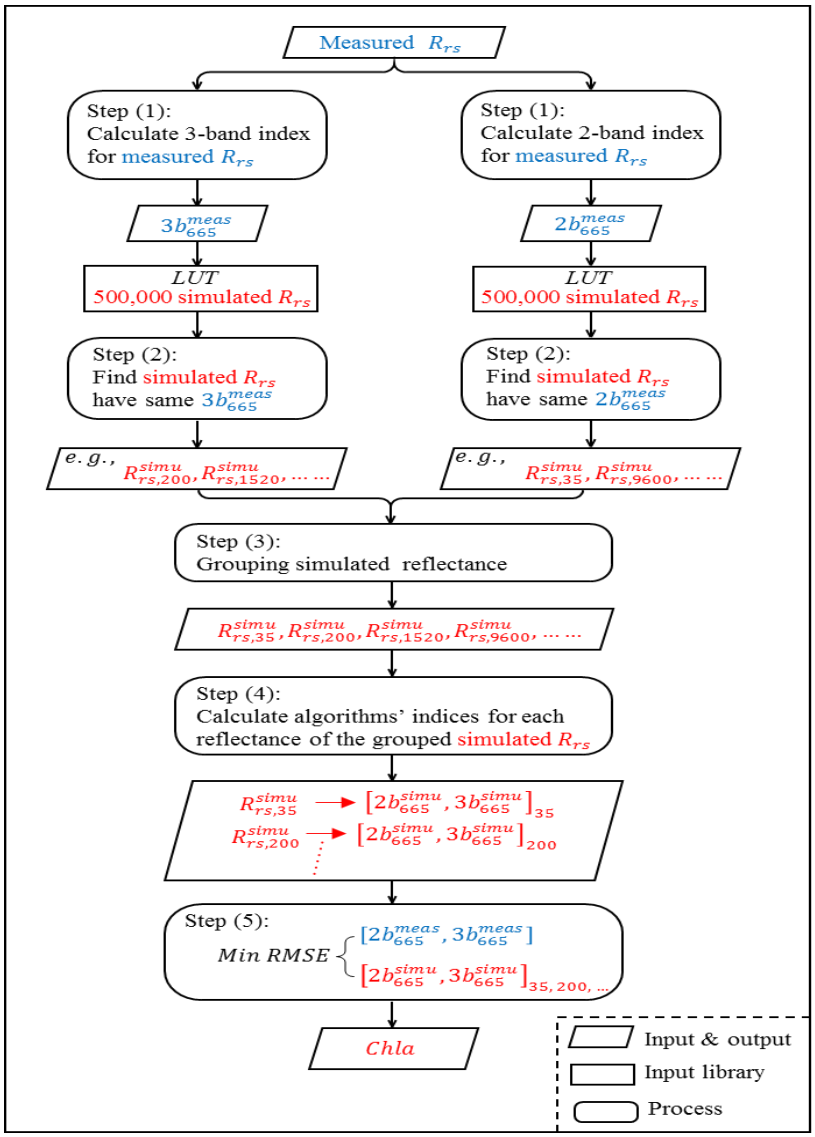

Fig. 5.4. Concept and schematic flowchart of MAIN-LUT technique for the 2-indices-[665] combination. For other combinations in Table 5.2, similar concept was employed. $2b_{665}$ stands for 2b [665, 709] algorithm's index $(= R_{rs}(709)/R_{rs}(665))$; $3b_{665}$ refers to the 3b [665, 709, 754] algorithm's index $(= [1/R_{rs}(665) - 1/R_{rs}(665)] * R_{rs}(754))$; *LUT* represents the look-up table; numbers like 35 in $R_{rs,35}^{simu}$ represents the tagged number for each simulated Rrs that range from 1 to 500,000; and *meas*, and *simu* denote measured and simulated, respectively. The blue and red color highlight the measured and simulated parameters, respectively.

5.4. Results and discussion

5.4.1. Validation using in-situ measurements

The in-situ data collected from Tokyo Bay between 2010 to 2013 (71 stations) were used to investigated the retrieval accuracy of the MAIN-LUT technique. The MAIN-LUT technique does not require a calibration process because Chla concentrations are directly retrieved from the look-up table. Therefore, all the measured Rrs passed through the MAIN-LUT steps (from step 1 to step 5 as explained in previous section) to retrieve Chla concentrations. For the eight algorithms' combinations proposed in Table 5.2, the Chla concentrations for each combination were retrieved from the MAIN-LUT and compared with the measured Chla (Fig. 5.5). In general, the results of MAIN-LUT revealed that most of algorithms' combinations could accurately retrieve Chla concentrations (Fig. 5.5). The 3-indices-[665] combination outperformed other combinations in terms of coefficient of determination (R^2) of 0.692 with RMSE and MARE of 21.4 mg m^{-3} and 142.6%, respectively (Fig. 5.5e). Overall, 3-indices-[665], 4-indices-[665], and 2-indices-[665] provided highest retrieval accuracy with average R^2, RMSE and MARE of 0.681, 21.43 mg m^{-3} and 141.87 %, respectively. In contrast, 4-indices-[680], and 3-indices-[680] introduced the lowest averaged retrieval accuracy (R^2 = 0.277, RMSE = 22.7 mg m^{-3}, MARE = 233.6 %) (Figs. 5.5g and 5.5h).

The performance of the MAIN-LUT was also examined with in-situ measurements from Lake Kasumigaura collected in 2016 with total sampling points of 68 stations. Although the simulated Rrs data of the MAIN-LUT technique was generated based of IOPs values from Tokyo Bay, the MAIN-LUT produced higher Chla retrieval accuracy for Lake Kasumigaura than Tokyo Bay for different algorithms' combinations (Figs. 5.5 and 5.6). This result can be attributed to the fact that the four algorithms incorporated with MAIN-LUT (Eqs. (**5.1**) - (**5.4**)) are mainly developed for Case 2 waters with high Chla and TSS concentrations. Comparing the characteristics of these two water bodies revealed that water conditions in Lake Kasumigaura (Chla = 55.86 mg m^{-3}, TSS = 21.71 g m^{-3}, Table 2.2) is more correlated with the algorithms assumption than Tokyo Bay (Chla = 25.14 mg m^{-3}, TSS = 8.29 g m^{-3}). In addition, the MARE values for all combinations were very high for Tokyo Bay comparing with same combinations at lake kasumigaura (Figs. 5.5 and 5.6). The reason is mainly due to the fact that the MARE is a relative error assesses the Chla retrieval over a relatively low range of Chla concentration in Tokyo Bay. As a result, any small difference between the measured and retrieved Chla concentrations would cause a high relative error.

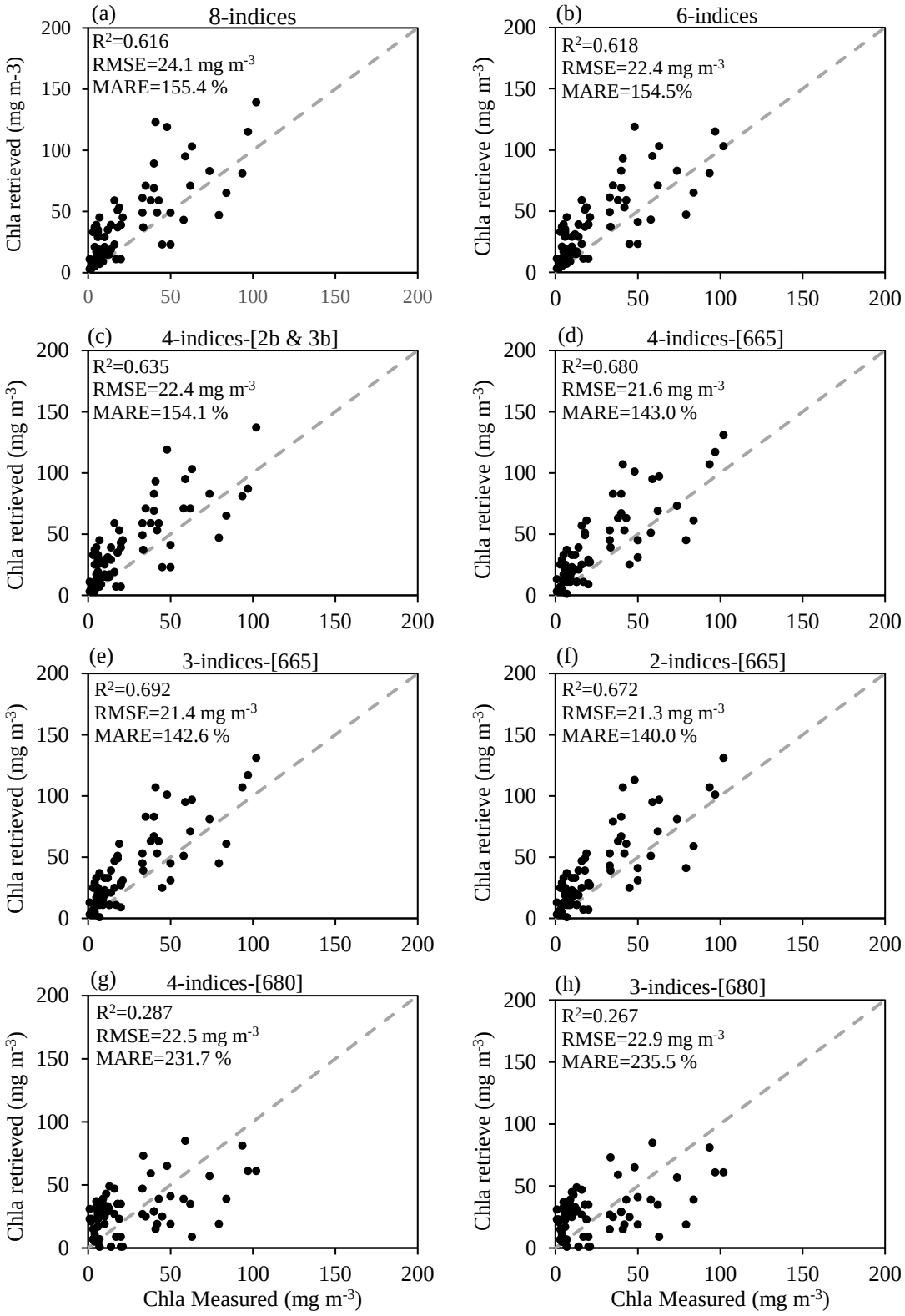

Fig. 5.5. Validation plots between Chla measured in Tokyo Bay (71 stations collected between 2010 and 2013) and retrieved Chla from different algorithms' combinations assessed for MAIN-LUT.

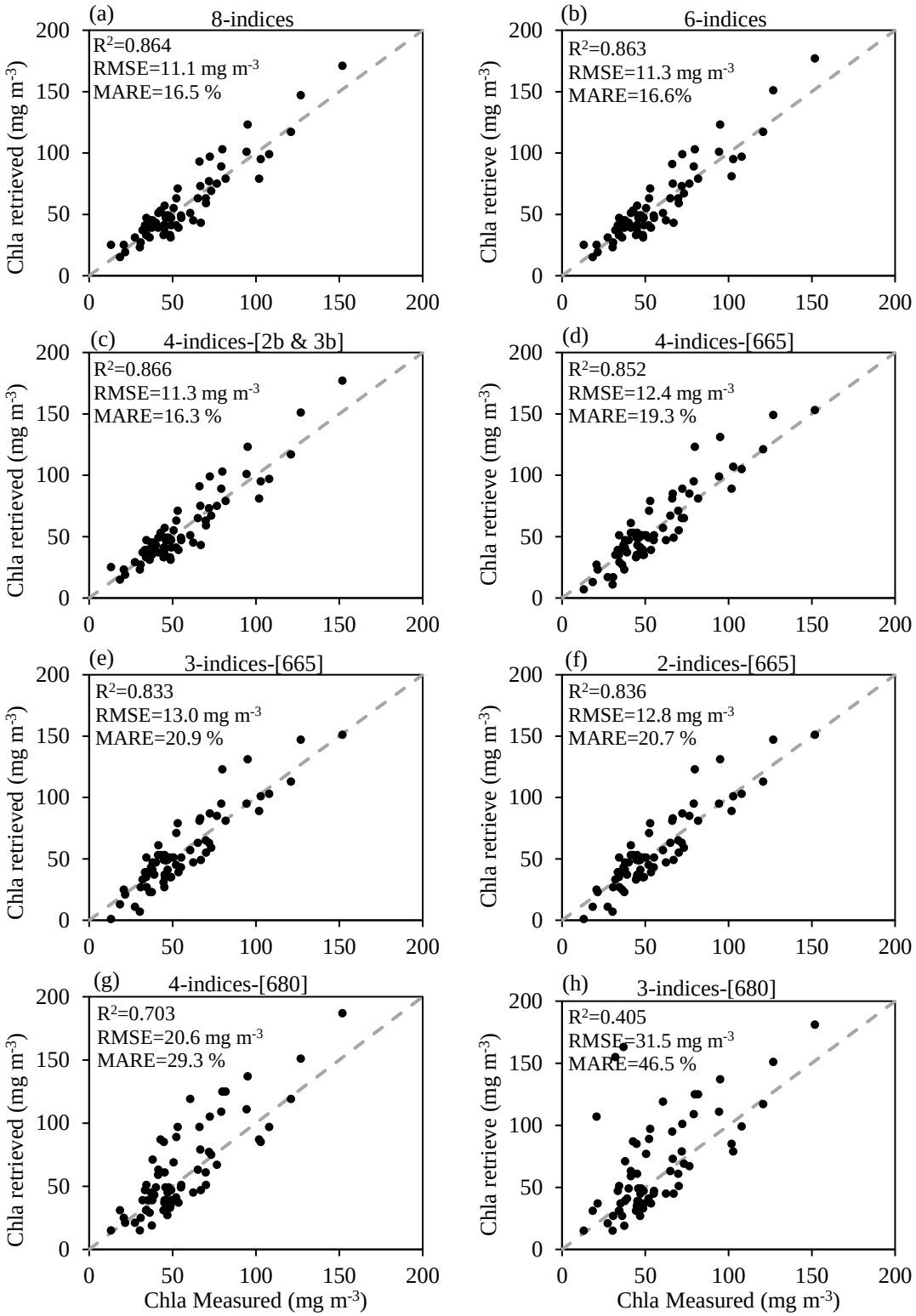

Fig. 5.6. Validation plots between Chla measured in Lake Kasumigaura (68 stations collected in 2016) and retrieved Chla from different algorithms' combinations assessed for MAIN-LUT.

The highest retrieval accuracy for Lake Kasumigaura was achieved by 4-indices-[2b & 3b] combination with R^2 of 0.866, RMSE of 11.3 mg m^{-3}, and MARE of 16.3% (Fig. 5.6c). The top three combinations in terms of Chla retrieval were 4-indices-[2b & 3b], 8-indices, and

6-indices with average R^2, RMSE, and MARE of 0.866, 11.23 mg m^{-3} and 16.47 %, respectively. The second tier of algorithms' combinations were 3-indices-[665], 4-indices-[665], and 2-indices-[665] which introduced slightly high retrieval accuracy, with R^2, RMSE and MARE of 0.840, 12.73 mg m^{-3} and 20.3 %, respectively. The retrieval accuracy of 4-indices-[680] combination significantly improved in terms of R^2 (from 0.287 to 0.703) and MARE (from 231.7 % to 29.3 %) (Figs. 5.5g and 5.6g). The 3-indices-[680] combination was also improved comparing with Tokyo Bay (Figs. 5.5h and 5.6h).

5.4.2. Validation using MERIS data

MAIN-LUT technique was also validated using MERIS satellite data. A matchup process executed between field observation campaigns in lake kasumigaura and MERIS images acquired at same day or 1-day difference during 2002 - 2012, resulting in 130 matched stations. However, the final number of stations that used during validation process reduced to 77 stations (Table 2.2 – Dataset2), due to flags occur through images processing. Therefore, MERIS reflectance spectra were used as an input for MAIN-LUT to retrieve Chla concentrations which were compared with the measured Chla during the field campaigns. In general, all algorithms' combinations provided relatively acceptable Chla retrieval, even for 4-indices-[680] and 3-indices-[680] which introduced lowest retrieval accuracy for Tokyo Bay and lake kasumigaura (Fig. 5.7). This can be attribute to the fact that the neural network atmospheric correction module does not include the inelastic reflectance (e.g., fluorescence) for the simulated dataset that used to train the module, which will affect the accuracy of the water-leaving reflectance of MERIS data in the red and near infrared (Red-NIR) region of spectrum (Binding et al., 2011).

The 4-indices-[680] provided the highest accuracy in terms of RMSE of 28.9 mg m^{-3}. Furthermore, the disruption of scatter plot of the 4-indices-[680] combination was close to a 1:1 line (Fig. 5.7g) compared to most of other combinations which underestimated Chla > 50 mg m^{-3} (Fig. 5.7a – Fig. 5.7f). This is mainly due to the fact that the simulated dataset of the MAIN-LUT considered the fluorescence reflectance in contrast to the EUL atmospheric correcting module that neglected the fluorescence reflectance during the training process. Thus, the magnitude of atmospherically corrected reflectance particularly in the Red-NIR in lower than the simulated reflectance of MAIN-LUT for the same Chla concentration. The 2-indices-[665] outperformed other combinations with R^2 of 0.57. The retrieval accuracy of 2-indices-[665], 3-indices-[665], and 4-indices-[665] were the highest combinations in terms of R^2 and MARE (R^2 = 0.564, RMSE = 32.47 mg m^{-3}, MARE = 43.4 %) (Figs. 5.7d – 5.7f). Although,

the scatter plot distribution of 3-indices-[680] was also close to the 1:1 line (Fig. 5.7h), it produced the lowest retrieval accuracy (R^2 = 0.385, RMSE = 37.8 mg m^{-3}, MARE = 74.3 %).

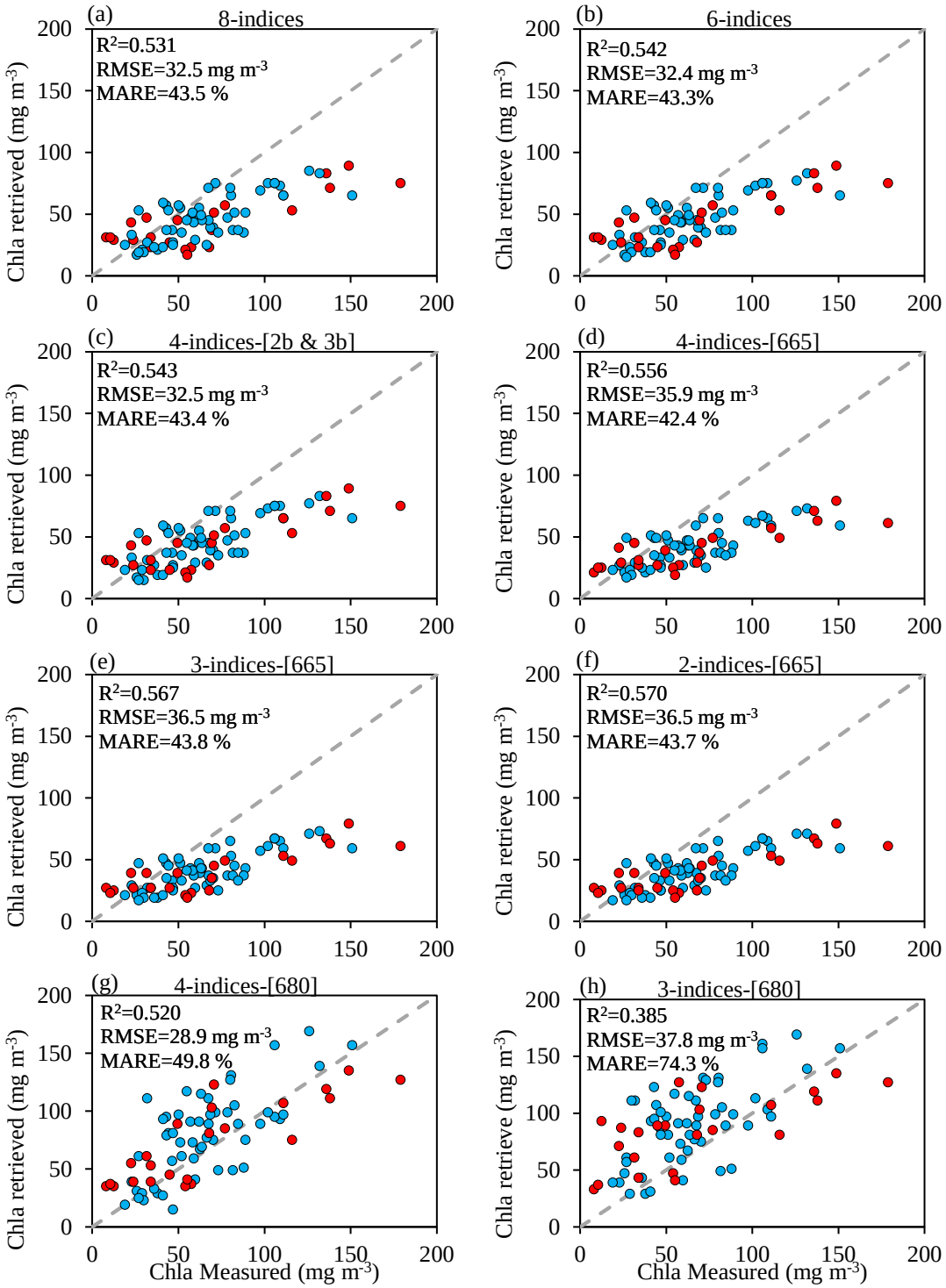

Fig. 5.7. Validation plots between Chla measured in Lake Kasumigaura (77 stations matched MERIS images and collected during 2002 - 2012) and retrieved Chla from different algorithms' combinations assessed for MAIN-LUT. The red and blue dots highlighted stations that matched MERIS images at same day and one day difference, respectively.

The MAIN-LUT technique was also applied to MERIS images (pixel by pixel) to retrieve and illustrate the spatial distribution of Chla concentration along Lake Kasumigaura. Fig. 5.8a and Fig. 5.8b illustrate the spatial distribution of Chla concentrations on July 2004 and May 2009, respectively. The Chla concentrations were up to 90 mg m^{-3} on May 2009 higher than that on July 2004 with Chla up to 50 mg m^{-3}. The scatter plot between the measured and the retrieved Chla shown in Fig. 5.8d reveals that the MAIN-LUT could retrieved Chla concentrations accurately for low and high Chla. In general, the Chla spatial distributions were relatively high near station 1 and station 6 (i.e., St. 1 and St. 6) as illustrated in Fig. 5.8a and Fig. 5.8b due to the nutrient-rich inflow from Koise river and Sakura River into the lake near St. 1 and St. 6 (Fig. 5.8c), respectively.

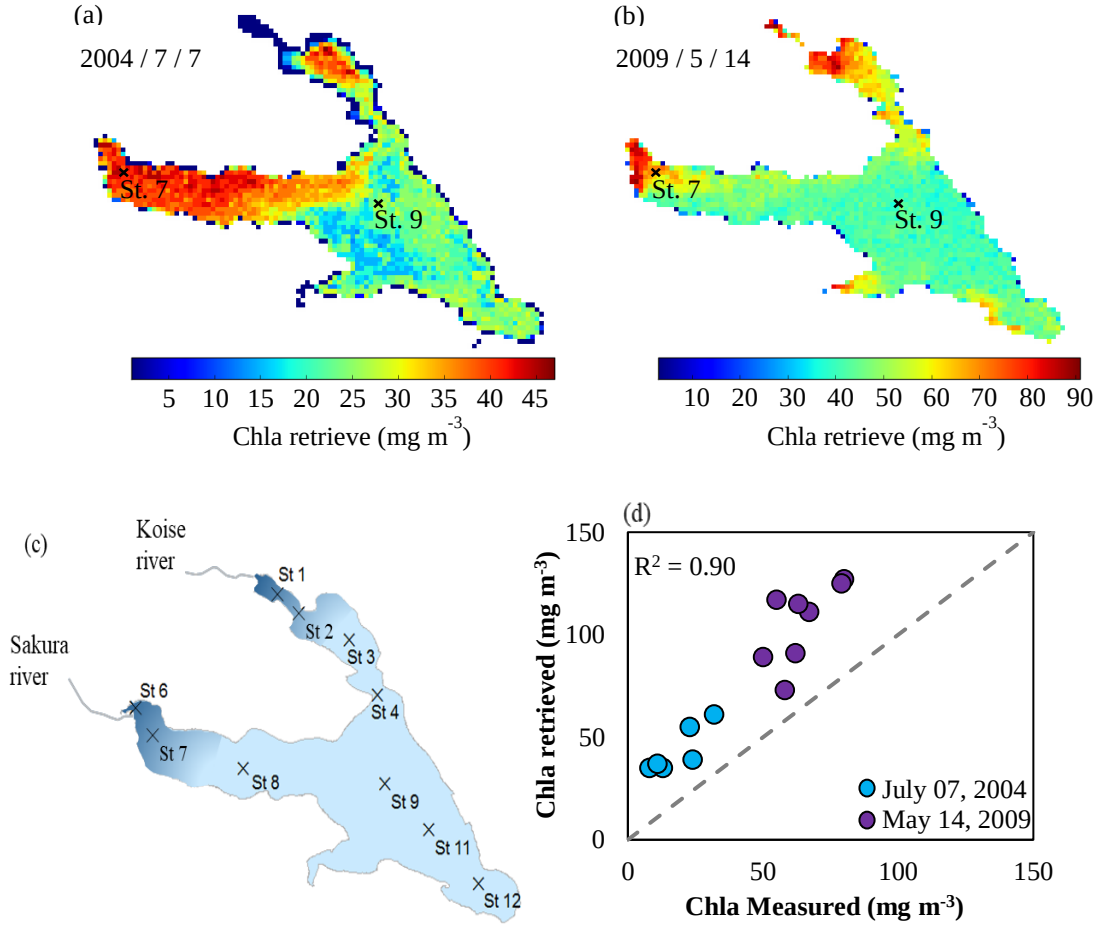

Fig. 5.8. Spatial distribution of Chla concentration for Lake Kasumigaura using MAIN-LUT in two different MERIS images. Images were acquired on (a) July 7, 2004; and (b) May 14, 2009. (c) illustrates the main rivers flow into Lake Kasumigaura. (d) scatter plot between the measured and retrieved Chla for the two images acquired on July 7, 2004; and May 14, 2009.

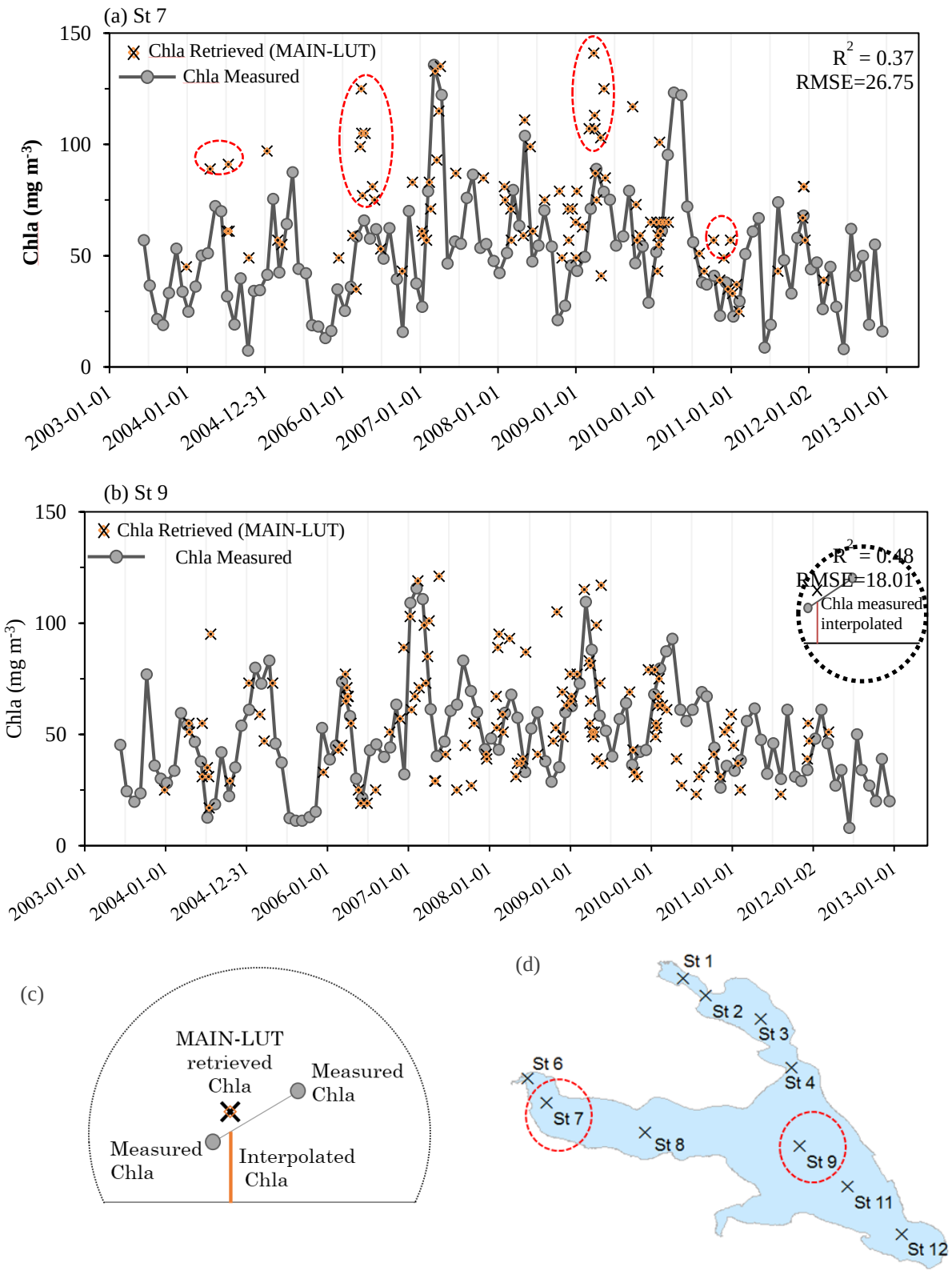

Fig. 5.9. Time series of measured chlorophyll-a (Chla) versus retrieved Chla from MAIN-LUT technique using 10-year of MERIS clear images at (a) station 7 (St 7) and (b) station 9 (St 9). (c) The linear interpolation technique was used to estimate measured Chla at the same day of available satellite data. (d) The location of St. 7 and St. 9 at Lake Kasumigaura.

The Chla retrieved accuracy of MAIN-LUT technique was investigated over Lake Kasumigaura using 10-year of MERIS data. A total of 122 clear or partially clear MERIS images were first processed using Eutrophic Lake Processor (EUL) to covert the top of atmosphere radiance to water leaving reflectance. Then, the available water leaving reflectance at St. (7) and St. (9) were processed using MAIN-LUT technique to retrieve Chla concentrations. The Chla concentrations are measured monthly at ten stations of Lake Kasumigaura since 1970s by NIES (NIES, 2016). Fig. 5.9a and Fig. 5.9b shows the time series of measured Chla at St. (7) and St. (9), respectively. Additionally, the retrieved Chla from MAIN-LUT is illustrated in Fig. 5.9a and Fig. 5.9b.

The visual comparison between the measured and retrieved Chla revealed that the MAIN-LUT could follow the seasonal and annual pattern of Chla concentrations during 2002 – 2012, except for slight overestimation at St. 7 and St. 9 during the spring seasons of 2004, 2006, 2008 and 2009 (Figs. 9a and 9d). Similar overestimation trend during the spring time was observed for the outputs of MCI_L1 and C2R processors which could be attribute to two reasons: (1) Diatom blooming which occur during spring time (i.e., April to June) in Lake Kasumigaura (CEBES, 2001) which required further investigation to examine the possible influence of phytoplankton species on the processors' performances., or (2) inaccurate neural network output. The linear interpolation was used to estimate the measure Chla at the same day of the acquired MERIS images (Fig. 5.9c). The Accuracy of MAIN-LUT was lower at St. 7 (R^2 = 0.37, RMSE = 26.75 mg m^{-3}) comparing with St. 9 (R^2 = 0.48, RMSE = 18.01 mg m^{-3}) due to the overestimation on the spring time.

5.4.3. Comparing MAIN-LUT with locally tuned algorithms

All algorithms incorporated with algorithms' combinations of MAIN-LUT (Table 5.2) were locally tuned and compared with MAIN-LUT. Each dataset (Tokyo Bay, lake kasumigaura dataset 1 and dataset2) shown in Table 2.2 was randomly divided to 70 % and 30 % for calibration and validation processes, respectively. Linear regression was adopted during calibration process. Table 5.3 summarizes R^2, slope and intercept derived during the calibration process for each dataset. In general, the algorithm which provided the highest correlation varied among dataset (Table 5.3). The 3b [680, 709, 754], 3b [665, 709, 754], and 2b [680, 709] algorithms outperformed other algorithms for Tokyo Bay, Lake Kasumigaura dataset 1 and lake kasumigaura dataset 2, respectively. All algorithms of Lake Kasumigaura dataset 1 comparatively introduced higher correlation than that for Tokyo Bay. These results were mainly due to the fact that these algorithms are much more suitable for high-turbidity water in Lake Kasumigaura than Tokyo Bay.

The result from validation process showed that the locally tuned algorithms provided slightly higher retrieval accuracy comparing with MAIN-LUT technique (Table 5.4). However, the MAIN-LUT have two major advantages over the locally tuned algorithms: (1) the MAIN-

LUT does not require calibration process, and (2) the MAIN-LUT introduced comparatively high retrieval accuracy for in-situ and satellite dataset, even with look-up table generated from Tokyo Bay. Moreover, locally tuned algorithms produced different relation for different dataset at the same algorithms which emphasize the limitation of derived relation to be applied for different locations or conditions.

Table 5.3 Algorithms evaluation during the calibrations stage using MERIS data.

	Tokyo Bay (In situ data)				Lake Kasumigaura (Dataset 1)				Lake Kasumigaura (Dataset 2)			
	N = 49				N = 47				N = 53			
Algorithms	R^2	a_0	a_1	SD (R^2)	R^2	a_0	a_1	SD (R^2)	R^2	a_0	a_1	SD (R^2)
2b [665, 709]	0.67	68.52	-42.85	0.04	0.85	109.31	-81.19	0.02	0.52	143.98	-95.37	0.05
2b [680, 709]	0.61	126.25	-60.07	0.05	0.84	113.42	-88.35	0.03	**0.54**	**127.26**	**-93.89**	**0.05**
3b [665, 709, 754]	0.60	235.05	26.32	0.05	**0.91**	**267.05**	**26.95**	0.02	0.52	490.74	43.67	0.05
3b [680, 709, 754]	**0.67**	**464.98**	**64.40**	0.04	0.84	268.25	24.69	0.04	**0.54**	**358.01**	**35.77**	0.05
MCI [665, 709, 754]	0.66	55421.74	3.78	0.05	0.53	10289.16	10.44	0.07	0.06	7023.47	48.00	0.03
MCI [680, 709, 754]	0.65	94031.85	22.29	0.06	0.53	9633.17	18.75	0.08	0.07	6218.31	53.15	0.03
NDCI [665, 709]	0.61	130.19	27.76	0.04	0.83	273.10	24.10	0.02	0.48	356.96	48.64	0.05
NDCI [680, 709]	0.58	200.35	65.21	0.05	0.82	321.06	19.69	0.03	0.50	307.39	37.50	0.05

Data highlighted in bold represents the best algorithm performance with the highest R^2 during the calibration stage. Lake kasumigaura *Dataset 1* and *Dataset 2* represent measurements collected in 2016 and during 2002 – 2012, respectively. a_0, and a_1 represent slope and intercept for linear regression approach. The variable "*N*" denotes the number of samples used during the calibration stage. *SD (R^2)* represents the standard deviation of R^2 value that was calculated 500 time (i.e., each time a random resampling for calibration (70 %) and validation (30 %) and running the models, saving the R^2, and repeating the process to find the datasets that provide mean R^2).

Table 5.4 Algorithms retrieval accuracies during the validation stage using MERIS data.

	Tokyo Bay (In situ data)			Lake Kasumigaura (Dataset 1)			Lake Kasumigaura (Dataset 2)		
	N = 22			N = 21			N = 24		
Algorithms	R^2	RMSE	SD (R^2)	R^2	RMSE	SD (R^2)	R^2	RMSE	SD (R^2)
2b [665, 709]	0.67	15.42	0.10	0.85	7.65	0.05	0.52	28.99	0.11
2b [680, 709]	0.62	16.81	0.12	0.83	9.83	0.07	0.54	26.17	0.11
3b [665, 709, 754]	0.58	19.24	0.12	**0.89**	**8.49**	0.07	0.52	28.61	0.11
3b [680, 709, 754]	**0.70**	**17.51**	**0.11**	0.84	8.62	0.07	**0.55**	**27.81**	0.11
MCI [665, 709, 754]	0.68	15.35	0.11	0.51	23.93	0.14	0.08	33.96	0.08
MCI [680, 709, 754]	0.67	18.12	0.12	0.51	16.93	0.14	0.10	39.09	0.08
NDCI [665, 709]	0.63	14.04	0.08	0.84	9.51	0.05	0.50	19.70	0.12
NDCI [680, 709]	0.58	17.45	0.12	0.81	11.27	0.06	0.52	19.31	0.12
MAIN-LUT	0.69	21.40	---	0.85	11.3	---	0.57	36.50	---

Data highlighted in bold represents the best algorithm performance with the highest R2.
SD (R^2) represents the standard deviation of R^2 value that was calculated 500 time (i.e., each time a random resampling for calibration (70 %) and validation (30 %) and running the models, saving the R^2, and repeating the process to find the datasets that provide mean R^2).

5.5. Conclusions

A multi-algorithm indices and look-up table (MAIN-LUT) technique was proposed to retrieve Chla concentration for optically complex Case 2 waters. The MAIN-LUT technique combine the advantage of a look-up table that covering wide ranges of trophic status with the ability of the existing Chla algorithms which provide indices correlated with Chla concentration. Multi-algorithms should be used to match algorithms' indices estimated from measured reflectance with the indices of simulated reflectance library. In-situ measurements and MERIS data were used to validate MAIN-LUT over turbid and highly turbid water bodies. The result presented in this study reveal the ability of MAIN-LUT to accurately retrieve Chla concentration. Although the simulated dataset was generated based on IOPs from Tokyo Bay, the MAIN-LUT provided high retrieval accuracy for Lake Kasumigaura with in-situ measurements and MERIS data. Eight algorithms' combinations were investigated for the MAIN-LUT. Six out of the eight combinations provided comparable high retrieval accuracy for Tokyo Bay (R^2 = 0.65, RMSE = 22.2 mg m^{-3}, MARE = 148.27 %), Lake Kasumigaura (R^2 = 0.85, RMSE = 11.98 mg m^{-3}, MARE = 18.38 %), and MERIS data (R^2 = 0.552, RMSE = 34.38 mg m^{-3}, MARE = 43.35 %). Accordingly, the 2-indices-[665] combination is proposed for MAIN-LUT. In addition, 4-indices-[680] combination is recommended for MERIS data to overcome the limitation of other combinations which underestimated Chla concentration > 50 mg m^{-3}. The spatial and temporal distribution of Chla concentration was also captured using MAN-LUT for MERIS images.

CHAPTER 6

Conclusions and future work

6.1. Conclusions

The objectives of the current research can be divided into three major points: (1) evaluation of seven processors developed for chlorophyll-a (Chla) retrieval from MERIS sensor; (2) evaluation of seven semi-analytical algorithms that are widely used for Chla retrieve in Case 2 waters; (3) developing a novel technique that combine the strength of these algorithms and approaches.

The evaluation of seven processors based on neural network and band height that developed for MERIS sensor reveals that the maximum chlorophyll index (MCI) and fluorescence line height (FLH) processors outperformed other processors. Both the MCI and FLH require MERIS L1 products as inputs which leads to avoidance of errors arising from atmospheric correction. The evaluation of five out of the seven processors that provide direct Chla concentration (i.e., Eutrophic Lake (EUL), Boreal Lake (BOL), Case 2 Regional (C2R), Free University of Berlin (FUB), and and Maximum Peak Height (MPH)) shows that theses processors underestimate or overestimate Chla concentration. Thus, the seven require local tuning which limit the ability of these processors to be applied globally.

The second evaluation study conducted for seven semi-analytical algorithms using different band combinations (i.e., multispectral and hyperspectral bands) and three regression approaches (i.e., linear, quadratic polynomial and power regression). Results show that the selection of regression approaches has low influence on Chla retrieval; whereas, the selection of algorithms' indices has significant influence on retrieval accuracy. The two-, three-, four-band algorithms and normalized different chlorophyll index tend to provide high retrieval accuracy than ocean color V4 (OC4E), maximum chlorophyll index and synthetic chlorophyll index. The spatial distribution of the most accurate algorithms for different concentrations of Chla (1 – 200 mg m^{-3}) and NAP (1 – 200 g m^{-3}) indicate that no single algorithms can produce outstanding retrieval accuracy for different concentration of Chla and NAP. In addition, the retrieved relationship for semi-analytical algorithms are location and data limited.

Based on the previous evaluation that indicate the strength and limitation of these algorithms and approaches, the Multi-Algorithm Indices and Look-Up Table (MAIN-LUT) technique was proposed. The MAIN-LUT combines the strength of both the semi-analytical algorithms (i.e., provide indices that highly correlated with Chla concentrations) and look-up

table (i.e., simulated dataset covers different trophic statuses). In addition, the MAIN-LUT technique can be applied for multispectral ocean color sensors. Results reveal that the MAIN-LUT provide high Chla retrieval accuracy that is similar to accuraty of locally tuned algorithms. Furthermore, the MAIN-LUT could accurately retrieve Chla concentration in Lake Kasumigaura, despite the fact that the look-up table was created based on inherent optical properties (IOPs) from Tokyo Bay. Thus, the MAIN-LUT could be applied in similar water bodies. The Spatial and temporal distribution of Chla concentration are accurately retrieved from MERIS data.

6.2. Future work

The concept of the Multi-Algorithm Indices and Look-Up Table (MAIN-LUT) technique can be applied to retrieve chlorophyll-a concentrations in a global scale. This hypothesis based on two reasons: (1) the look-up table of MAIN-LUT could simulate water leaving reflectance in different properties; and (2) although the look-up table of MAIN-LUT was developed based on IOPs from Tokyo Bay, the MAIN-LUT provided high retrieval accuracy in Lake Kasumigaura. Availability of in-situ measurements for inland lakes and coastal areas represents the major challenge to apply and validate the MAIN-LUT in a global scale. However, the Global Observatory of Lake Responses to Environmental Change (GLOBOLAKES) project provides a solution to overcome this obstacle. The GLOBOLAKES project belongs to University of Stirling, UK and it collects the data from around 250 lakes and reservoirs all over the world. This dataset covers various trophic status. Upgrading the look-up table of MAIN-LUT to include these water bodies could allow the MAIN-LUT to monitor chlorophyll-a concentrations for the whole world.

REFERENCES

American Public Health Association., 2005. Standard methods for the examination of water and wastewater. American Public Health Association, Washington, D.C.

Augusto-Silva, P.B., Ogashawara, I., Barbosa, C.C.F., de Carvalho, L.A.S., Jorge, D.S.F., Fornari, C.I., Stech, J.L., 2014. Analysis of MERIS reflectance algorithms for estimating chlorophyll-a concentration in a Brazilian reservoir. Remote Sens. 6, 11689–11707. doi:10.3390/rs61211689

Austin, R.W., 1980. Gulf of Mexico, ocean-color surface-truth measurements. Boundary-Layer Meteorol. 18, 269–285. doi:10.1007/BF00122024

Austin, R.W., Petzold, T.J., 1981. The determination of the diffuse attenuation coefficient of sea water using the Coastal Zone Color Scanner, in: Oceanography from Space; Barale, V., Gower, J.F.R., Alberotanza, L., Eds. Springer, Boston, MA, USA, pp. 239–256. doi:10.1017/CBO9781107415324.004

Baruah, P.J., Tamura, M., Oki, K., Nishimura, H., 2001. Neural network modeling of lake surface chlorophyll and sediment content from Landsat TM imagery, in: Proceedings of the Paper Presented at the 22nd Asian Conference on Remote Sensing, Singapore, 5–9 November 2001. p. 9.

Binding, C.E., Greenberg, T.A., Jerome, J.H., Bukata, R.P., Letourneau, G., 2011. An assessment of MERIS algal products during an intense bloom in Lake of the Woods. J. Plankton Res. 33, 793–806. doi:10.1093/plankt/fbq133

Boyer, J.N., Kelble, C.R., Ortner, P.B., Rudnick, D.T., 2009. Phytoplankton bloom status: Chlorophyll a biomass as an indicator of water quality condition in the southern estuaries of Florida, USA. Ecol. Indic. 9, S56–S67. doi:10.1016/j.ecolind.2008.11.013

Brando, V.E., Anstee, J.M., Wettle, M., Dekker, A.G., Phinn, S.R., Roelfsema, C., 2009. A physics based retrieval and quality assessment of bathymetry from suboptimal hyperspectral data. Remote Sens. Environ. 113, 755–770. doi:10.1016/j.rse.2008.12.003

Bresciani, M., Stroppiana, D., Odermatt, D., Morabito, G., Giardino, C., 2011. Assessing remotely sensed chlorophyll-a for the implementation of the Water Framework Directive in European perialpine lakes. Sci. Total Environ. 409, 3083–3091. doi:10.1016/j.scitotenv.2011.05.001

Buiteveld, H., Hakvoort, J.H.M., Donze, M., 1994. Optical properties of pure water, in: Jaffe, J.S. (Ed.), Ocean Optics XII. International Society for Optics and Photonics, Bellingham, WA, USA, pp. 174–183. doi:10.1117/12.190060

Campbell, G., Phinn, S.R., Dekker, A.G., Brando, V.E., 2011. Remote sensing of water quality in an Australian tropical freshwater impoundment using matrix inversion and MERIS images. Remote Sens. Environ. 115, 2402–2414. doi:10.1016/j.rse.2011.05.003

Carder, K.L., Chen, F.R., Lee, Z.P., Hawes, S.K., Kamykowski, D., 1999. Semianalytic Moderate-Resolution Imaging Spectrometer algorithms for chlorophyll a and absorption with bio-optical domains based on nitrate-depletion temperatures. J. Geophys. Res. 104, 5403. doi:10.1029/1998JC900082

CEBES, 2001. Lake Kasumigaura Database, Interpretations of observed data [WWW Document]. URL http://db.cger.nies.go.jp/gem/moni-e/inter/GEMS/database/kasumi/pdf/methods/interpretation2001.pdf (accessed 6.27.17).

Ciotti, A.M., Lewis, M.R., Cullen, J.J., 2002. Assessment of the relationships between dominant cell size in natural phytoplankton communities and the spectral shape of the

absorption coefficient. Limnol. Oceanogr. 47, 404–417.

Dall'Olmo, G., Gitelson, A.A., 2006. Effect of bio-optical parameter variability and uncertainties in reflectance measurements on the remote estimation of chlorophyll-a concentration in turbid productive waters: modeling results. Appl. Opt. 45, 3577. doi:10.1364/AO.45.003577

Dall'Olmo, G., Gitelson, A.A., Rundquist, D.C., 2003. Towards a unified approach for remote estimation of chlorophyll-a in both terrestrial vegetation and turbid productive waters. Geophys. Res. Lett. 30, 1938. doi:10.1029/2003GL018065

Dalponte, M., Bruzzone, L., Gianelle, D., 2012. Tree species classification in the Southern Alps based on the fusion of very high geometrical resolution multispectral/hyperspectral images and LiDAR data. Remote Sens. Environ. 123, 258–270. doi:10.1016/j.rse.2012.03.013

Dekker, A.G., 1993. Detection of optical water quality parameters for eutrophic waters by high resolution remote sensing.

Dekker, A.G., Phinn, S.R., Anstee, J., Bissett, P., Brando, V.E., Casey, B., Fearns, P., Hedley, J., Klonowski, W., Lee, Z.P., 2011. Intercomparison of shallow water bathymetry, hydro-optics, and benthos mapping techniques in Australian and Caribbean coastal environments. Limnol. Oceanogr. Methods 9, 396–425. doi:10.4319/lom.2011.9.396

Doerffer, R., Helmut, S., 2000. Neural network for retrieval of concentrations of water constituents with the possibility of detecting exceptional out of scope spectra, in: Proceedings of the IGARSS 2000: IEEE 2000 International Geoscience and Remote Sensing Symposium, Honolulu, HI, USA, 24–28 July 2000. IEEE, Piscataway, NJ, USA, pp. 714–717.

Doerffer, R., Schiller, H., 2008. MERIS lake water algorithm for BEAM—MERIS algorithm theoretical basis document. V1.0, 10 June 2008. Geesthacht, Germany: GKSS Research Center.

Doerffer, R., Schiller, H., 2007. The MERIS Case 2 water algorithm. Int. J. Remote Sens. 28, 517–535. doi:10.1080/01431160600821127

Dogliotti, A.I., Ruddick, K.G., Nechad, B., Doxaran, D., Knaeps, E., 2015. A single algorithm to retrieve turbidity from remotely-sensed data in all coastal and estuarine waters. Remote Sens. Environ. 156, 157–168. doi:10.1016/j.rse.2014.09.020

El-Alem, A., Chokmani, K., Laurion, I., El-Adlouni, S.E., 2012. Comparative analysis of four models to estimate chlorophyll-a concentration in case-2 waters using MODerate resolution imaging spectroradiometer (MODIS) imagery. Remote Sens. 4, 2373–2400. doi:10.3390/rs4082373

ESA, 2015. European Space Agency, Earthnet Online [WWW Document]. URL http://earth.esa.int/ (accessed 3.10.15).

ESA, 2012. MERIS Frequently Asked Questions [WWW Document]. URL http://earth.esa.int/pub/ESA_DOC/ENVISAT/MERIS/VT-P017-DOC-005-E-01-01_meris.faq.1_1.pdf (accessed 6.23.17).

Fernandez-Jaramillo, A.A., Duarte-Galvan, C., Contreras-Medina, L.M., Torres-Pacheco, I., de J Romero-Troncoso, R., Guevara-Gonzalez, R.G., Millan-Almaraz, J.R., 2012. Instrumentation in developing chlorophyll fluorescence biosensing: a review. Sensors 12, 11853–69. doi:10.3390/s120911853

Finger, D., Wüest, A., Bossard, P., 2013. Effects of oligotrophication on primary production

in peri-alpine lakes. Water Resour. Res. 49, 4700–4710. doi:10.1002/wrcr.20355

Garver, S.A., Siegel, D.A., 1997. Inherent optical property inversion of ocean color spectra and its biogeochemical interpretation: 1. Time series from the Sargasso Sea. J. Geophys. Res. Ocean. 102, 18607–18625. doi:10.1029/96JC03243

Gholizadeh, M.H., Melesse, A.M., Reddi, L., 2016. A Comprehensive Review on Water Quality Parameters Estimation Using Remote Sensing Techniques. Sensors 16, 1298.

Giardino, C., Brando, V.E., Dekker, A.G., Strömbeck, N., Candiani, G., 2007. Assessment of water quality in Lake Garda (Italy) using Hyperion. Remote Sens. Environ. 109, 183–195. doi:10.1016/j.rse.2006.12.017

Gilerson, A.A., Gitelson, A.A., Zhou, J., Gurlin, D., Moses, W., Ioannou, I., Ahmed, S.A., 2010. Algorithms for remote estimation of chlorophyll-a in coastal and inland waters using red and near infrared bands. Opt. Express 18, 24109–25. doi:10.1364/OE.18.024109

Gilerson, A., Zhou, J., Hlaing, S., Ioannou, I., Schalles, J., Gross, B., Moshary, F., Ahmed, S., 2007. Fluorescence component in the reflectance spectra from coastal waters. Dependence on water composition. Opt. Express 15, 15702–15721. doi:10.1364/OE.15.015702

Gitelson, A.A., Dall'Olmo, G., Moses, W., Rundquist, D.C., Barrow, T., Fisher, T.R., Gurlin, D., Holz, J., 2008. A simple semi-analytical model for remote estimation of chlorophyll-a in turbid waters: Validation. Remote Sens. Environ. 112, 3582–3593. doi:10.1016/j.rse.2008.04.015

Gokul, E.A., Shanmugam, P., Sundarabalan, B., Sahay, A., Chauhan, P., 2014. Modelling the inherent optical properties and estimating the constituents′ concentrations in turbid and eutrophic waters. Cont. Shelf Res. 84, 120–138. doi:10.1016/j.csr.2014.05.013

Gons, H.J., 1999. Optical Teledetection of Chlorophyll a in Turbid Inland Waters. Environ. Sci. Technol. 33, 1127–1132. doi:10.1021/es9809657

Gons, H.J., Auer, M.T., Effler, S.W., 2008. MERIS satellite chlorophyll mapping of oligotrophic and eutrophic waters in the Laurentian Great Lakes. Remote Sens. Environ. 112, 4098–4106. doi:10.1016/j.rse.2007.06.029

Gons, H.J., Burger-Wiersma, T., Otten, J.H., Rijkeboer, M., 1992. Coupling of phytoplankton and detritus in a shallow, eutrophic lake (Lake Loosdrecht, The Netherlands). Hydrobiologia 233, 51–59. doi:10.1007/BF00016095

Gordon, H., Brown, J., Brown, O., Evans, R., Smith, R., 1988. A semianalytic radiance model of ocean color. J. Geophys. Res. 93, 10909–10924.

Gordon, H.R., Morel, A., 1983. Remote Assessment of Ocean Color for Interpretation of Satellite Visible Imagery. A review. Lecture notes on coastal and estuarine studies. Springer, Berlin, Germany.

Gower, J., King, S., Borstad, G., Brown, L., 2008a. The importance of a band at 709 nm for interpreting water-leaving spectral radiance. Can. J. Remote Sens. 34, 287–295.

Gower, J., King, S., Borstad, G., Brown, L., 2005. Detection of intense plankton blooms using the 709 nm band of the MERIS imaging spectrometer. Int. J. Remote Sens. 26, 2005–2012. doi:10.1080/01431160500075857

Gower, J., King, S., Goncalves, P., 2008b. Global monitoring of plankton blooms using MERIS MCI. Int. J. Remote Sens. 29, 6209–6216. doi:10.1080/01431160802178110

Gower, J.F.R., Doerffer, R., Borstad, G.A., 1999. Interpretation of the 685nm peak in water-

leaving radiance spectra in terms of fluorescence, absorption and scattering, and its observation by MERIS. Int. J. Remote Sens. 20, 1771–1786. doi:10.1080/014311699212470

Gurlin, D., Gitelson, A.A., Moses, W.J., 2011. Remote estimation of chl-a concentration in turbid productive waters — Return to a simple two-band NIR-red model? Remote Sens. Environ. 115, 3479–3490. doi:10.1016/j.rse.2011.08.011

Ha, N., Koike, K., Nhuan, M., 2013. Improved Accuracy of Chlorophyll-a Concentration Estimates from MODIS Imagery Using a Two-Band Ratio Algorithm and Geostatistics: As Applied to the Monitoring of Eutrophication Processes over Tien Yen Bay (Northern Vietnam). Remote Sens. 6, 421–442. doi:10.3390/rs6010421

HAN, L., RUNDQUIST, D.C., LIU, L.L., FRASER, R.N., SCHALLES, J.F., 1994. The spectral responses of algal chlorophyll in water with varying levels of suspended sediment. Int. J. Remote Sens. 15, 3707–3718. doi:10.1080/01431169408954353

Hedley, J., Roelfsema, C., Phinn, S.R., 2009. Efficient radiative transfer model inversion for remote sensing applications. Remote Sens. Environ. 113, 2527–2532. doi:10.1016/j.rse.2009.07.008

HIGANO, Y., SAWADA, T., 1995. The Dynamic Optimal Policy to Improve the Water Quality of Lake Kasumigaura. Stud. Reg. Sci. 26, 75–86. doi:10.2457/srs.26.75

Hirawake, T., Suzuki, K., Kishino, M., Furuya, K., Taguchi, S., Saitoh, S., Saino, T., Matsumoto, K., Harimoto, T., Sasaki, H., Fujiki, T., Kobara, S., Kashiwa, T., 2001. A Protocol for Measuring the Absorption Coefficient of Phytoplankton using QFT(Quantitative Filter Technique)and a Submersible Spectrophotometer. Oceanogr. Japan 10, 471–484. doi:10.5928/kaiyou.10.471

Hock, R., Jensen, H., 1999. Application of kriging interpolation for glacier mass balance computations. Geogr. Ann. Ser. A, Phys. … 81, 611–619. doi:10.1111/j.0435-3676.1999.00089.x

Huang, C., Zou, J., Li, Y., Yang, H., Shi, K., Li, J., Wang, Y., Chena, X., Zheng, F., 2014. Assessment of NIR-red algorithms for observation of chlorophyll-a in highly turbid inland waters in China. ISPRS J. Photogramm. Remote Sens. 93, 29–39. doi:10.1016/j.isprsjprs.2014.03.012

Huang, Y., Jiang, D., Zhuang, D., Fu, J., 2010. Evaluation of hyperspectral indices for chlorophyll-a concentration estimation in Tangxun Lake (Wuhan, China). Int. J. Environ. Res. Public Health 7, 2437–51. doi:10.3390/ijerph7062437

IOCCG, 2014. Phytoplankton Functional Types from Space, Reports of the International Ocean Colour Coordinating Group. IOCCG, Dartmouth, Canada.

IOCCG, 2010. Atmospheric Correction for Remotely-Sensed Ocean-Colour Products, Reports of the International Ocean Colour Coordinating Group. IOCCG, Dartmouth, Canada.

IOCCG, 2006. Remote Sensing of Inherent Optical Properties: Fundamentals, Tests of Algorithms, and Applications, Reports of the International Ocean Colour Coordinating Group. IOCCG, Dartmouth, Canada.

IOCCG, 2000. Remote Sensing of Ocean Colour in Coastal, and Other Optically-Complex, Waters, Reports of the International Ocean Colour Coordinating Group. IOCCG, Dartmouth, Canada.

Jaelani, L.M., Matsushita, B., Yang, W., Fukushima, T., 2013. Evaluation of four MERIS atmospheric correction algorithms in Lake Kasumigaura, Japan. Int. J. Remote Sens.

JMA, 2017. Monthly mean percentage of possible sunshine, Mito station, Japan Meteorological Agency [WWW Document]. URL http://www.data.jma.go.jp/obd/stats/etrn/view/monthly_s3_en.php?block_no=47629&view=10 (accessed 3.4.17).

Kirk, J.T.O., 1984. Dependence of relationship between inherent and apparent optical properties of water on solar altitude. Limnol. Oceanogr. 29, 350–356. doi:10.4319/lo.1984.29.2.0350

Kishino, M., Takahashi, M., Okami, N., Ichimura, S., 1985. Estimation of the spectral absorption coefficients of phytoplankton in the sea. Bull. Mar. Sci. 37, 634–642.

Klonowski, W.M., Fearns, P.R., Lynch, M.J., 2007. Retrieving key benthic cover types and bathymetry from hyperspectral imagery. J. Appl. Remote Sens. 1, 11505. doi:10.1117/1.2816113

Kutser, T., 2004. Quantitative detection of chlorophyll in cyanobacterial blooms by satellite remote sensing. Limnol. Oceanogr. 49, 2179–2189. doi:10.4319/lo.2004.49.6.2179

Kutser, T., Metsamaa, L., Strömbeck, N., Vahtmäe, E., 2006. Monitoring cyanobacterial blooms by satellite remote sensing. Estuar. Coast. Shelf Sci. 67, 303–312. doi:10.1016/j.ecss.2005.11.024

Le, C., Hu, C., Cannizzaro, J., English, D., Muller-Karger, F., Lee, Z., 2013. Evaluation of chlorophyll-a remote sensing algorithms for an optically complex estuary. Remote Sens. Environ. 129, 75–89. doi:10.1016/j.rse.2012.11.001

Le, C., Li, Y., Zha, Y., Sun, D., Huang, C., Lu, H., 2009. A four-band semi-analytical model for estimating chlorophyll a in highly turbid lakes: The case of Taihu Lake, China. Remote Sens. Environ. 113, 1175–1182. doi:10.1016/j.rse.2009.02.005

Le, C., Li, Y., Zha, Y., Sun, D., Huang, C., Zhang, H., 2011. Remote estimation of chlorophyll a in optically complex waters based on optical classification. Remote Sens. Environ. 115, 725–737. doi:10.1016/j.rse.2010.10.014

Lee, Z., Carder, K.L., Arnone, R.A., 2002. Deriving Inherent Optical Properties from Water Color: a Multiband Quasi-Analytical Algorithm for Optically Deep Waters. Appl. Opt. 41, 5755. doi:10.1364/AO.41.005755

Lee, Z., Carder, K.L., Chen, R.F., Peacock, T.G., 2001. Properties of the water column and bottom derived from Airborne Visible Infrared Imaging Spectrometer (AVIRIS) data. J. Geophys. Res. Ocean. 106, 11639–11651. doi:10.1029/2000JC000554

Lee, Z., Carder, K.L., Mobley, C.D., Steward, R.G., Patch, J.S., 1999. Hyperspectral remote sensing for shallow waters: 2 Deriving bottom depths and water properties by optimization. Appl. Opt. 38, 3831. doi:10.1364/AO.38.003831

Lee, Z., Carder, K.L., Mobley, C.D., Steward, R.G., Patch, J.S., 1998. Hyperspectral remote sensing for shallow waters. I. A semianalytical model. Appl. Opt. 37, 6329–6338. doi:10.1364/AO.37.006329

Lesser, M.P., Mobley, C.D., 2007. Bathymetry, water optical properties, and benthic classification of coral reefs using hyperspectral remote sensing imagery. Coral Reefs 26, 819–829. doi:10.1007/s00338-007-0271-5

Levrini, G., Delvart, S., 2011. MERIS Product Handbook, European Space Agency (ESA).

Li, L., Li, L., Song, K., Li, Y., Tedesco, L.P., Shi, K., Li, Z., 2013. An inversion model for deriving inherent optical properties of inland waters: Establishment, validation and application. Remote Sens. Environ. 135, 150–166. doi:10.1016/j.rse.2013.03.031

Loisel, H., Vantrepotte, V., Ouillon, S., Ngoc, D.D., Herrmann, M., Tran, V., Mériaux, X., Dessailly, D., Jamet, C., Duhaut, T., Nguyen, H.H., Van Nguyen, T., 2017. Assessment and analysis of the chlorophyll-a concentration variability over the Vietnamese coastal waters from the MERIS ocean color sensor (2002–2012). Remote Sens. Environ. 190, 217–232. doi:10.1016/j.rse.2016.12.016

Louchard, E.M., Reid, R.P., Stephens, F.C., Davis, C.O., Leathers, R.A., Downes, T.V., 2002. Optical remote sensing of benthic habitats and bathymetry in coastal environments at Lee Stocking Island, Bahamas: A comparative spectral classification approach. DTIC Document: Fort Belvoir, VA, USA.

Lyons, M., Phinn, S., Roelfsema, C., 2011. Integrating Quickbird Multi-Spectral Satellite and Field Data: Mapping Bathymetry, Seagrass Cover, Seagrass Species and Change in Moreton Bay, Australia in 2004 and 2007. Remote Sens. 3, 42–64. doi:10.3390/rs3010042

Lyu, H., Li, X., Wang, Y., Jin, Q., Cao, K., Wang, Q., Li, Y., 2015. Evaluation of chlorophyll-a retrieval algorithms based on MERIS bands for optically varying eutrophic inland lakes. Sci. Total Environ. 530–531, 373–82. doi:10.1016/j.scitotenv.2015.05.115

Majozi, N.P., Salama, M.S., Bernard, S., Harper, D.M., Habte, M.G., 2014. Remote sensing of euphotic depth in shallow tropical inland waters of Lake Naivasha using MERIS data. Remote Sens. Environ. 148, 178–189. doi:10.1016/j.rse.2014.03.025

Mannino, A., Russ, M.E., Hooker, S.B., 2008. Algorithm development and validation for satellite-derived distributions of DOC and CDOM in the U.S. Middle Atlantic Bight. J. Geophys. Res. 113, C07051. doi:10.1029/2007JC004493

Matsushita, B., Yang, W., Chang, P., Yang, F., Fukushima, T., 2012. A simple method for distinguishing global Case-1 and Case-2 waters using SeaWiFS measurements. ISPRS J. Photogramm. Remote Sens. 69, 74–87. doi:10.1016/j.isprsjprs.2012.02.008

Matsushita, B., Yang, W., Jaelani, L.M., Setiawan, F., Fukushima, T., 2016. Monitoring Water Quality with Remote Sensing Image Data, in: Remote Sensing for Sustainability, Remote Sensing Applications Series. CRC Press, pp. 163–189. doi:doi:10.1201/9781315371931-10

Matsushita, B., Yang, W., Yu, G., Oyama, Y., Yoshimura, K., Fukushima, T., 2015. A hybrid algorithm for estimating the chlorophyll-a concentration across different trophic states in Asian inland waters. ISPRS J. Photogramm. Remote Sens. 102, 28–37. doi:10.1016/j.isprsjprs.2014.12.022

Matthews, M.W., 2014. Eutrophication and cyanobacterial blooms in South African inland waters: 10years of MERIS observations. Remote Sens. Environ. 155, 161–177. doi:10.1016/j.rse.2014.08.010

Matthews, M.W., 2011. A current review of empirical procedures of remote sensing in inland and near-coastal transitional waters. Int. J. Remote Sens. 32, 6855–6899. doi:10.1080/01431161.2010.512947

Matthews, M.W., Bernard, S., Robertson, L., 2012. An algorithm for detecting trophic status (chlorophyll-a), cyanobacterial-dominance, surface scums and floating vegetation in inland and coastal waters. Remote Sens. Environ. 124, 637–652. doi:10.1016/j.rse.2012.05.032

Matthews, M.W., Bernard, S., Winter, K., 2010. Remote sensing of cyanobacteria-dominant algal blooms and water quality parameters in Zeekoevlei, a small hypertrophic lake, using MERIS. Remote Sens. Environ. 114, 2070–2087.

Mélin, F., Vantrepotte, V., Clerici, M., D'Alimonte, D., Zibordi, G., Berthon, J.-F., Canuti, E., 2011. Multi-sensor satellite time series of optical properties and chlorophyll-a concentration in the Adriatic Sea. Prog. Oceanogr. 91, 229–244. doi:10.1016/j.pocean.2010.12.001

Mishra, S., Mishra, D.R., 2012. Normalized difference chlorophyll index: A novel model for remote estimation of chlorophyll-a concentration in turbid productive waters. Remote Sens. Environ. 117, 394–406. doi:10.1016/j.rse.2011.10.016

Mitchell, B.G., Kahru, M., Wieland, J., Stramska, M., Mueller, J.L., 2002. Determination of spectral absorption coefficients of particles, dissolved material and phytoplankton for discrete water samples. Ocean Opt. Protoc. Satell. Ocean Color Sens. validation, Revis. 3, 231–257.

Mobley, C.D., 1999. Estimation of the Remote-Sensing Reflectance from Above-Surface Measurements. Appl. Opt. 38, 7442. doi:10.1364/AO.38.007442

Mobley, C.D., Sundman, L.K., Davis, C.O., Bowles, J.H., Downes, T.V., Leathers, R.A., Montes, M.J., Bissett, W.P., Kohler, D.D.R., Reid, R.P., Louchard, E.M., Gleason, A., 2005. Interpretation of hyperspectral remote-sensing imagery by spectrum matching and look-up tables. Appl. Opt. 44, 3576. doi:10.1364/AO.44.003576

Moore, T.S., Dowell, M.D., Bradt, S., Verdu, A.R., 2014. An optical water type framework for selecting and blending retrievals from bio-optical algorithms in lakes and coastal waters. Remote Sens. Environ. 143, 97–111. doi:10.1016/j.rse.2013.11.021

Morel, A., 1974. Optical properties of pure water and pure sea water. Opt. Asp. Oceanogr. 1, 1–24.

Morel, A., Prieur, L., 1977. Analysis of variations in ocean color. Limnol. Oceanogr. 22, 709–722. doi:10.4319/lo.1977.22.4.0709

Neville, R.A., Gower, J.F.R., 1977. Passive remote sensing of phytoplankton via chlorophyll α fluorescence. J. Geophys. Res. 82, 3487–3493.

NIES, 2016. Lake Kasumigaura Database, National Institute for Environmental Studies, Japan. [WWW Document]. URL http://db.cger.nies.go.jp/gem/moni-e/inter/GEMS/database/kasumi/index.html (accessed 11.20.16).

NLNI, 2017. Lakes Data, National Land Numerical Information , Japan [WWW Document]. URL http://nlftp.mlit.go.jp/ksj/ (accessed 3.14.17).

O'Reilly, J.E., Maritorena, S., Mitchell, B.G., Siegel, D.A., Carder, K.L., Garver, S.A., Kahru, M., McClain, C., 1998. Ocean color chlorophyll algorithms for SeaWiFS. J. Geophys. Res. 103, 24937. doi:10.1029/98JC02160

O'Reilly, J.E., Maritorena, S., O'Brien, M.C., Siegel, D.A., Toole, D., Menzies, D., Smith, R.C., Mueller, J.L., Mitchell, B.G., Kahru, M., 2000a. SeaWiFS postlaunch calibration and validation analyses, part 3. NASA Tech. Memo 2000–20689, 3–8.

O'Reilly, J.E., Maritorena, S., Siegel, D.A., O'Brien, M.C., Toole, D., Mitchell, B.G., Kahru, M., Chavez, F.P., Strutton, P., Cota, G.F., 2000b. Ocean color chlorophyll a algorithms for SeaWiFS, OC2, and OC4: Version 4. SeaWiFS postlaunch calibration Valid. Anal. Part 3, 9–23.

Odermatt, D., Pomati, F., Pitarch, J., Carpenter, J., Kawka, M., Schaepman, M., Wüest, A., 2012. MERIS observations of phytoplankton blooms in a stratified eutrophic lake. Remote Sens. Environ. 126, 232–239. doi:10.1016/j.rse.2012.08.031

Oki, K., 2010. Why is the Ratio of Reflectivity Effective for Chlorophyll Estimation in the Lake Water? Remote Sens. 2, 1722–1730. doi:10.3390/rs2071722

Oki, K., Yasuoka, Y., 2002. Estimation of Chlorophyll Concentration in Lakes and Inland Seas with a Field Spectroradiometer above the Water Surface. Appl. Opt. 41, 6463. doi:10.1364/AO.41.006463

Oki, K., Yasuoka, Y., 1996. Estimation of Chlorophyll-a Concentration in Rich Chlorophyll Water Area from Near-infrared and Red Spectral Signature. J. Remote Sens. Soc. Japan 16, 315–323. doi:10.11440/rssj1981.16.315

Oki, K., Yasuoka, Y., Tamura, M., 2001. Estimation of Chlorophyll- a and Suspended Solids Concentration in Rich Concentration Water Area with Remote Sensing Technique. J. Remote Sens. Soc. Japan 21, 449–457. doi:10.11440/rssj1981.21.449

Oyama, Y., Matsushita, B., Fukushima, T., Matsushige, K., Imai, A., 2009. Application of spectral decomposition algorithm for mapping water quality in a turbid lake (Lake Kasumigaura, Japan) from Landsat TM data. ISPRS J. Photogramm. Remote Sens. 64, 73–85. doi:10.1016/j.isprsjprs.2008.04.005

Palmer, S.C.J., Hunter, P.D., Lankester, T., Hubbard, S., Spyrakos, E., N. Tyler, A., Présing, M., Horváth, H., Lamb, A., Balzter, H., Tóth, V.R., Palmer, S.C.J., Hunter, P.D., Lankester, T., Hubbard, S., Spyrakos, E., N. Tyler, A., Présing, M., Horváth, H., Lamb, A., Balzter, H., Tóth, V.R., 2015. Validation of Envisat MERIS algorithms for chlorophyll retrieval in a large, turbid and optically-complex shallow lake. Remote Sens. Environ. 157, 158–169. doi:10.1016/j.rse.2014.07.024

Palmer, S.C.J., Odermatt, D., Hunter, P.D., Brockmann, C., Présing, M., Balzter, H., Tóth, V.R., 2015. Satellite remote sensing of phytoplankton phenology in Lake Balaton using 10years of MERIS observations. Remote Sens. Environ. 158, 441–452. doi:10.1016/j.rse.2014.11.021

Ruiz-Verdú, A., Koponen, S., Heege, T., Doerffer, R., Brockmann, C., Kallio, K., Pyhälahti, T., Peña, R., Polvorionos, A., Heblinski, J., 2008. Development of MERIS lake water algorithms: Validation results from Europe, in: Proceedings of The“ 2nd MERIS/(A) ATSR User Workshop”, Frascati, Italy, 22– 26 September 2008 (ESA SP-666, November 2008).

Salem, S., Higa, H., Kim, H., Kazuhiro, K., Kobayashi, H., Oki, K., Oki, T., 2017a. Multi-Algorithm Indices and Look-Up Table for Chlorophyll-a Retrieval in Highly Turbid Water Bodies Using Multispectral Data. Remote Sens. 9, 556. doi:10.3390/RS9060556

Salem, S., Higa, H., Kim, H., Kobayashi, H., Oki, K., Oki, T., 2017b. Assessment of Chlorophyll-a Algorithms Considering Different Trophic Statuses and Optimal Bands. Sensors 17, 1746. doi:10.3390/S17081746

Santer, R., Carrere, V., Dubuisson, P., Roger, J.C., 1999. Atmospheric correction over land for MERIS. Int. J. Remote Sens. 20, 1819–1840. doi:10.1080/014311699212506

Schroeder, T., Schaale, M., Fischer, J., 2007. Retrieval of atmospheric and oceanic properties from MERIS measurements: A new Case-2 water processor for BEAM. Int. J. Remote Sens. 28, 5627–5632. doi:10.1080/01431160701601774

Schueler, C., Yoder, J., Antoine, D., Castillo, C., Evans, R., Mengelt, C., Mobley, C., Sarmiento, J., Sathyendranath, S., Siegel, D., Wilson, C., 2011. Assessing Requirements for Sustained Ocean Color Research and Observations, in: Proceedings of the AIAA SPACE 2011 Conference & Exposition, Long Beach, CA, USA, 27–29 September 2011. American Institute of Aeronautics and Astronautics, Reston, VA, USA. doi:doi:10.2514/6.2011-7361

Shen, F., Zhou, Y.-X., Li, D.-J., Zhu, W.-J., Suhyb Salama, M., 2010. Medium resolution imaging spectrometer (MERIS) estimation of chlorophyll- a concentration in the turbid

sediment-laden waters of the Changjiang (Yangtze) Estuary. Int. J. Remote Sens. 31, 4635–4650. doi:10.1080/01431161.2010.485216

Shi, K., Li, Y., Li, L., Lu, H., Song, K., Liu, Z., Xu, Y., Li, Z., 2013. Remote chlorophyll-a estimates for inland waters based on a cluster-based classification. Sci. Total Environ. 444, 1–15. doi:10.1016/j.scitotenv.2012.11.058

Shi, K., Zhang, Y., Liu, X., Wang, M., Qin, B., 2014. Remote sensing of diffuse attenuation coefficient of photosynthetically active radiation in Lake Taihu using MERIS data. Remote Sens. Environ. 140, 365–377. doi:10.1016/j.rse.2013.09.013

Song, K., Li, L., Tedesco, L.P.P., Li, S., Duan, H., Liu, D., Hall, B.E.E., Du, J., Li, Z., Shi, K., Zhao, Y., 2013. Remote estimation of chlorophyll-a in turbid inland waters: Three-band model versus GA-PLS model. Remote Sens. Environ. 136, 342–357. doi:10.1016/j.rse.2013.05.017

Su, H., Liu, H., Wang, L., Filippi, A.M., Heyman, W.D., Beck, R.A., 2014. Geographically Adaptive Inversion Model for Improving Bathymetric Retrieval From Satellite Multispectral Imagery. IEEE Trans. Geosci. Remote Sens. 52, 465–476. doi:10.1109/TGRS.2013.2241772

Sun, D., Li, Y., Le, C., Shi, K., Huang, C., Gong, S., Yin, B., 2013. A semi-analytical approach for detecting suspended particulate composition in complex turbid inland waters (China). Remote Sens. Environ. 134, 92–99. doi:10.1016/j.rse.2013.02.024

Suzuki, R., Ishimaru, T., 1990. An improved method for the determination of phytoplankton chlorophyll using N, N-dimethylformamide. J. Oceanogr. Soc. Japan 46, 190–194. doi:10.1007/BF02125580

Terauchi, G., Tsujimoto, R., Ishizaka, J., Nakata, H., 2014. Preliminary assessment of eutrophication by remotely sensed chlorophyll-a in Toyama Bay, the Sea of Japan. J. Oceanogr. 70, 175–184. doi:10.1007/s10872-014-0222-z

Tyler, A.N., Hunter, P.D., Spyrakos, E., Groom, S., Constantinescu, A.M., Kitchen, J., 2016. Developments in Earth observation for the assessment and monitoring of inland, transitional, coastal and shelf-sea waters. Sci. Total Environ. 572, 1307–1321. doi:10.1016/j.scitotenv.2016.01.020

Usali, N., Ismail, M.H., 2010. Use of Remote Sensing and GIS in Monitoring Water Quality. J. Sustain. Dev. 3, 228–238. doi:10.5539/jsd.v3n3p228

Vollenweider, R.A., Kerekes, J., 1982. Eutrophication of waters. Monitoring, assessment and control. Organ. Econ. Co-Operation Dev. (OECD), Paris 156.

Watanabe, F., Alcântara, E., Rodrigues, T., Imai, N., Barbosa, C., Rotta, L., 2015. Estimation of Chlorophyll-a Concentration and the Trophic State of the Barra Bonita Hydroelectric Reservoir Using OLI/Landsat-8 Images. Int. J. Environ. Res. Public Health 12, 10391–10417. doi:10.3390/ijerph120910391

Werdell, P.J., Bailey, S.W., Franz, B.A., Harding, L.W., Feldman, G.C., McClain, C.R., 2009. Regional and seasonal variability of chlorophyll-a in Chesapeake Bay as observed by SeaWiFS and MODIS-Aqua. Remote Sens. Environ. 113, 1319–1330. doi:10.1016/j.rse.2009.02.012

Xu, J., Li, F., Zhang, B., Song, K., Wang, Z., Liu, D., Zhang, G., 2009. Estimation of chlorophyll-a concentration using field spectral data: a case study in inland Case-II waters, North China. Environ. Monit. Assess. 158, 105–16. doi:10.1007/s10661-008-0568-z

Yang, W., Matsushita, B., Chen, J., Fukushima, T., 2011a. Estimating constituent

concentrations in case II waters from MERIS satellite data by semi-analytical model optimizing and look-up tables. Remote Sens. Environ. 115, 1247–1259. doi:10.1016/j.rse.2011.01.007

Yang, W., Matsushita, B., Chen, J., Fukushima, T., 2011b. A Relaxed Matrix Inversion Method for Retrieving Water Constituent Concentrations in Case II Waters: The Case of Lake Kasumigaura, Japan. IEEE Trans. Geosci. Remote Sens. 49, 3381–3392. doi:10.1109/TGRS.2011.2126048

Yang, W., Matsushita, B., Chen, J., Yoshimura, K., Fukushima, T., 2013. Retrieval of Inherent Optical Properties for Turbid Inland Waters From Remote-Sensing Reflectance. IEEE Trans. Geosci. Remote Sens. 51, 3761–3773. doi:10.1109/TGRS.2012.2220147

Ylöstalo, P., Kallio, K., Seppälä, J., 2014. Absorption properties of in-water constituents and their variation among various lake types in the boreal region. Remote Sens. Environ. 148, 190–205. doi:10.1016/j.rse.2014.03.023

Yoder, J.A., McClain, C.R., Blanton, J.O., Oeymay, L.-Y., 1987. Spatial scales in CZCS-chlorophyll imagery of the southeastern U.S. continental shelf. Limnol. Oceanogr. 32, 929–941. doi:10.4319/lo.1987.32.4.0929

Yu, G., Yang, W., Matsushita, B., Li, R., Oyama, Y., Fukushima, T., 2014. Remote Estimation of Chlorophyll-a in Inland Waters by a NIR-Red-Based Algorithm: Validation in Asian Lakes. Remote Sens. 6, 3492–3510. doi:10.3390/rs6043492

Zhang, F., Li, J., Shen, Q., Zhang, B., Wu, C., Wu, Y., Wang, G., Wang, S., Lu, Z., 2015. Algorithms and Schemes for Chlorophyll a Estimation by Remote Sensing and Optical Classification for Turbid Lake Taihu, China. IEEE J. Sel. Top. Appl. Earth Obs. Remote Sens. 8, 350–364. doi:10.1109/JSTARS.2014.2333540

Zhang, Y.L., Liu, M.L., Wang, X., Zhu, G.W., Chen, W.M., 2009. Bio-optical properties and estimation of the optically active substances in Lake Tianmuhu in summer. Int. J. Remote Sens. 30, 2837–2857. doi:10.1080/01431160802558592

Zhou, L., Roberts, D.A., Ma, W., Zhang, H., Tang, L., 2014. Estimation of higher chlorophylla concentrations using field spectral measurement and HJ-1A hyperspectral satellite data in Dianshan Lake, China. ISPRS J. Photogramm. Remote Sens. 88, 41–47. doi:10.1016/j.isprsjprs.2013.11.016

Zhou, Z., Zhao, Y., 2011. Research on the Water Quality Monitoring System for Inland Lakes based on Remote Sensing. Procedia Environ. Sci. 10, 1707–1711. doi:10.1016/j.proenv.2011.09.268

Zhu, W., Yu, Q., Tian, Y.Q., Becker, B.L., Zheng, T., Carrick, H.J., 2014. An assessment of remote sensing algorithms for colored dissolved organic matter in complex freshwater environments. Remote Sens. Environ. 140, 766–778. doi:10.1016/j.rse.2013.10.015

Zimba, P. V., Gitelson, A., 2006. Remote estimation of chlorophyll concentration in hyper-eutrophic aquatic systems: Model tuning and accuracy optimization. Aquaculture 256, 272–286. doi:10.1016/j.aquaculture.2006.02.038